THESIS

Michigan State
University
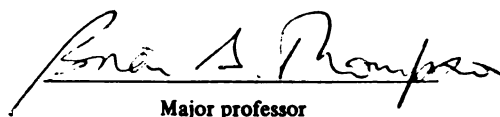
This is to certify that the

thesis entitled

An Analytical and experimental investigation
of the dynamic response of a four bar mechanism
with clearance in the coupler-rocker bearing

presented by

Mehrnam Sharif-Bakhtiar

has been accepted towards fulfillment
of the requirements for

___M.S.___ degree in __Mechanical__ Engineering

_____
Major professor

Date _2 Nov 1984_

O-7639

AN ANALYTICAL AND EXPERIMENTAL

INVESTIGATION OF THE DYNAMIC RESPONSE

OF A FOUR BAR MECHANISM WITH CLEARANCE

IN THE COUPLER-ROCKER BEARING

By

Mehrnam Sharif-Bakhtiar

A THESIS

Submitted to

Michigan State University

in partial fulfillment of the requirement

for the degree of

MASTER OF SCIENCE

Department of Mechanical Engineeing

1984

ABSTRACT

AN ANALYTICAL AND EXPERIMENTAL

INVESTIGATION OF THE DYNAMIC RESPONSE

OF A FOUR BAR MECHANISM WITH CLEARANCE

IN THE COUPLER-ROCKER BEARING

By

Mehrnam Sharif-Bakhtiar

Design problems of mechanisms in industry which were considered
of secondary importance until about a decade ago, are now receiving
more extensive attention due to the ever-increasing demand for
high-speed machinery. One of the major problems associated with the
operation of such machinery is the inevitable existence of clearance
in one or more of the bearings of the system, which results in a
number of undesirable effects such as excessive vibrations and defor-
mations in the parts, the generation of large forces in the bearings
with clearance due to the vibro-impact phenomenon which can create
high levels of acoustic radiation, overloading of the driving motor,
and also premature failure of the bearings.

The work presented here deals with this specific problem, namely, the existence of clearance in the bearings of a mechanism. A four bar linkage with a finite clearance in the coupler-rocker bearing has been chosen as the mechanism to be studied. Governing equations of motion for one full revolution of the crank are developed which consider the occurence of contact-loss in the bearing with clearance along with subsequent impacts. To perform this task, a specific theoretical model based on some simplifying assumptions has been developed and simulated. An attempt has been made to compare and correlate the theoretical results to experimental data. The principal objective of this study is to investigate the sole effect of bearing clearance on the kinetic and kinematic behavior of the system, whose links are assumed to be rigid and hence free of deflection. This project is by no means intended to be a thorough analysis of the subject of bearing clearance in high-speed machinery, but rather as a means of developing guidelines and criteria for the design of mechanisms, and to help provide a better insight into this relatively new phenomenological problem.

This work is dedicated to my parents, who taught me that there is no failure except in nolonger trying.

ACKNOWLEDGEMENTS

TABLE OF CONTENTS

LIST OF TABLES

LIST OF FIGURES

CHAPTER ONE

INTRODUCTION

The presence of clearances in the joints of mechanisms is inevitable if plain journal bearings are incorporated into the system. Owing to the high-speed operation of machinery, more interest is currently drawn to the study of this problem due to the undesirable effects of existence of bearing clearance such as excessive noise radiation, links' deflection, force generation in the bearings and so forth. The complex effects associated with the existence of clearance in a bearing cannot be confined to the bearing alone, rather it influences the behavior of the system as a whole.

During the high-speed operation of a mechanism, intermittent motions are generated in the bearing(s) with clearance. This, in turn, causes high levels of impactive forces in the bearing(s). Large pulses of forces are transmitted throughout the mechanism causing

extensive vibrations and deflections in the parts, which can partly reduce the longevity of the links. These pulses are also a major cause of premature failure of the bearings with clearance due to the generation of large impulses and subsequent ovality of the bearings, and also frequent overheating of the driving motor primarily due to the inability of the motor to withstand high levels of torque-pulses transmitted to its driving shaft.

The induced vibrations of the links of the mechanism due to the intermittent motions of the system, can become a primary source of excessive acoustic radiation. In addition, these vibratory motions of the links tend to decrease the accuracy of the mechanism in tracing a prescribed path, which is a crucial factor in precision instrumentation and some areas related to robotics.

Numerous researchers have studied the effects of bearing clearances from different points of views. The vast amount of literature available ranges from studies wherein the primary focus of the research is on the on the behavior of the pin within the bushing of the bearing with the links of the mechanism assumed to be free of deflection [1-11], to ones which concentrate on mechanisms whose links are elastic [12-20], that investigate the response of the system to the presence of bearing clearances. Mechanisms with only one of the bearings with clearance [1,2,5,6,21-24] or with multiple clearances in the bearings [16,25-29] have been taken under study to investigate the difference in the behavior of the mechanism based on the number of

clearances and also, the dependency of the response of the system on the size of the clearance(s).

In more specialized studies, some related investigations have been performed on the nature and mechanics of contact between the surfaces of the two components of the bearing, the pin and the bushing [30-34]. Some attempt has been made to mathematically model the bearing components [35-39] in order to observe the effect of such physical and geometrical parameters as damping and the hydrodynamic phenomenon associated with the bearing lubrication.

As previously mentioned, the mechanics of the intermittent motion of a system is primarily due to the impacts generated in the bearing(s) as a consequence of trajectory motion of the pin within the bushing after contact between the two components has been lost [36,40-62]. This in turn, brings about the problem of determining the extent of acoustic radiation transmitted to the surroundings [63-71] caused by the links' resonant vibrations. The intensity of such noise radiation can become high enough that the employees adjacent to the machine are exposed to doses of acoustic radiation in excess of that specified by federal regulations.

Due to the nature of the problem, no one literature can contain all the aforementioned issues associated with the subject of bearing clearances in a comprehensive form, for the subject is too broad and diverse. Thus, one has to acquire a good deal of expertise in several

areas of scientific endeavor in order to be able to analyse and comprehend the thorough behavior of all the issues. However, any attempt in this field provides a basis for further investigation, and helps provide a better insight into the problem as a whole. For instance, the results of an investigation which has focused on the magnitude of the forces generated in the bearing of a rigid-linked mechanism due to the vibro-impact behavior, can serve as an intuitive guideline for the prediction of the size of the deflections occuring in the links of the mechanism, if the links were elastic.

Although the primary effort in all of the investigations has been to model and predict the behavior, in various conditions, of a mechanism with intermittent motions, there has been some work concentrating on the feasibility of adaption of different methods to prevent these vibro-impact motions. For instance, Perera et al. [40] have suggested the use of 'properly sized torsional springs' fitted into the bearing of a mechanism that has clearance to prevent the occurence of the intermittent motion. The results that are presented in this work are plausible to some extent. But, the optimum solution to this problem is a well-founded and indepth understanding of its nature, for once this task has been accomplished, then sound and optimum preventive methods can be developed, which are more likely to be effective. Some recent work [82] has also been carried out on the effect of using different types of materials, such as composites, in order to reduce the acoustic radiation emitted from the links of mechanism with bearing clearances, which show some promising results.

For the interested reader, there is a vast number of publications and investigations devoted to the subject of bearing clearances, which focus on different aspects of the problem, and one can select to concentrate on any one of the aspects of this issue that suits one's interest. These may be reviewed in a survey paper by Haines [83].

CHAPTER TWO

ASSUMPTIONS AND GOVERNING MODES

In order to study and develop the governing equations of motion of a planar four bar linkage with clearance in the coupler-rocker bearing, some simplifying assumptions need to be imposed upon the system, to ease the way for modeling the system. The primary use of these assumptions is to eliminate some of the uncertainties associated with the system which could significantly influence the outcome of the simulation. Prior to listing these assumptions, the term 'nominal mechanism' should be explained; this phrase refers to a mechanism with no clearance in any of its bearings.

2.1- Assumptions

1. The nominal mechanism has one degree of freedom associated with a

crank shaft drive, running at constant angular velocity. In other words, the motor driving the crank is theoretically capable of supplying any magnitude of torque required to keep the crank speed constant.

2. The mechanism, be it nominal or otherwise, is perfectly planar, with co-planar dynamic and static loads. This assumption eliminates the forces and bending moments acting in the direction perpendicular to the plane of the mechanism, thus reducing the problem to that of a two-dimensional one.

3. All of the link and the bearing surfaces are rigid, implying that the elastodynamic behavior of the system can be ignored. Hence, problems such as deflections of the links and/or nature of contact of the bearing surfaces can be bypassed.

4. Friction is light, and can be neglected. In other words, there is no energy dissipation in any of the bearings. Also any hydrodynamic phenomena due to the lubrication of the bearings is assumed to have negligible effect on the results.

5. The radial clearance in the coupler-rocker bearing is very small compared to any dimensionally similar expression associated with the nominal mechanism. The magnitude of the clearance is at least of the order of 10^{-3} times that of any other longitudinal dimension in the mechanism.

Upon imposition of these assumptions on the system, a theoretical model can be constructed whose governing equations of motion and their

behavior will be investigated in the subsequent chapters. Since the nominal mechanism plays a significant role in this study, some of its governing equations, which will be referred to later, are braught here (for a thorough derivation the reader is referred to the paper by Smith and Maunder [72]) with a typical plot of their behavior over one full crank revolution. The ordinates of the plots are insignificant and hence are omitted. Figure (2.1) is a schematic view of the nominal mechanism with its corresponding notation. Figures (2.2) to (2.4) show the angular displacement, velocity, and acceleration of the coupler link, respectively.

The angular displacements of the coupler and rocker, respectively, can be expressed as follows

$$\cos\theta_3 = A \cdot B/D^2 \pm \left[(A \cdot B/D^2)^2 - (B^2 - C^2)/D^2 \right]^{1/2} \qquad (2.1\text{-}1a)$$

where

$$A = 2l_3(l_2\cos\theta_2 - l_1)$$

$$B = l_4^2 - l_1^2 - l_2^2 - l_3^2 + 2l_1l_2\cos\theta_2$$

$$C = 2l_2l_3\sin\theta_2$$

$$D = (A^2 + C^2)^{1/2}$$

$$\cos\theta_4 = (l_2\cos\theta_2 + l_3\cos\theta_3 - l_1)/l_4 \qquad (2.1\text{-}1b)$$
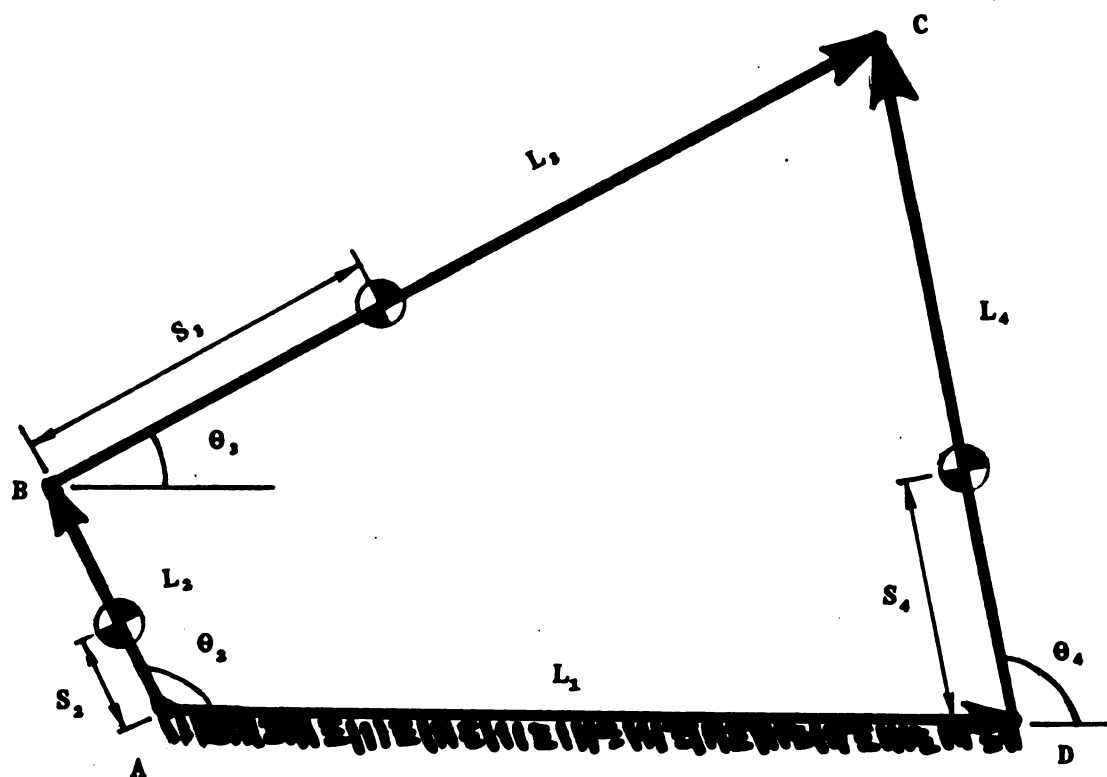
FIGURE 2.1.   SCHEMATIC VIEW OF THE NOMINAL MECHANISM
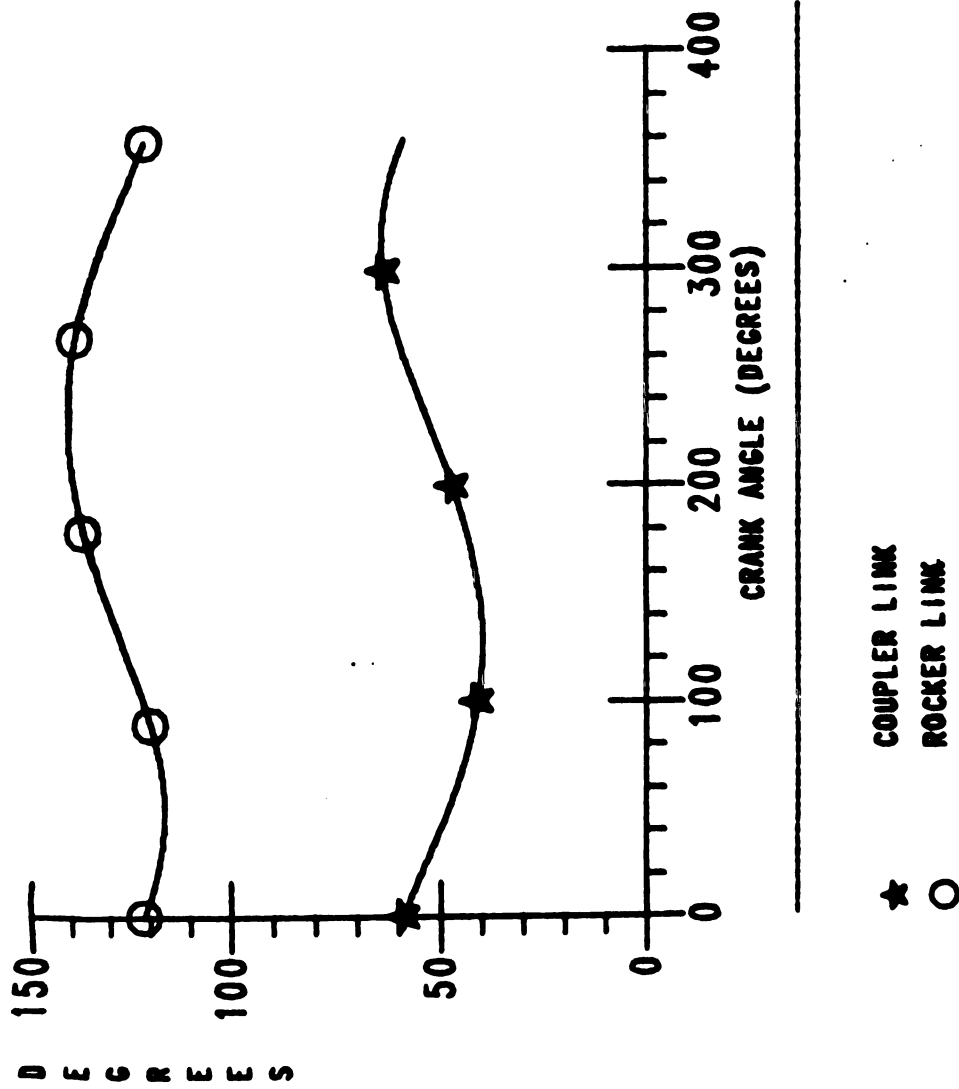
FIGURE 2.2. ANGULAR DISPLACEMENT
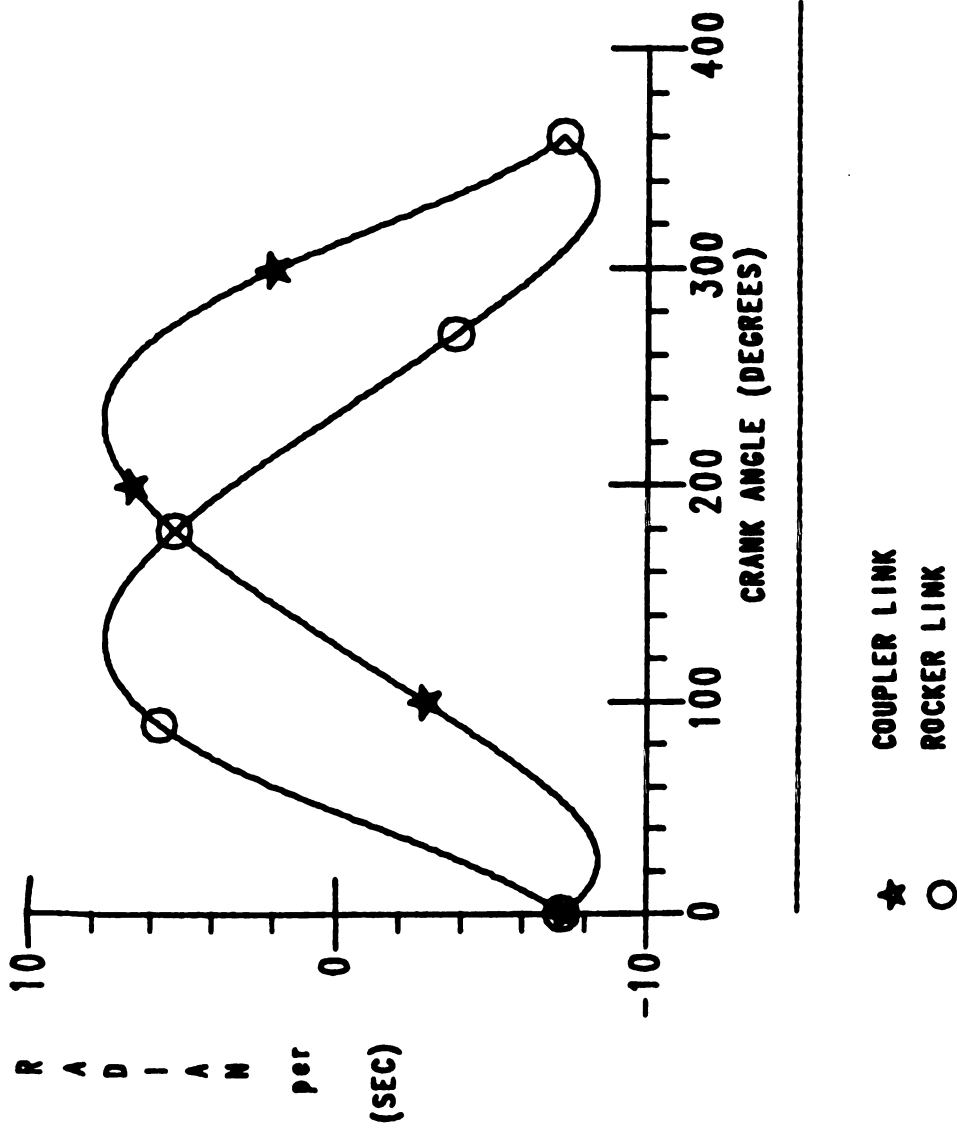
FIGURE 2.3. ANGULAR VELOCITY
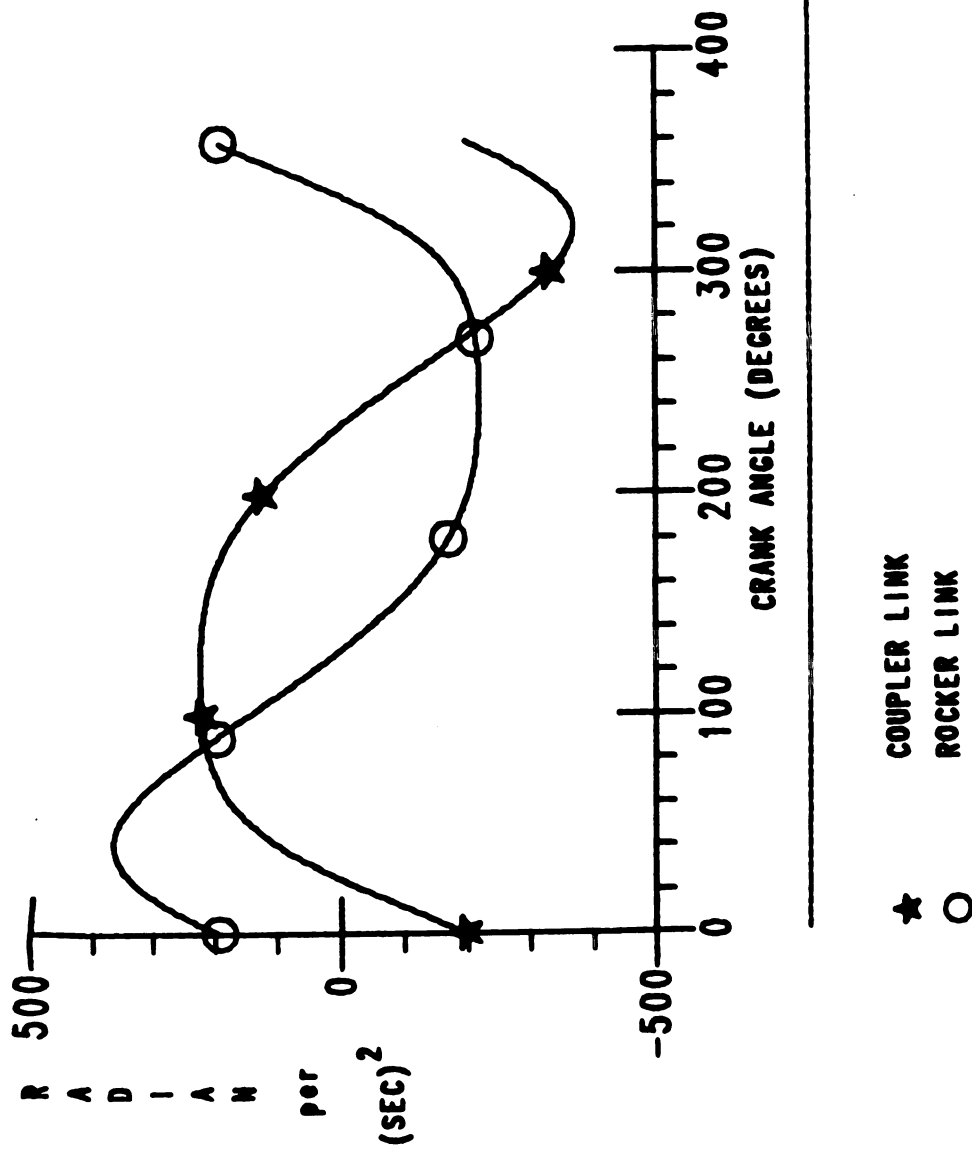
FIGURE 2.4. ANGULAR ACCELERATION

The angular velocities of the coupler, and rocker, respectively are

$$\omega_3 = -\omega_2[l_2\sin(\theta_2-\theta_4)]/[l_3\sin(\theta_3-\theta_4)] \qquad (2.1-2a)$$

$$\omega_4 = -\omega_2[l_2\sin(\theta_2-\theta_3)]/[l_4\sin(\theta_3-\theta_4)] \qquad (2.1-2b)$$

and, the angular accelerations of the coupler, and rocker, respectively, are

$$\alpha_3 = (\omega_3/\omega_2)\alpha_2 - [\omega_2^2 l_2\cos(\theta_2-\theta_4)$$

$$+\omega_3^2 l_3\cos(\theta_3-\theta_4-\omega_4^2 l_4]/l_3\sin(\theta_3-\theta_4)$$

$$(2.1-3a)$$

$$\alpha_4 = (\omega_4/\omega_2)\alpha_2 - [\omega_2^2 l_2\cos(\theta_2-\theta_3)$$

$$-\omega_4^2 l_4\cos(\theta_3-\theta_4)+\omega_3^2 l_3]/l_4\sin(\theta_3-\theta_4)$$

$$(2.1-3b)$$

2.2- Modes of Behavior

Figure (2.5) shows a four bar linkage with clearance in the coupler-rocker bearing. Following considerable deliberation, cogita-

tion and, consideration of the physics of the problem, it is postulated that the dynamic behavior of such a system can be primarily contained within three modes at all times. This section is concerned with explaining this hypothesis.

The first mode, called the "following" mode (Fig. 2.5), refers to a particular configuration, in which the pin and the bushing of the bearing under study are in contact at all times. The question of whether the pin and bushing slip against each other or stick together in any given time in this mode, is a matter that will be dealt with later in its proper place. The second mode, referred to as the "free-flight" mode, describes the system at times when contact has been lost between the two components of the coupler-rocker bearing, the pin and the bushing. In this mode, the pin moves along a particular trajectory path inside the bushing. Figure (2.6) shows the system in the free-flight mode. The third mode, called the "impact" mode (Fig. 2.7), which always occurs in succession with the free-flight mode, primarily describes the system at the instant of time when the pin collides with the bushing at the termination of the free-flight mode.

Once the equations of motion for each mode are derived, they can be related together using appropriate boundary and initial conditions, to yield a set of equations which describe th complete behavior of the system. The next three chapters are devoted to the derivation of the governing equations of each mode, and chapter six deals with
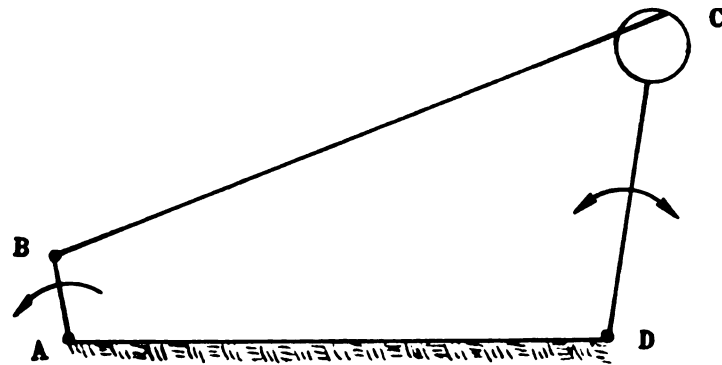
(a)- Following mode
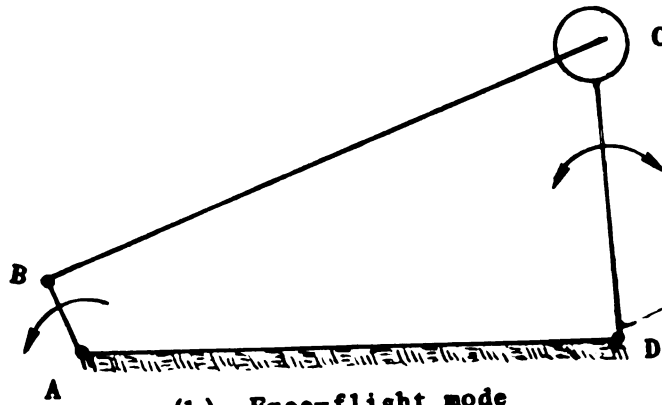
(b)- Free-flight mode
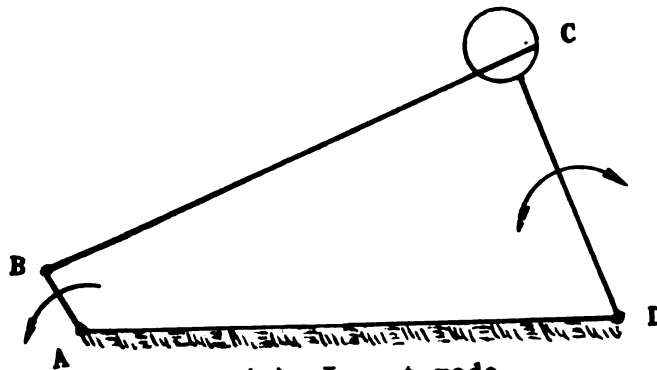
(c)- Impact mode

FIGURE 2.5.   MODES OF BEHAVIOR OF THE MECHANISM

relating these modes and their numerical solution along with the corresponding results. Chapter seven describes the experimental instrumentation along with some digitized results. In chapter eight the numerical and experimental results have been correlated. Finally, chapter nine will contain the closing remarks.

CHAPTER THREE

THE FOLLOWING MODE

In order to study the four bar linkage in the following mode, the clearance in the coupler-rocker bearing can be represented as a massless fifth link, whose length remains constant (as proposed by Earles and Wu [3] and Grant and Fawcett [8]. Figure (3.1) shows such a linkage with the notation that will be used throughout this chapter. By examining this diagram, it is observed that such a system has a total of seven degrees of freedom associated with its dynamic motion. These are the four angular displacements of the crank, coupler, rocker, and the 'clearance link', along with the crank torque, and the X- and Y-components of the coupler-rocker bearing reaction. The latter force acts in order to sustain the mechanism in a prescribed configuration.

As suggested by several authors [3,5,10,29,79], The Lagrangian

approach is employed here in order to develop the governing equations of motions, i.e.,

$$d/dt\left[\partial T/\partial q_i\right]-\partial T/\partial q_i = Q_i + \sum(\lambda_j \cdot \partial f_j/\partial q_i) \qquad (3-1)$$

where

T : Total kinetic energy of the system

q_i : Generalized coordinates

Q_i : Generalized forces

λ_j : Lagrange multipliers

f_j : Constraint equations

The following notes regarding equation (3.1) should be considered:

1. The generalized coordinates, as previously mentioned, are Θ_2, Θ_3, Θ_4, and Θ_{c_3}.

2. The Lagrange multipliers include the remaining three unknowns, namely,

λ_1 : crank torque

λ_2 : Y-component of the coupler-rocker bearing reaction

λ_3 : X-component of the coupler-rocker bearing reaction

3. The summation on the right hand side of the equation is over parameter j, for j=1,...,n ,where n is the number of Lagrange multipliers.

4. The number of constraint equations should be equal to the number of Langrange multipliers. The first constraint equation can be deduced from the first assumption stated in section (2.1) that, the crank has constant angular velocity. This can be expressed in mathematical form as

$$f_1 = \theta_2 - \omega_2 \cdot t \qquad (3-2)$$

where the term t denotes time. In what follows an overdot on a parameter indicates the derivative of that variable with respect to time.

The other two constraint equations can be obtained by writing the vector loop-closure equation of the mechanism (fig. 3.1), namely,

$$\bar{I}_2 + \bar{I}_3 + \bar{C}_3 = \bar{I}_1 + \bar{I}_4 \qquad (3-3)$$

where the overbar indicates vector quantity.

However, any vector, $\bar{L}_j$, can be expressed in complex form as

$$L_i = L \cdot e^{j\theta} = L\cos\theta + jL\sin\theta \qquad (3-4)$$

Thus, decomposing equation (3-3) according to (3-4) and seperating the real and imaginary parts yields the two constraint equations, f_2 and f_3, i.e.,

$$f_2 = l_2\sin\theta_2 + l_3\sin\theta_3 + C_3\sin\theta_{c_3} - l_4\sin\theta_4 \qquad (3-6)$$

$$f_3 = l_2\cos\theta_2 + l_3\cos\theta_3 + C_3\cos\theta_{c_3} - l_1 - l_4\cos\theta_4 \qquad (3-7)$$

5. The generalized forces, which will be discussed in detail later in section 3.2, generally include both conservative and nonconservative forces.

3.1- Total Kinetic Energy of the System

The total kinetic energy, T, of the mechnism (fig. 3.1) can be expressed as

$$T = T_2 + T_3 + T_4 \qquad (3.1-1)$$

where the subscripts 2, 3, and 4 denote the crank, coupler, and rocker

links, respectively. Note that there is no kinetic energy associated with the clearance link for it is assumed to be massless. The objective is to express the total kinetic energy in terms of the angular velocities of the links to be suitable for substitution into the Lagrange's equation (3-1).

3.1.1- Crank kinetic Energy, T_2

The kinetic energy of the crank can be formulated as (fig. 3.2)

$$T_2 = (1/2)m_2 S_2^2 \omega_2^2 + (1/2)I_{G_2}\omega_2^2 \qquad (3.1.1-1)$$

which is readily in the desired form, and where I_{G_i} denotes the mass moment of inertia of link i about its mass center.

3.1.2- Coupler Kinetic Energy, T_3

Refering to Figure (3.2), the kinetic energy of the coupler may be written as

$$T_3 = (1/2)m_3 V_3^2 + (1/2)I_{G_3}\omega_3^2 \qquad (3.1.2-1)$$

However, using the law of relative velocities
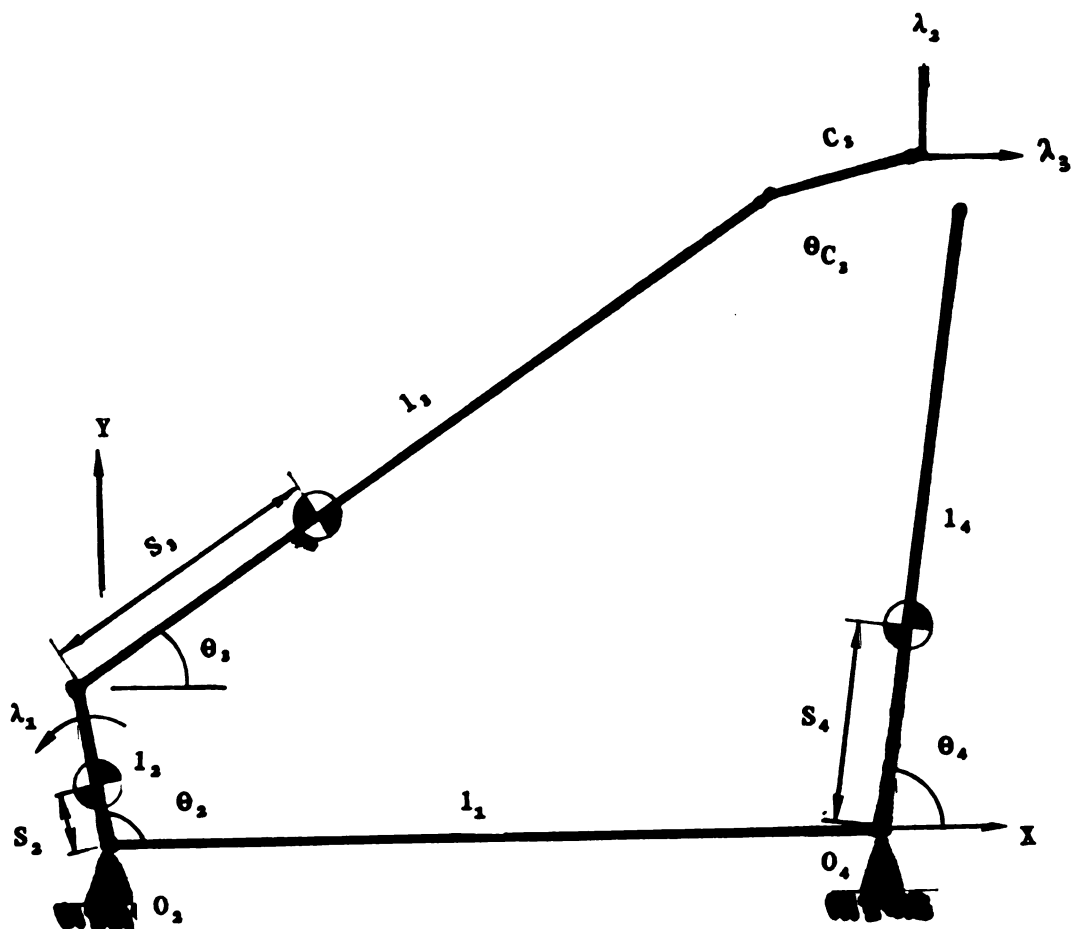
FIGURE 3.1. MECHANISM IN THE FOLLOWING MODE

$$\bar{V}_s = \bar{V}_B + \bar{V}_{C/B} \qquad (3.1.2\text{-}2)$$

where V_s is the absolute velocity of the mass center of the coupler link. But,

$$V_B = 1_2 \omega_2 \qquad (3.1.2\text{-}3)$$

and

$$V_{C/B} = S_s \omega_s \qquad (3.1.2\text{-}4)$$

Construction of the vector diagram of equation (3.1.2-2) is shown in Figure (3.3). Refering to this Figure and using the law of cosines V_s can be written as

$$V_s^2 = 1_2^2 \omega_2^2 + S_s^2 \omega_s^2 - 21_2 S_s \omega_2 \omega_s \cos(\theta_2 - \theta_s) \qquad (3.1.2\text{-}5)$$

Substitution of equation (3.1.2-5) into (3.1.2-1) yields the expression for the kinetic enegy of the coupler as

$$T_s = (1/2) m_s [1_2^2 \omega_2^2 + S_s^2 \omega_s^2 - 21_2 S_s \omega_2 \omega_s$$

$$\cos(\theta_2 - \theta_s)] + (1/2) I_{G_s} \omega_s^2$$

$$(3.1.2\text{-}6)$$
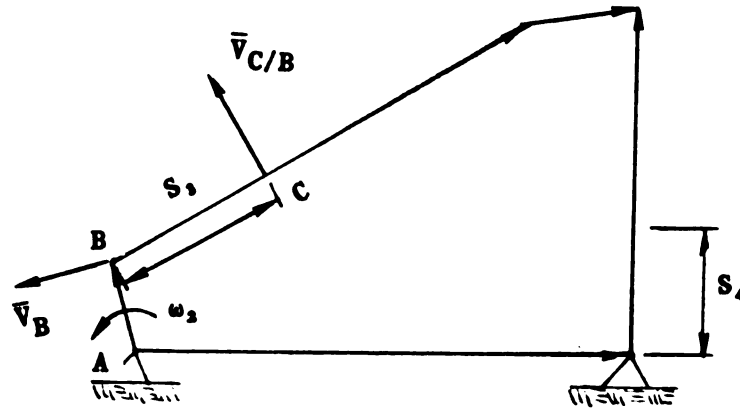
FIGURE 3.2. VELOCITY DIRECTION OF THE COUPLER'S MASS CENTER
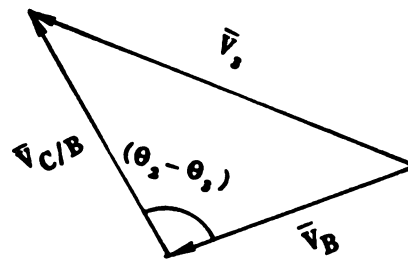
FIGURE 3.3. VECTOR REPRESSENTATION OF V_s

3.1.3- Rocker Kinetic Energy, T_4

Observing Figure (3.2), the kinetic energy of the rocker can be written as

$$T_4=(1/2)m_4 S_4 \omega_4{}^2+(1/2)I_{G_4}\omega_4{}^2 \tag{3.1.3-1}$$

Substitution of equations (3.1.1-1), (3.1.2-6), and (3.1.3-1) into equation (3.1-1) results in the final expression for the total kinetic energy of the system in the desired form as

$$T=(1/2)m_2 S_2{}^2 \omega_2{}^2+(1/2)I_{G_2}\omega_2{}^2+(1/2)m_3[1_2{}^2\omega_2{}^2$$

$$+S_3{}^2\omega_3{}^2-21_2 S_3 \omega_2 \omega_3 \cos(\theta_2-\theta_3)]+(1/2)I_{G_3}\omega_3{}^2$$

$$+(1/2)m_4 S_4 \omega_2{}^2+(1/2)I_{G_4}\omega_4{}^2$$

$$\tag{3.1-2}$$

3.2- Generalized Forces

The generalized forces, Q_i, are obtained using the Hamiltonian method and principle of virtual work [80]. The reader can refer to any advanced calculus or mechanics book for a thorough description of

these methods. Thus, for breviety, only the principal features of the derivation of the generalized forces will be indicated here.

If p forces act upon a system, then the virtual work can be stated as

$$\delta W = \sum_j \overline{F}_j \cdot \delta \overline{r}_j \qquad j=1,\ldots,p \qquad (3.2-1)$$

Since $\overline{r}_j$, the vector position of the point of action of any one of the forces, such as $\overline{F}_j$, can be written as

$$\overline{r}_j = \overline{r}_j(q_1,q_2,\ldots,q_n,t) \qquad (3.2-2)$$

where q_i indicates the ith generalized coordinate and t represents the time. Hence the variation of $\overline{r}_j$ can be expressed as

$$\delta \overline{r}_j = (\partial \overline{r}_j/\partial q_1)\delta q_1 + (\partial \overline{r}_j/\partial q_2)\delta q_2 + \ldots + (\partial \overline{r}_j/\partial q_n)\delta q_n \qquad (3.2-3)$$

Hence, equation (3.2-1) can be written as

$$\delta W = \sum_j [\overline{F}_j \cdot (\partial \overline{r}_j/\partial q_1)\delta q_1 + \overline{F}_j \cdot (\partial \overline{r}_j/\partial q_2)\delta q_2 + \ldots + \overline{F}_j \cdot (\partial \overline{r}_j/\partial q_n)\delta q_n]$$

$$j=1,\ldots,p$$

$$(3.2-4)$$

On the other hand, one can express the virtual work as the product of n 'generalized forces', Q_k, acting over n generalized virtual displacements δq_k . The directions of these generalized forces coincide with the corresponding directions of the generalized displacements, so one writes

$$\delta W = Q_1 \delta q_1 + Q_2 \delta q_2 + \ldots + Q_n \delta q_n = \sum_k Q_k \delta q_k \qquad k=1,\ldots,n$$

(3.2-5)

The generalized forces, Q_k, take the place of the single forces acting upon each particle. These forces form the components of an n-dimensional vector in the configuration space. The configuration space of a system is a point in an n-dimensional space, corresponding to values of n generalized coordinates defining the instantaneous configuration of the system. In other words, the configuration of the system at any instant of time can be represented as only one point in an n-dimensional reference frame whose axes are the n generalized coordinates.

Note that the generalized force, Q_k, does not necessarily represent a force. Its units, however, must be such that $Q_k \cdot \delta q_k$ has units of work. For instance, Q_k could be a moment, in which case δq_k represents an angular displacement.

Comparing equations (3.2-4) and (3.2-5) one concludes that

$$Q_k = \sum_j \bar{F}_j \cdot (\partial \bar{r}_j / \partial q_k) \qquad j=1,\ldots,p \qquad (3.2\text{-}6)$$

The generalized force, Q_k, in general contains both conservative and nonconservative force fields. One can distinguish between the two by noting that the conservative force, Q_{k_c}, can be derived from the potential energy expression V, and the nonconservative force, $Q_{k_{nc}}$, may include internal dissipative forces or any external forces which are not derivable from a potential function, so that

$$Q_k = Q_{k_c} + Q_{k_{nc}} \qquad (3.2\text{-}7)$$

The system under study (fig. 3.1) is assumed to be acted upon by a conservative field, since the friction (dissipative) forces are assumed to be negligible, and also no external forces (path independent) act on the system. Note that the crank torque and the X- and Y-components of the coupler-rocker bearing reaction have been accounted for as Lagrange multipliers. For a conservative field

$$W_c(q_k) = -V(q_k) \qquad (3.2\text{-}8)$$

because in such a field, the work is the negative of the change in the potential energy. But

$$\delta W_c(q_k) = \sum_k Q_{k_c} \delta q_k \qquad (3.2\text{-}9)$$

and

$$\delta W_c(q_k) = -\delta V(q_k) = -\sum_k (\partial V/\partial q_k)\delta q_k \qquad (3.2-10)$$

Comparison of the equations (3.2-9) and (3.2-10) yields

$$Q_{k_c} = -\partial V/\partial q_k \qquad (3.2-11)$$

3.2.1- Total Potential Energy, V

Refering to Figure (3.2), the potential energy of the crank can be written as

$$V_2 = m_2 g S_2 \sin\theta_2 \qquad (3.2.1-1)$$

and that of the coupler is

$$V_3 = m_3 g(l_2 \sin\theta_2 + S_3 \sin\theta_3) \qquad (3.2.1-2)$$

and for the rocker

$$V_4 = m_4 g S_4 \sin\theta_4 \qquad (3.2.1-3)$$

Hence, the total potential energy of the mechanism can be expressed as

$$V = m_2 g S_2 \sin\theta_2 + m_3 g(l_2 \sin\theta_2 + S_3 \sin\theta_3) + m_4 g S_4 \sin\theta_4 \qquad (3.2.1-4)$$

Application of equation (3.2-11) to (3.2.1-4) yields the expressions for the generalized conservative forces as

$$Q_{2_c} = -(m_2 S_2 + m_3 l_2) g \cos\theta_2 \qquad (3.2\text{-}12a)$$

$$Q_{3_c} = -m_3 g S_3 \cos\theta_3 \qquad (3.2\text{-}12b)$$

$$Q_{c_{3_c}} = 0 \qquad (\text{clearance link}) \qquad (3.2\text{-}12c)$$

$$Q_{4_c} = -m_4 g S_4 \cos\theta_4 \qquad (3.2\text{-}12d)$$

where g in the above equations represents the component of the gravitational acceleration in the plane of the mechanism.

3.3- Resulting Equations of Motion

Having all the parameters expressed in the desired form, the Lagrange's equation (equation 3-1) can now be written for each generalized coordinate. The explicit expression of equation (3-1) on the first generalized coordinate, θ_2, is

$$-\lambda_1-(l_2\cos\theta_2)\lambda_2+(l_2\sin\theta_2)\lambda_3+[m_3 l_2 S_3\cos(\theta_2-\theta_3)]\alpha_3$$

$$=-m_2 g S_2\cos\theta_2-m_3 g l_2\cos\theta_2-m_3 l_2 S_3\sin(\theta_2-\theta_3)\omega_3^2$$

$$(3.3-1)$$

Note that α_2 is zero.

For θ_3 we have

$$-(l_3\cos\theta_3)\lambda_2+(l_3\sin\theta_3)\lambda_3+(I_{G_3}+m_3 S_3^2)\alpha_3$$

$$=-m_3 g S_3\cos\theta_3+m_3 l_2 S_3\sin(\theta_2-\theta_3)\omega_2^2$$

$$(3.3-2)$$

and for θ_{c_3} we have

$$-(C_3\cos\theta_{c_3})\lambda_2+(C_3\sin\theta_{c_3})\lambda_3=0 \qquad (3.3-3)$$

and finally, for θ_4 one can write

$$(l_4\cos\theta_4)\lambda_3-(l_4\sin\theta_4)\lambda_3+(I_{G_4}+m_4 S_4^2)\alpha_4=$$

$$-m_4 g S_4\cos\theta_4$$

$$(3.3-4)$$

Assuming that, at the time of start the angular displacements of all the links are known, along with the angular velocities of the

links (section 3.4), the only remaining unknowns in equations (3.3-1) to (3.3-4) are the angular accelerations of the links (α_i, i=2,3,4,c,) and also the Lagrange multipliers (λ_j, j=1,2,3). Hence, at initial condition (section 3.4), there are six unknowns embedded in these four nonlinear equations. The other two necessary equations to solve for the unknowns can be derived from the constraint equations f_2 and f_3 (equations 3-6 and 3-7), which represent the real and imaginary components of the loop closure equation of the mechanism. However, in order to have these two latter equations be compatible with equations (3.3-1) to (3.3-4) in terms of the linearity of the unknowns, the second time derivative of these constraint equations shall be used. Thus, equation (3-6) yields

$$\partial^2 f_2 / \partial t^2 = 0$$

or

$$-(l_4 \sin\theta_4)\alpha_4 + (l_3 \sin\theta_3)\alpha_3 + (C_3 \sin\theta_{c_3})\alpha_{c_3}$$

$$= l_4 \cos\theta_4 \omega_4{}^2 - l_3 \cos\theta_3 \omega_3{}^2 - C_3 \cos\theta_{c_3} \omega_{c_3}{}^2 - l_2 \cos\theta_2 \omega_2{}^2$$

$$(3.3-5)$$

and equation (3-7) yields

$$\partial^2 f_3 / \partial t^2 = 0$$

or

$$-(1_4\cos\Theta_4)\alpha_4+(1_3\cos\Theta_3)\alpha_3+(C_3\cos\Theta_{c_3})\alpha_3$$

$$=1_2\sin\Theta_2\omega_2^{\ 2}+1_3\sin\Theta_3\omega_3^{\ 2}+C_3\sin\Theta_{c_3}\omega_{c_3}^{\ 2}-1_4\sin\Theta_4\omega_4^{\ 2}$$

$$(3.3-6)$$

Note that, the constraint equation f_1 (equation 3-2) which states that the crank has a constant angular velocity, has not been ignored, rather its first time derivative ,i.e.

$$\partial f_1/\partial t = \alpha_2 = 0$$

has been substituted into the other six equations to eliminate α_2 .

A glance at the equations (3.3-1) to (3.3-6) reveals the fact that these equations are nonlinear in terms of the angular displace- ments and velocities. However, they are linear in terms of the angu- lar accelerations and the Lagrange's multipliers. Hence, they can be written in a matrix form as

$$[A][X]=[B] \qquad (3.3-7)$$

where matrix [A] is

$$
\begin{bmatrix}
-1 & -l_2\cos\theta_2 & l_2\sin\theta_2 & 0 & m_3 l_2 S_3 \cos\beta & 0 \\
0 & -l_3\cos\theta_3 & l_3\sin\theta_3 & 0 & I_{G_3}+m_3 S_3{}^2 & 0 \\
0 & -C_3\cos\theta_{C_3} & C_3\sin\theta_{C_3} & 0 & 0 & 0 \\
0 & l_4\cos\theta_4 & -l_4\sin\theta_4 & I_{G_4}+m_4 S_4{}^2 & 0 & 0 \\
0 & 0 & 0 & -l_4\sin\theta_4 & l_3\sin\theta_3 & C_3\sin\theta_{C_3} \\
0 & 0 & 0 & -l_4\cos\theta_4 & l_3\cos\theta_3 & C_3\cos\theta_{C_3}
\end{bmatrix}
$$

(3.3-8a)

Where $\beta=\theta_3-\theta_3$. Vector [X] can be written as

$$
\begin{bmatrix}
\lambda_1 \\
\lambda_2 \\
\lambda_3 \\
\alpha_4 \\
\alpha_3 \\
\alpha_{C_3}
\end{bmatrix}
$$

(3.3-8b)

and vector [B] is

$$
\begin{bmatrix}
-m_3 g S_3 \cos\theta_3 - m_3 g l_2 \cos\theta_2 - m_3 l_2 S_3 \sin(\theta_2-\theta_3)\omega_2^2 \\[2ex]
-m_3 g S_3 \cos\theta_3 + m_3 l_2 S_3 \sin(\theta_2-\theta_3)\omega_2^2 \\[2ex]
0 \\[2ex]
-m_4 g S_4 \cos\theta_4 \\[2ex]
l_4\cos\theta_4\omega_4^2 - l_3\cos\theta_3\omega_3^2 - C_3\cos\theta_{c_3}\omega_{c_3}^2 - l_2\cos\theta_2\omega_2 \\[2ex]
l_2\sin\theta_2\omega_2^2 + l_3\sin\theta_3\omega_3^2 + C_3\sin\theta_{c_3}\omega_{c_3}^2 - l_4\sin\theta_4\omega_4^2
\end{bmatrix}
\qquad (3.3\text{-}8c)
$$

3.4- Initial Conditions

Since the solution of equation (3.3-7) is an inital value prob-
lem, the state of the system at some time is required. The criteria
for selecting a particular instant of time as the initial time is not
universal and primarily depends on the geometrical aspects of the
mechanism under study. For instance, Earles and Wu in their paper [3]
use a certain position called the dead-center-point (d.c.p.), which is
referred to the instant of time when the crank and the coupler are in
line, and the clearance (being in the crank-coupler bearing) link has
a translatory motion without any rotational component. Obviously,
this criterion cannot be generalized to be applicable to any typical
mechanism, for this condition requiring the existense of a so-called

d.c.p. would only occur in a few mechanisms with similar geometric dimensions to that of the Earles and Wu's.

However, a rather customary approach is to assume that at the initial time, the clearance link's direction is coincident with the direction of the bearing force in a corresponding 'nominal mechanism'. Such an assumption is relatively well-founded, as investigated by Haines [1]. In this paper, the expression for the angle of lag, S, of the clearance link relative to the bearing reaction has been derived. Then it is shown that with light damping, the system will rapidly approach a state where the angle of lag is negligibly small. At any rate, for reasons to be discussed in six, the determination of the initial condition will be based on a trial and error approach.

3.5- Termination of the Following Mode

As previously mentioned in this chapter, the fundamental assumption of the following mode is the representation of the clearance as a massless fifth link, whose length remains constant. However, at some time t the contact between the pin and the bushing within the coupler-rocker bearing is lost and the above assumption no longer prevails. Once this occurs the following mode's equations of motion cease to apply. Hence, the task is now to determine such a point in time when contact-loss occurs between the bearing components.

Again, this problem has had no unique method of approach, and it is, to some extent, based on intuition and the characteristics of the mechanism under study. Also, the accuracy and capabilities of the available digital computer play a significant role, as to how sensitive the method of contact-loss detection should be. Earles and Wu in their work [3], have adapted a criterion for determining the occurence of contact-loss which is solely dependent on the shape of the polar force plot of the bearing under study. In other words, contact-loss is assumed to take place when the force vector plot passes through the origin with a finite slope. Obviously, such a method seems to be too specialized and cannot be given a universal status as a method of determination of contact-loss.

The second criterion proposed by Earles and Wu [4] is based on monitoring the rate of change of direction of the bearing reaction under study. It states that, the contact-loss positions are located at the points where the rate of change of direction of the force in the bearing is maximum and, simultaneously, the magnitude of this force is at or near its minimum value. This may be formulated mathematically as

$$(\gamma_e / R_{min}) > 1.0 \ (rad/N/sec)$$

where

γ_e : rate of change of direction of the bearing reaction

R_{min} : the corresponding minimum value of bearing reaction

This method, although being more general than the preceding criterion, is not sufficiently accurate and sensitive. According to Haines [83], impacts (a subsequent of contact-loss) have been recorded (albeit small) for (γ_e/R_{min}) as low as 0.32, whereas no impacts have been recorded (at small clearance) in one case where this term is as high as 220.

Grant and Fawcett [84], have interpreted the latter criterion developed by Earles and Wu [4] as indicating that the actual time when contact is lost between the pin and the bushing of the bearing corresponds to the instant of time when (γ_e/R_{min}) equals unity (rad/N/sec). But, this condition would be met in rather specialized mechanisms and, again, cannot be generalized. In another case [8], Fawcett et. al. have made use of the fact that the 'clearance link' can only be in tension. Hence, once in compressive force field, contact-loss occurs. However, it has not been clarified as to how these two conditions are identified.

Two distinct but interrelated methods have been adapted here to predict the occurence of contact-loss, which are basically modified forms of those used by Earles and Wu [3], and Grant and Fawcett [84]. The first method is based on the angular displacement of the 'clearance link' relative to the reaction force in the bearing. Figure (3.4a) shows the bearing at a time when there is contact

(a)- Continuous contact

(b)- Imminent contact-loss
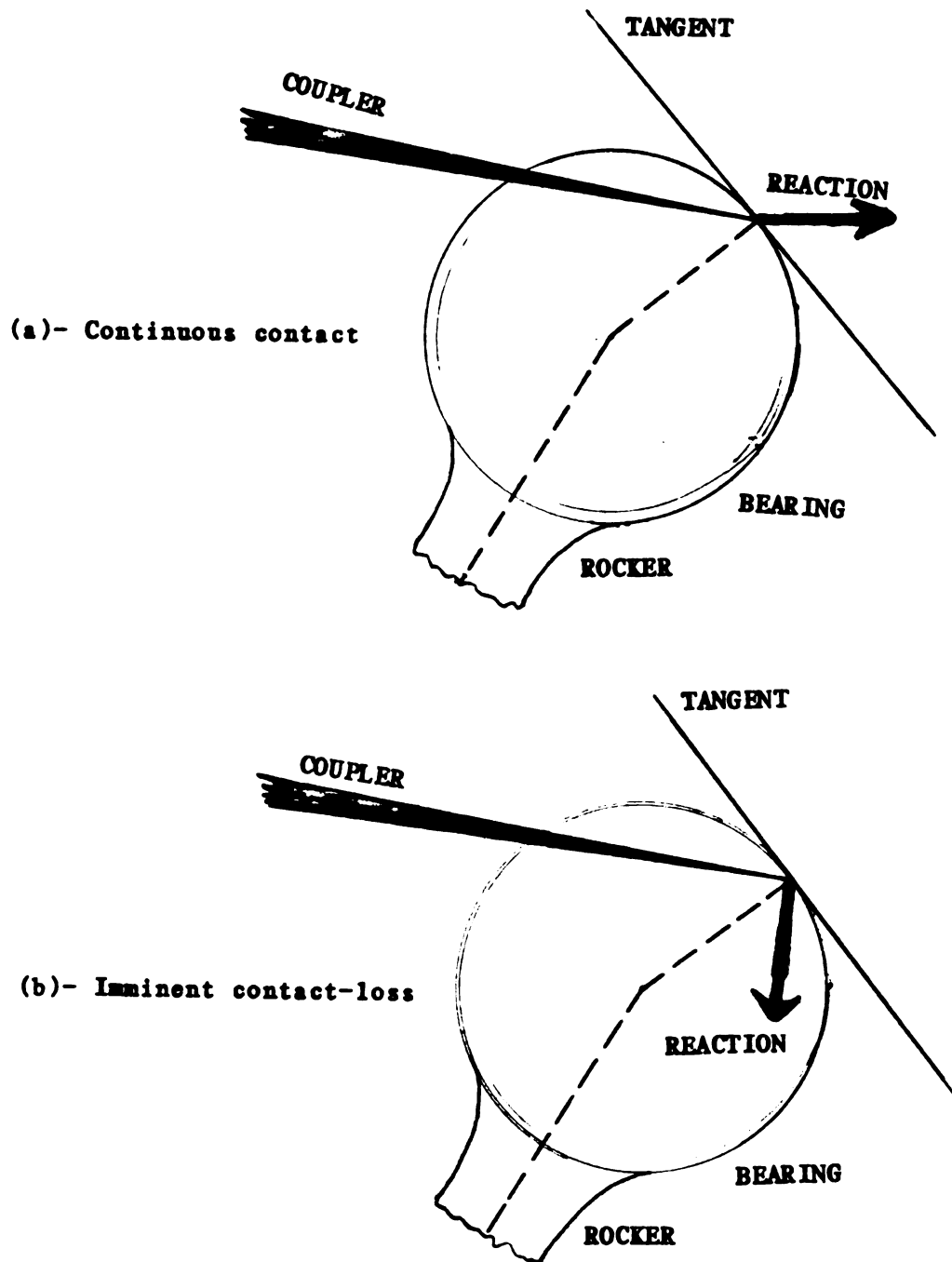
FIGURE 3.4. COUPLER-ROCKER BEARING

between the pin and the bushing, while Figure (3.4b) illustrates the imminent occurence of contact-loss in the bearing at some later time. In a sense, these two figures depict the clearance link as being in compression (contact) and tension (contact-loss), respectively. In other words, if the bearing reaction, F, is in a direction such that the clearance link would acquire an acceleration directed towards the center of the bearing, then the bearing components would seperate and lose contact (fig. 3.4b). On the other hand, so long as the direction of the acceleration is inclined towards the 'outside' of the bearing, it implies that the pin is pressing against the bushing, indicating a continuous contact between the two (fig. 3.4a).

The second method detects the occurence of the contact-loss by sensing the magnitude of the bearing reaction. That is, contact is lost if the magnitude of this force drops to small values in the neighborhood of zero, indicating that contact-loss is imminent. This method acts as a complimentary sensor to the first one and has been developed in order to compensate for the precision errors generated during the numerical solution of the equations of motion.

Once contact has been lost between the pin and the bushing, the system no longer abides by the equations of motion developed for the following mode. At this point the mechanism enters the second mode, called the free-flight mode, which is discussed in the next chapter.

CHAPTER FOUR

THE FREE-FLIGHT MODE

Once the criterion for contact-loss has been met, the pin in the coupler-rocker bearing seperates from the bushing, and the mechanism enters the free-flight mode. Unlike the following mode, the system does not act as an integrated mechanism in this mode, but rather as two independent systems (fig. 4.1) with specific boundary conditions and constraint equations. The crank and coupler represent a compound pendulum, while the rocker, which is seperated from the coupler, represents a simple pendulum. As suggested by Mansour et. al. [5-7], to find the governing equations of motion of these two pendulums a Newtonian approach appears more attractive than the Lagrangian method, since there are less number of unknowns in this mode than in the following mode. Note that the only assumption made at this stage is that the driving torque acting on the crank is ignored in order to reduce the degree of indeterminacy of the compound pendulum, and make
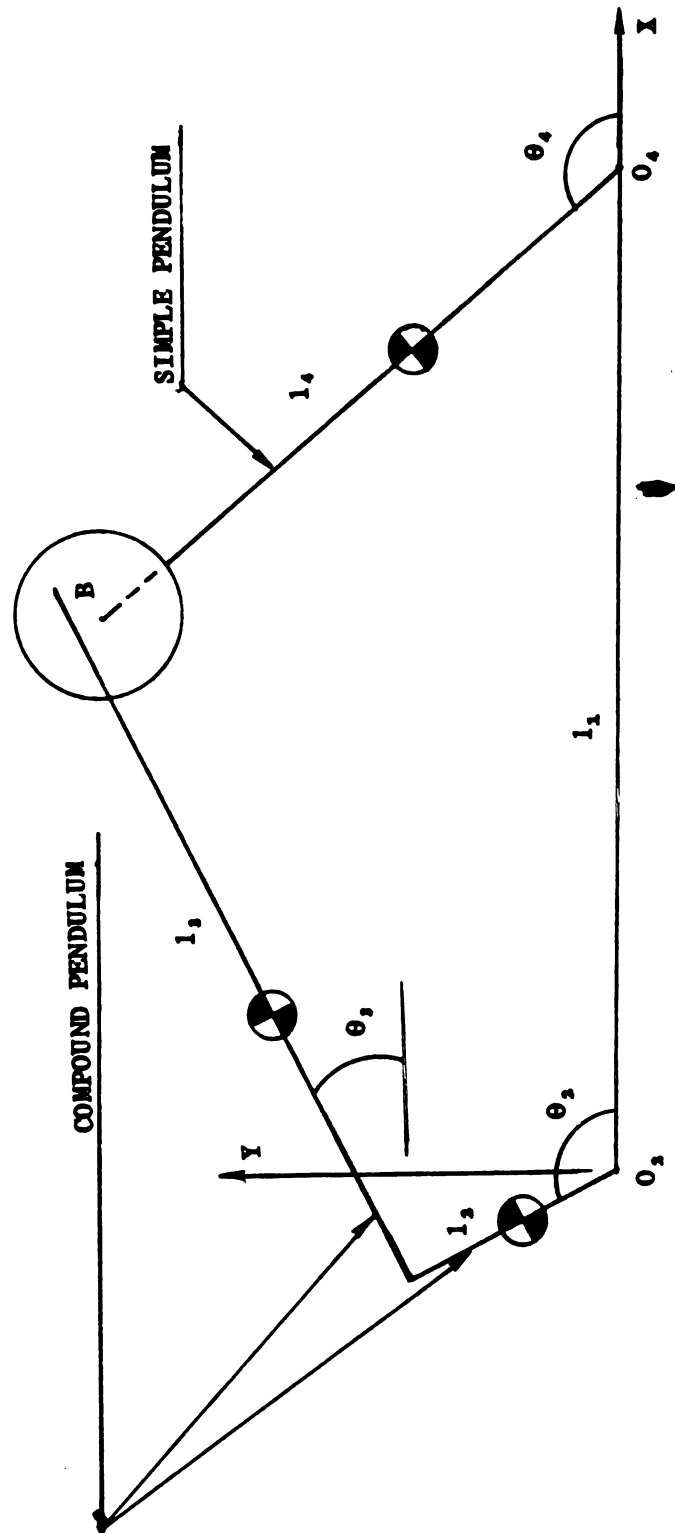
FIGURE 4.1. MECHANISM IN THE FREE-FLIGHT MODE

it possible to find the remaining unknown parameters. However, the assumption of the crank having constant angular velocity still prevails.

4.1- Compound pendulum (crank and coupler)

Figure (4.2) shows the crank and coupler in an integrated manner along with the pertaining notation. Figure (4.3) shows a free-body diagram of the crank. Writing the two equations of motion in the X- and Y-direction yields

$$\sum F_X = m_2 a_X$$

$$F_X - R_X = m_2 a_X \qquad (4.1-1)$$

where a_X is the absolute acceleration of the mass center of the crank in the X-direction. But,

$$a_X = a_n \sin\beta = S_2 \omega_2^2 \sin(\theta_2 - \pi/2)$$

or

$$a_X = -S_2 \omega_2^2 \cos\theta_2 \qquad (4.1-2)$$

where, hereafter, subscripts n and t denote the components in the
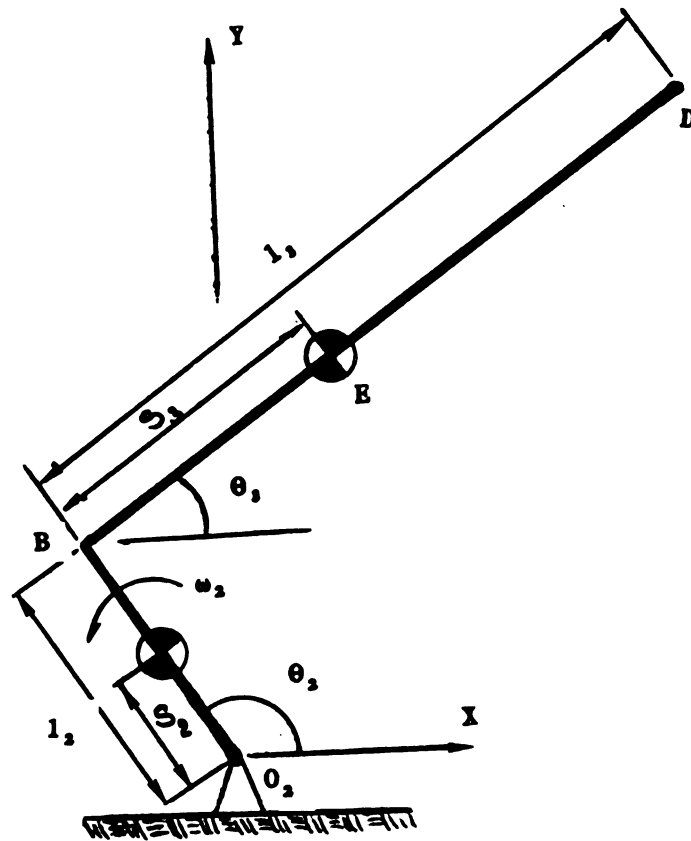
FIGURE 4.2. COMPOUND PENDULUM (CRANK AND COUPLER)

positive normal and tangential directions, respectively. Combining equations (4.1-1) and (4.1-2) yield

$$f_x - R_x = -m_2 S_2 \omega_2^2 \cos\theta_2 \qquad (4.1-3)$$

also

$$\sum F_y = m_2 a_y$$

$$F_y - R_y - m_2 g = m_2 a_y \qquad (4.1-4)$$

and

$$a_y = -a_n \cos\beta = -S_2 \omega_2^2 \cos(\theta_2 - \pi/2)$$

or

$$a_y = -S_2 \omega_2^2 \sin\theta_2 \qquad (4.1-5)$$

Combining (4.1-4) and (4.1-5) results in

$$F_y - R_y = m_2(g + S_2 \omega_2^2 \sin\theta_2) \qquad (4.1-6)$$

Taking moments about the pivot point A (fig. 4.3)

$$\sum M_A = I_{A_2} \alpha_2 = 0$$

since $\alpha_2 = 0$
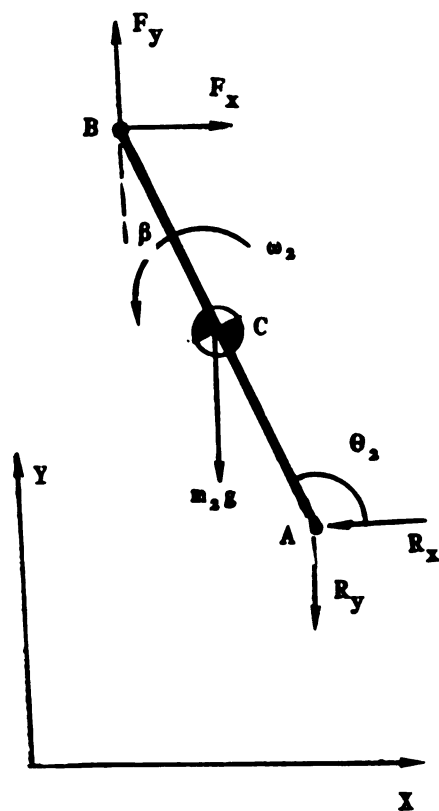
FIGURE 4.3.   CRANK FREE-BODY DIAGRAM

Note that I_{i_j} denotes the mass moment of inertia of link j about point i. Hence,

$$-F_x 1_2 \sin\theta_2 + F_y 1_2 \cos\theta_2 = m_2 g S_2 \cos\theta_2 \qquad (4.1-7)$$

Equations (4.1-3), and (4.1-6), and (4.1-7) are such that all the terms on the left hand sides are unknowns, and, the ones on the right hand side are known.

Figure (4.4) is a free-body diagram of the coupler. Again, applying the first two Newton's equations results in

$$\sum F_x = m_3 a_{E_x}$$

or

$$-F_x = m_3 a_{E_x} \qquad (4.1-8)$$

and

$$\sum F_y = m_3 a_{E_y}$$

or

$$F_y = -m_3 (a_{E_y} + g) \qquad (4.1-9)$$

Applying the moment law about point A for this link yields
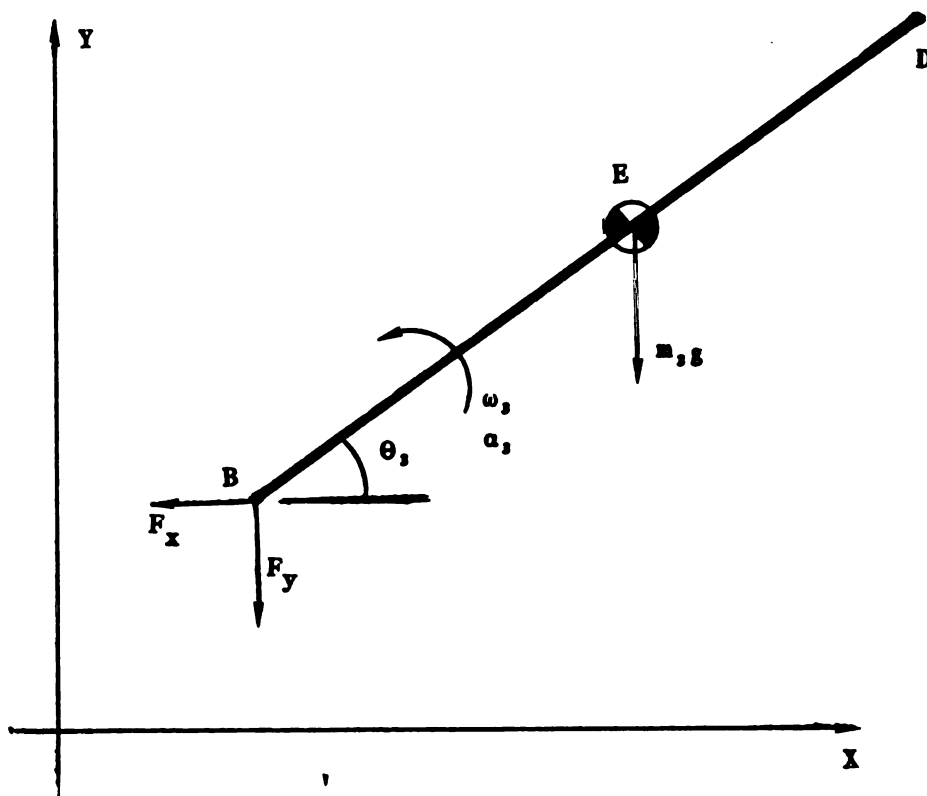
FIGURE 4.4. COUPLER FREE-BODY DIAGRAM

$$\sum M_E = I_{E_3} \alpha_3$$

or

$$F_y S_3 \cos\theta_3 - F_x S_3 \sin\theta_3 = I_{E_3} \alpha_3 \qquad (4.1\text{-}10)$$

However, in equations (4.1-8) to (4.1-10), the X- and Y-components of the linear acceleration of the mass center, point E, of the coupler, a_{E_x} and a_{E_y} respectively, and the angular acceleration of the coupler link, α_3, along with the forces F_x and F_y are unknown. The absolute acceleration of the mass center can be written in vector form using the laws of non-inertial reference frames [73,74]. Thus,

$$\bar{a}_E = \bar{a}_B + \bar{a}_{E/B} \qquad (4.1\text{-}11)$$

where $\bar{a}_{i/j}$ denotes the acceleration of point i relative to point j. Decomposition of (4.1-11) into its X- and Y-components yields

$$a_{E_x} = a_{B_x} + a_{E/B_x} \qquad (4.1\text{-}12a)$$

$$a_{E_y} = a_{B_y} + a_{E/B_y} \qquad (4.1\text{-}12b)$$

But

$$a_{B_x} = -l_2 \omega_2^2 \cos\theta_2 \qquad (4.1\text{-}13a)$$

$$a_{B_y} = -l_2 \omega_2^2 \sin\theta_2 \qquad (4.1\text{-}13b)$$

also

$$a_{E/B_x} = -a_{E_n}\cos\theta_3 - a_{E_t}\sin\theta_3 \qquad (4.1\text{-}14a)$$

$$a_{E/B_y} = -a_{E_n}\sin\theta_3 + a_{E_t}\cos\theta_3 \qquad (4.1\text{-}14b)$$

where

$$a_{E_n} = S_3\omega_3^2 \qquad (4.1\text{-}15a)$$

$$a_{E_t} = S_3\alpha_3 \qquad (4.1\text{-}15b)$$

Combining equations (4.1-12) to (4.1-15) yields

$$a_{E_x} = -l_2\omega_2^2\cos\theta_2 - S_3\omega_3^2\cos\theta_3 - S_3\alpha_3\sin\theta_3 \qquad (4.1\text{-}16)$$

and

$$a_{E_y} = -l_2\omega_2^2\sin\theta_2 - S_3\omega_3^2\sin\theta_3 + S_3\alpha_3\cos\theta_3 \qquad (4.1\text{-}17)$$

Hence, there are six unknowns, namely, F_x, F_y, R_x, R_y, ω_3, and α_3. The six equations needed to find these unknowns are (4.1-3), (4.1-6), (4.1-7), (4.1-10), (4.1-8), and (4.1-9), where in the latter two equations, the acceleration components a_{E_x} and a_{E_y} have been replaced by equations (4.1-16) and (4.1-17), respectively.

For ease of reference, these six equations are rearranged and written in the following

$$F_x - R_x = -m_3 S_3 \omega_3{}^2 \cos\theta_3 \qquad (4.1-18a)$$

$$F_y - R_y = m_3(g + S_3 \omega_3{}^2 \sin\tau_3) \qquad (4.1-18b)$$

$$F_x l_2 \sin\theta_3 - F_y l_2 \cos\theta_3 = -m_3 g S_3 \cos\theta_3 \qquad (4.1-18c)$$

$$-m_3 S_3 \sin\theta_3 \alpha_3 - m_3 S_3 \cos\theta_3 \omega_3{}^2 + F_x = m_3 l_{12} \omega_2{}^2 \cos\theta_2 \qquad (4.1-18d)$$

$$m_3 S_3 \cos\theta_3 \alpha_3 - m_3 S_3 \sin\theta_3 \omega_3{}^2 + F_y = m_3(l_2 \omega_2{}^2 \sin\theta_2 + g) \qquad (4.1-18e)$$

$$I_{E_3} \alpha_3 + F_x S_3 \sin\theta_3 - F_y S_3 \cos\theta_3 = 0 \qquad (4.1-18f)$$

Equations (4.1-18c) to (4.1-18f) can be solved simultaneously and independent of the first two, and then, (4.1-18a) and (4.1-18b) can be solved for R_x and R_y seperately. Writing the last four equations of (4.1-18) in a matrix form we have

$$[A]\{ X \} = \{ B \} \qquad (4.1-19)$$

where matrix [A] is

$$
\begin{bmatrix}
0 & 0 & l_2\sin\theta_3 & -l_2\cos\theta_3 \\
-m_3 S_3 \sin\theta_3 & -m_3 S_3 \cos\theta_3 & 1 & 0 \\
m_3 S_3 \cos\theta_3 & -m_3 S_3 \sin\theta_3 & 0 & 1 \\
I_{E_3} & 0 & S_3\sin\theta_3 & -S_3\cos\theta_3
\end{bmatrix}
$$

and, vector $\{ X \}$ is

$$
\begin{bmatrix}
\alpha_3 \\
\omega_3{}^2 \\
F_x \\
F_y
\end{bmatrix}
$$

and where vector $\{ B \}$ is

$$
\begin{bmatrix}
-m_3 g S_3 \cos\theta_3 \\
m_3 l_2 \omega_2{}^2 \cos\theta_2 \\
m_3 (l_2 \omega_2{}^2 \sin\theta_2 + g) \\
0
\end{bmatrix}
$$

Solving the matrix equation (4.1-19) yields the angular acceleration of the coupler as

$$
\alpha_3 = (m_3 S_3 / I_{E_3})[l_2 \omega_2{}^2 \sin(\theta_2-\theta_3)-g\cos\theta_3] \tag{4.1-20}
$$

The expression for other unknowns in (4.1-19) have been omitted here, and will be stated later as deemed necessary.

4.2- Simple Pendulum (rocker)

Figure (4.5) illustrates the rocker as a simple pendulum. The task of finding the angular acceleration of this link is less tedious than the case of the compound pendulum, and since it only involves taking the moments about point O_4 (fig. 4.5)

$$\sum M_{O_4} = I_{O_4} \alpha_4$$

or

$$\alpha_4 = -(m_4 S_4 / I_{O_4}) g \cdot \cos \theta_4 \qquad\qquad (4.2\text{-}1)$$

Hence, at this stage, the two required governing equations of motion, equations (4.1-20) and (4.2-1), of the four bar linkage which define the behavior of the system in the free-flight mode are obtained. These equations may be solved and integrated numerically using a digital computer, and other system parameters can be computed at any time once these two equations are solved.

4.3- Initial Conditions

As previously mentioned, the equations of motion of the free-flight mode are to be integrated numerically. Hence, some initial values are needed to start the iteration. Suppose at time $t=0$ the simulation starts with the mechanism assumed to be in the follow-
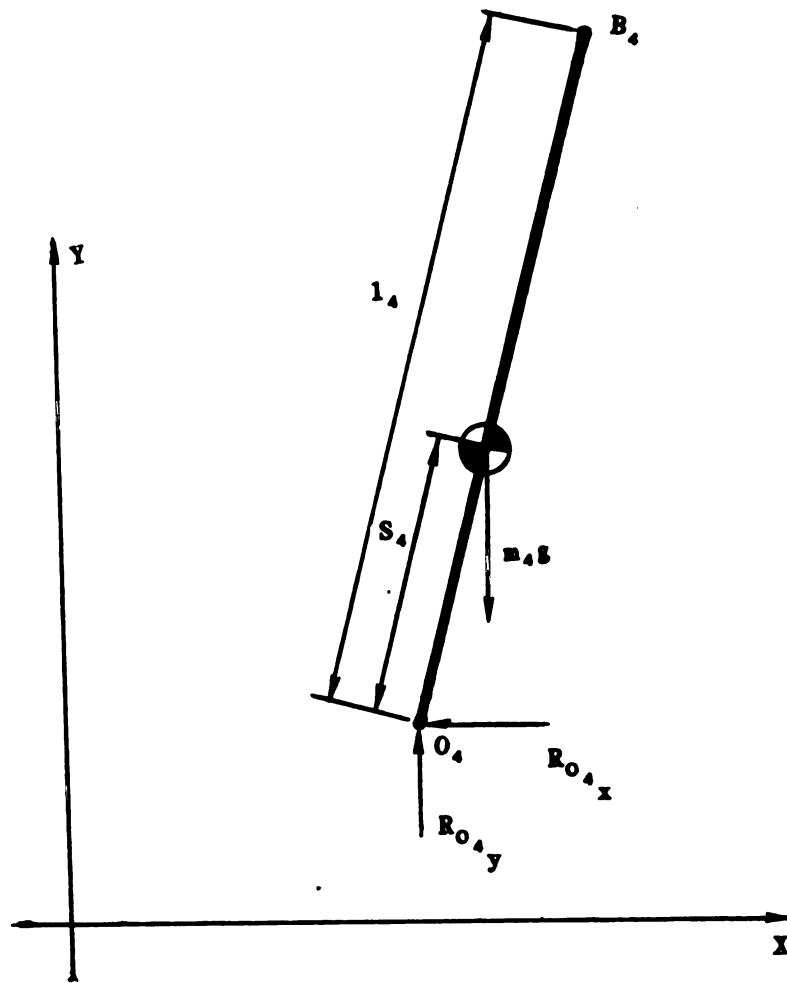
FIGURE 4.5. ROCKER FREE-BODY DIAGRAM

ing mode. If at time $t=t_1$ the pin and the bushing seperation phase has reached (refer to section 3.5), and the system enters the free-flight mode, then the initial values taken for the equations of motion of this mode are the corresponding values of the parameters in the following mode just prior to contact-loss. If the mesh size of iteration is small enough, the magnitude of the error tends to become negligible and does not enter the simulation results as a propagation error.

4.4- Termination of the Free-Flight Mode

The interval of time during which the mechanism is in the free-flight mode is finite and bounded. The lower bound of this interval is marked by the occurence of the contact-loss in the coupler-rocker bearing. Then, as time progresses, the pin travels along a trajectory path within the bushing until it collides with the bushing at some point in time, which is an indication of the termination of the free-flight mode. The extent of time-lapse for the duration of this mode is not fixed but depends on the relative location of the pin and the bushing, and in addition, on the kinematics of the two components of the bearing at the instant of contact-loss.

Once the pin is travelling inside the bearing housing in the free-flight mode, it is not constrained to move along a path prescribed by the inner surface of the bushing, as is the case in the following mode. Hence, the distance between the pin and the center of

the bushing, which was taken as the length of the clearance link in the following mode, becomes less than the actual clearance size of the bearing. Thus, the optimum method to ensure the prompt detection of the collision of the pin and the bushing is to monitor the distance between the pin and the center of the bushing. When this distance equals the clearance size of the bearing, it is an indication of the collision of the two surfaces, hence the termination of the free-flight mode.

Such a task can be performed on a digital computer by making use of the loop closure equation of the mechanism after each step of iteration. Figure (4.6) shows the mechanism in the free-flight mode whose loop closure equation in vector form can be written as

$$\bar{l}_2 + \bar{l}_3 + \bar{\Omega} = \bar{l}_1 + \bar{l}_4 \qquad (4.4\text{-}1)$$

where $\bar{\Omega}$ is the vector extended from the pin to the center of the bushing. Decomposing (4.4-1) into its real and imaginary components, and rearranging yields

$$-\Omega\cos\alpha = l_2\cos\theta_2 + l_3\cos\theta_3 - l_1 - l_4\cos\theta_4 \qquad (4.4\text{-}2a)$$

$$-\Omega\sin\alpha = l_2\sin\theta_2 + l_3\sin\theta_3 - l_4\sin\theta_4 \qquad (4.4\text{-}2b)$$

where α denotes the angular displacement of the vector $\bar{\Omega}$. Squaring
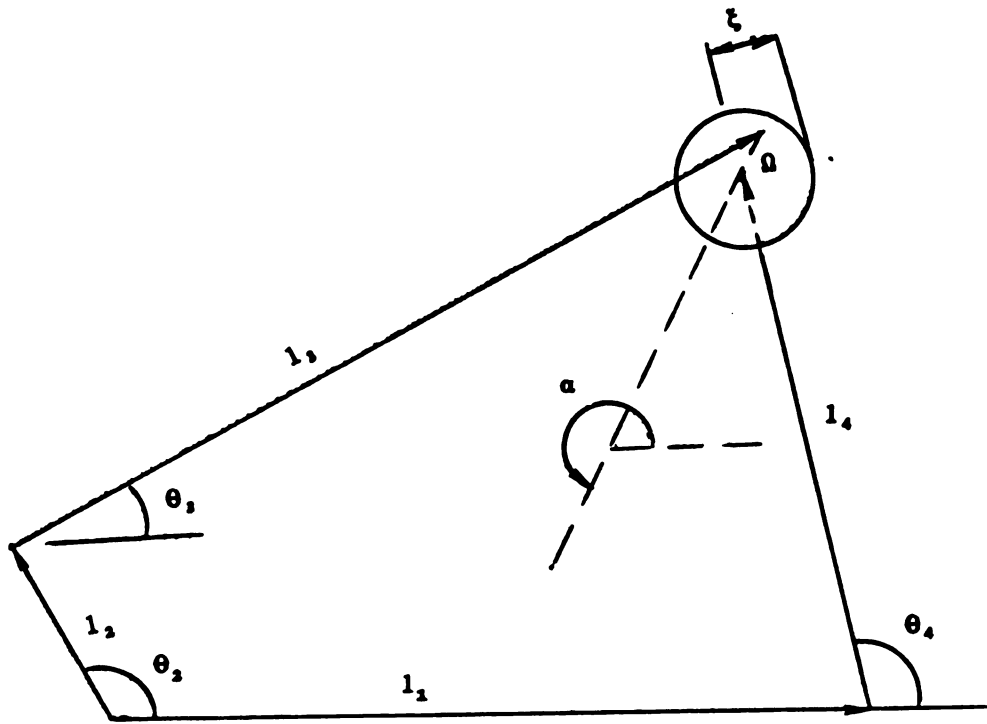
FIGURE 4.6. VECTOR PRESENTATION OF THE FREE-FLIGHT MODE

and adding equations (4.4-2) results in

$$\Omega^2=(l_2\cos\Theta_2+l_3\cos\Theta_3-l_1-l_4\cos\Theta_4)^2+(l_2\sin\Theta_2+l_3\sin\Theta_3-l_4\sin\Theta_4)^2$$

(4.4-3)

If the clearance size in the bearing is denoted by ξ , then the collision between the pin and the bushing occurs at the instant of time when

$$\Omega=\xi \quad \text{or} \quad \Omega^2=\xi^2 \qquad (4.4-4)$$

Hence, from equations (4.4-3) and (4.4-4) it can be deduced that the constraint equation for the free-flight mode can be expressed as

$$\Omega^2<\xi^2$$

or

$$(l_2\cos\Theta_2+l_3\cos\Theta_3-l_1-l_4\cos\Theta_4)^2+(l_2\sin\Theta_2+l_3\sin\Theta_3-l_4\sin\Theta_4)^2<\xi^2$$

(4.4-5)

In other words, the free-flight mode is terminated once the inequality (4.4-5) is violated. At this point the mechanism enters the third mode, namely, the impact mode, which is discussed in the next chapter.

CHAPTER FIVE

THE IMPACT MODE

The termination of the free-flight mode triggers the initiation of the third mode, namely, the impact mode. As previously mentioned in chapter one, a great deal of literature is available on the subject of impacts in the bearings with clearances and some related areas. According to Mansour [5], some of the analytical research carried out in the past [3,44,75-77] considered the idealization of the contacting surfaces by linear and nonlinear springs and dashpots. Veluswami, Crossley, and Horvay [78] showed experimentally that the dynamic behavior, the impact pattern, and the time of contact of impacting surfaces constitute a complex function of initial conditions, approaching velocities of the colliding surfaces, and the size of the clearance in the bearing. Mansour and Townsend [6,7] developed a different model which did not use the spring-dashpot approach. It was built around the momentum-exchange principles for impacting pairs.

This is the method that will be adapted here. In this method, instead of following the rather difficult traditional path of trying to define the force-time history during the impact, the total area under that curve is evaluated. This area, which is essentially the impulse associated with the impact, is all that is needed to determine the subsequent motion of impacting pair. This approach bypasses many unsettled issues regarding the exact nature of the stiffnesses of the contacting surfaces, and its dependence on the actual contact time. It also enables one to account for the actual geometry of the joint as well as for the surface roughness. These are what constitute the set of parameters which were difficult to handle by the previous approaches.

However, the primary difference between the work presented here, and Mansour's investigation is that, he has modeled the mechanism as being in only two modes of free-flight and impact mode, and does not take into account the intervals of time when the pin and the bushing of the bearing with clearance are in continuous contact. This deficiency is eliminated here by augmenting the third mode, or the following mode, to the first two modes, hence encompassing all the possible configurations the mechanism can acquire.

5.1- Governing Equations of Motion

Figure (5.1) depicts the four-bar linkage at the instant of impact, along with its corresponding notation. This notation will be
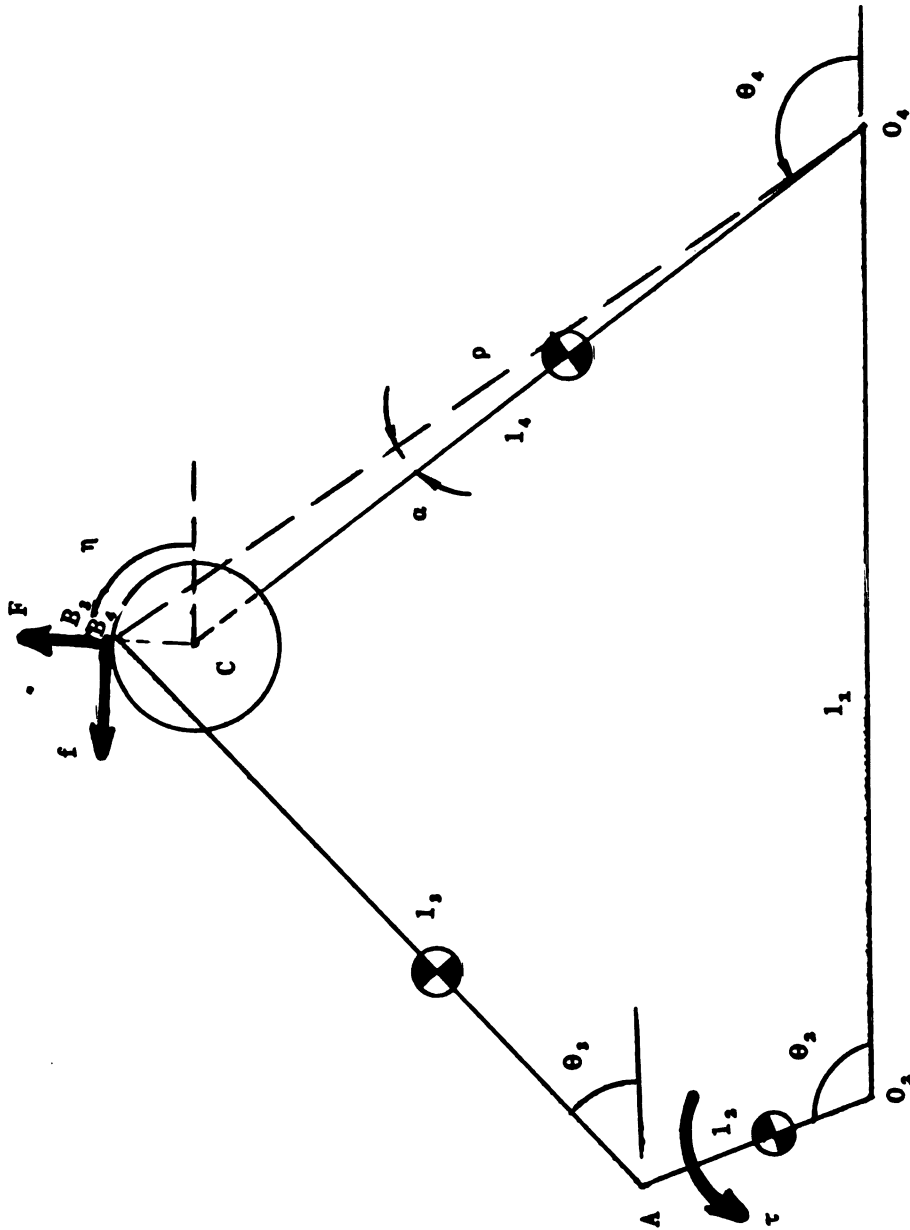
FIGURE 5.1. MECHANISM IN THE IMPACT MODE

clarified during the course of the derivation of the equations of motion.

As discussed in the preceding chapter (section 4.4), impact occurs when the following condition is violated

$$\mu_1^2 + \mu_2^2 < \zeta^2 \qquad\qquad (5.1\text{-}1)$$

where

$$\mu_1 = l_2\cos\theta_2 + l_3\cos\theta_3 - l_1 - l_4\cos\theta_4 \qquad\qquad (5.1\text{-}2a)$$

$$\mu_2 = l_2\sin\theta_2 + l_3\sin\theta_3 - l_4\sin\theta_4 \qquad\qquad (5.1\text{-}2b)$$

and where ζ is the size of the clearance.

Dubowsky and Freudenstein [76] estimated that the duration of the impact of a typical pin-connection is in the neighborhood of 10^{-4} seconds. This time is associated with about one degree-displacement for the driving link with operating speed of 2000 RPM or about 209 radians per second. Consequently, one can consider that the configuration of the mechanism is hardly changing during an impact with that speed.

Contact between the pin and the bushing at impact occurs at a clearance link's angle of η (fig. 5.2) given by the relation
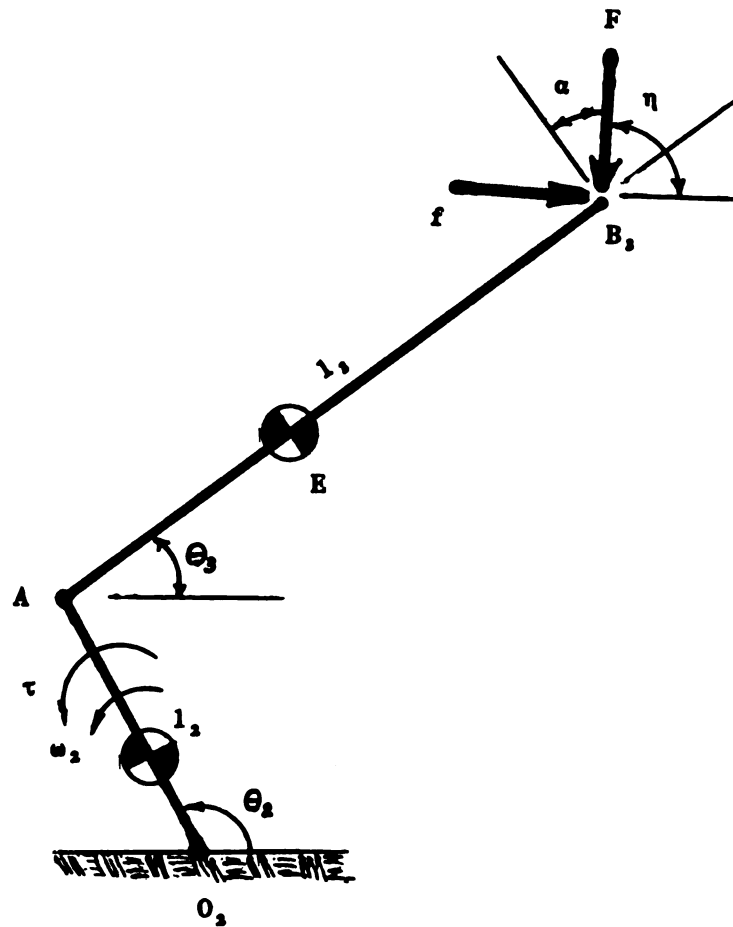
FIGURE 5.2. CRANK AND COUPLER LINKS AT IMPACT

$$\tan\eta = \mu_2/\mu_1 \tag{5.1-3}$$

where μ_1 and μ_2 are given in equations (5.1-2).

In what follows, the superscript (+) indicates a variable after impact. The principle of angular impulse-momentum [73] can be stated as

$$\int \sum \bar{M}_0 dt = \bar{H}_{0_2} - \bar{H}_{0_1} \tag{5.1-4}$$

where the integral in the above equation, which is vector form, is from t_1 to t_2, which is the duration of the impact, and denotes the angular momentum of the system, and the right hand side is merely the change in the angular impulse of the mechanism about a point O . The vector $\bar{H}_0$ indicates the angular momentum about point O . If point O is the mass center of the system, then

$$H_0 = I\omega \tag{5.1-5}$$

where I is the mass moment of inertia of the body about the mass center, and ω is the angular velocity of the body. However, if point O is different from the mass center, then

$$H_0 = I\omega + mVd \tag{5.1-6}$$

where m is the mass, V the linear velocity of the mass center, and d is the distance from point 0 to the mass center.

5.1.1- Equation of Motion for Crank

Figure (5.2) shows a free-body diagram of the crank and coupler at the instant of impact. Rewriting equation (5.1-1) for pivot O_2 we have

$$\int_t \sum M_{O_2} dt = (H_{O_2})_2 - (H_{O_2})_1 \tag{5.1.1-1}$$

where the integration interval on time, t, is from t_1 to t_2, and where subscripts 1 and 2 on H_{O_2} denote the variable at times t_1 and t_2, respectively. Also, for convenience, the vector notation has been omitted without loss of correctness since the equation is written for only one dimension at a time. Keeping in mind that the angular acceleration of the crank is zero at all times, the following expression may be derived

$$(H_{O_2})_1 = (I\omega_2 + m_2 V_2 S_2)_1 \tag{5.1.1-2}$$

and

$$(H_{O_2})_2 = (I\omega_2 + m_2 V_2 S_2)_2 \qquad\qquad (5.1.1-3)$$

The linear and angular velocity terms in equations (5.1.1-2) and (5.1.1-3) are unchanged before and after impact. Thus, the right hand sides of the above two equations are equal . This implies that the angular momentum of the crank is conserved and remains constant. Hence, the magnitude of angular impulse on this link due to the impact in the coupler-rocker bearing is zero. Consequently, the equations corresponding to this link can be omitted altogether from the remainder of the analysis.

5.1.2- Equations of Motion for the Coupler

Application of the angular impulse-momentum equation (5.1-1) to point A of the coupler (fig.5.2) yields

$$\int \sum M_A dt = (H_A)_2 - (H_A)_1 \qquad\qquad (5.1.2-1)$$

From here on, the limits of integration on all the integrals are eliminated, keeping in mind that the limits are for the duration of the impact, from t_1 to t_2. If F_n anf F_t (not shown on the figure) are forces in the normal and tangential directions with respect to the direction of approach, which are exerted on the pin at the end of the coupler at impact, respectively, then the moment of all forces acting on the coupler about point A can be written as

$$\sum M_A = -l_3 F_n \cos\alpha - l_3 F_t \cos(\pi/2-\alpha)$$

or

$$\sum M_A = -l_3 F_n \sin(\eta-\Theta_s) - l_3 F_t \cos(\eta-\Theta_s) \qquad (5.1.2-2)$$

Note that (5.1.2-2) is written for the general case, in the sense that F_n represents the force due to the collision of the approaching surfaces in the normal direction, and F_t indicates the force in the tangential direction due to the generation of friction between the two contacting surfaces at the time of impact.

Integrating equation (5.1.2-2) with respect to time from t_1 to t_2, which is the duration of impact, yields

$$\int \sum M_A dt = -\int l_3 F_n \sin(\eta-\Theta_s) dt - \int l_3 F_t \cos(\eta-\Theta_s) dt$$

$$(5.1.2-3)$$

As discussed in section (5.1), the configuration of the mechanism hardly changes during impact. This implies that the angular displacements can be assumed constant. Thus, taking the invariant parameters in equation (5.1.2-3) outside of the integrals on the right hand side results in

$$\int \sum M_A dt = -1_s \sin(\eta - \Theta_s) \int F_n dt - 1_s \cos(\eta - \Theta_s) \int F_t dt$$

$$(5.1.2-4)$$

The integrals on the right hand side of (5.1.2-4) are but expressions for the 'impulses' in the normal and tangential directions of the bushing, respectively. From here on, the normal impulse will be denoted by F, and the tangential impulse by f , i.e.,

$$F = \int F_n dt \qquad ; \qquad f = \int F_t dt \qquad (5.1.2-5)$$

Note that F and f are vector quantities as shown in Figure (5.1), that have the dimensions of FORCE x TIME. They will be refered to in this study as impulsive forces for ease of identification. The impulsive reactions at the bearings are also defined as the time integrals of the large reactions at the bearings during impact. Similarly, τ denotes the time integral of the large torque acting on the crank from time t_1 to t_2. It is referred to as the impulsive torque with the dimensions of FORCE x LENGTH x TIME.

Substitution of equation (5.1.2-5) into (5.1.2-4) yields the expression for the total impulse on the coupler, i.e.,

$$\int \sum M_A dt = -1_s F \sin(\eta - \Theta_s) - 1_s f \cos(\eta - \Theta_s) \qquad (5.1.2-6)$$

The angular momentum of the coupler link about point A (fig.

5.2) can be written as

$$H_{A_3} = I_{E_3}\omega_3 + m_3 V_{E_3} S_3 \qquad (5.1.2-7)$$

where V_{E_3} is the linear velocity of the mass center, E, of the coupler relative to point A. Noting that

$$V_{E_3} = S_3 \omega_3$$

equation (5.1.2-7) becomes

$$H_{A_3} = I_{E_3}\omega_3 + m_3 S_3^2 \omega_3$$

$$= I_{A_3}\omega_3 \qquad (5.1.2-8)$$

Hence, the change in angular momentum of the coupler during impact becomes

$$\Delta H_{A_3} = (H_{A_3})_2 - (H_{A_3})_1 \qquad (5.1.2-9)$$

$$\Delta H_{A_3} = I_{A_3}(\omega_3^+ - \omega_3) \qquad (5.1.2-10)$$

Substitution of equations (5.1.2-6), (5.1.2-9), and (5.1.2-10) into (5.1.2-1) yields

$$-1_3 F \sin(\eta - \Theta_3) - 1_3 f \cos(\eta - \Theta_3 = I_{A_3}(\omega_3^+ - \omega_3) \qquad (5.1.2-11)$$

which is the desired angular impulse-momentum equation for the coupler.

5.1.3- Equtions of Motion for the Rocker

Figure (5.3) depicts a diagram of the rocker at the time of impact, with corresponding normal, F, and tangential, f, impulses acting on the bushing. Using a similar argument as in the derivation of equation (5.1.2-10), the change in the angular momentum of the rocker about the pivot O_4 can be written as

$$H_{O_4} = I_{O_4} \omega_4 \qquad (5.1.3-1)$$

and the change in angular momentum becomes

$$\Delta H_{O_4} = (H_{O_4})_2 - (H_{O_4})_1$$

or

$$\Delta H_{O_4} = I_{O_4}(\omega_4^+ - \omega_4) \qquad (5.1.3-2)$$

Since the change in the angular momentum is with respect to point O_4, the angular impulse should also be expressed about the same point.
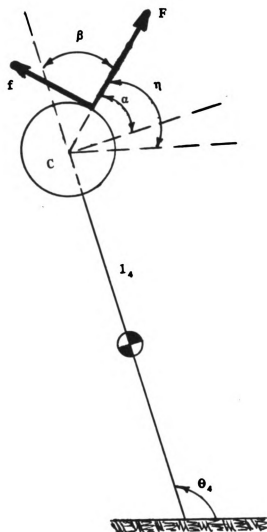
FIGURE 5.3. ROCKER LINK AT IMPACT

Taking moments about point O_4 yields

$$\sum M_{O_4} = -F_n l_4 \cos(\pi/2 - \Theta_4 + \eta) + F_t [l_4 \cos(\Theta_4 - \eta) + \xi]$$

(5.1.3-3)

where, again, F_n and F_t (not shown on the figure), are the impact forces whose corresponding integrals with respect to time yield the impulses F and f, respectively.

Integrating (5.1.3-3) with respect to time gives

$$\int \sum M_{O_4} dt = -\int F_n l_4 \cos(p/2 - \Theta_4 + \eta) dt + \int F_t [l_4 \cos(\Theta_4 - \eta) + \xi] dt$$

(5.1.3-4)

and since the angular displacements remain constant, equation (5.1.3-4) becomes

$$\int \sum M_{O_4} dt = -l_4 \cos(\pi/2 - \Theta_4 + \eta) \int F_n dt + [l_4 \cos(\Theta_4 - \eta) + \xi] \int F_t dt$$

(5.1.3-5)

Substituting equation (5.1.2-5) into (5.1.3-5) yields

$$\int \sum m_{0_4} dt = -Fl_4 \cos(\pi/2 - \Theta_4 + \eta) + f[l_4 \cos(\Theta_4 - \eta) + \xi]$$

$$(5.1.3-6)$$

Equating (5.1.3-2) and (5.1.3-6) yields

$$Fl_4 \sin(\eta - \Theta_4) + f[l_4 \cos(\eta - \Theta_4) + \xi] = I_{0_4}(\omega_4^+ - \omega_4)$$

$$(5.1.3-7)$$

which is the angular impulse-momentum expression for the rocker link.

A glance at the above equation and equation (5.1.2-11) reveals that these equations contain four unknown parameters. These are the normal and tangential impulses during impact, F and f, and also the angular velocities of the coupler and rocker after impact, ω_3^+ and ω_4^+, respectively. The remaining variables in these relations are quantites that are known from the end values of the preceding free-flight mode. Thus, two more equations are needed in terms of these parameters in order to find the unknowns. These two will be obtained by utilizing the theoretical arguments presented in the following section concerning the coefficient of restitution, and also, the effect of the smoothness of the surfaces of the colliding bodies, namely, the pin and the bushing of the coupler-rocker bearing.

5.2- Coefficient of Restitution, e

The definition of the coefficient of restitution, e, provides the third equation by relating ω_i and ω_i^+, since the values of these parameters as well as the impulses depend on the coefficient of restitution between the pin and the bushing. The parameter e formally relates the normal impulse of the approaching (compression) phase, to that in the receding (rebound) phase in the direction of the line of impact, which is essentially the η direction (Figures 5.2 and 5.3). For an external view of the impacts, an equivalent relation is used in terms of the normal velocities of approach (V_{B_3} and V_{B_4}) before and after impact. Thus, the coefficient of restitution is defined such that

$$V_{B_4}{}_n^+ - V_{B_3}{}_n^+ = e(V_{B_3}{}_n - V_{B_4}{}_n) \qquad (5.2-1)$$

Figure (5.4) on the following page illustrates the crank and coupler at a given configuration just prior to impact, and Figure (5.5) depicts a graphical representation of the velocity vectors of the two links. As can be seen from Figure (5.5) on the next page, the absolute velocity of the coupler end, V_{B_3}, is the vector addition of the crank end absolute linear velocity, V_{A_2}, whose magnitude and direction is $l_2\omega_2$ perpendicular to the crank at point A_2 in the direction of crank rotation, and the linear velocity of point B_3 relative to point A_3, which is directed normal to the coupler at B_3 in the direction of rotation of the coupler, and with magnitude of $l_3\omega_3$.
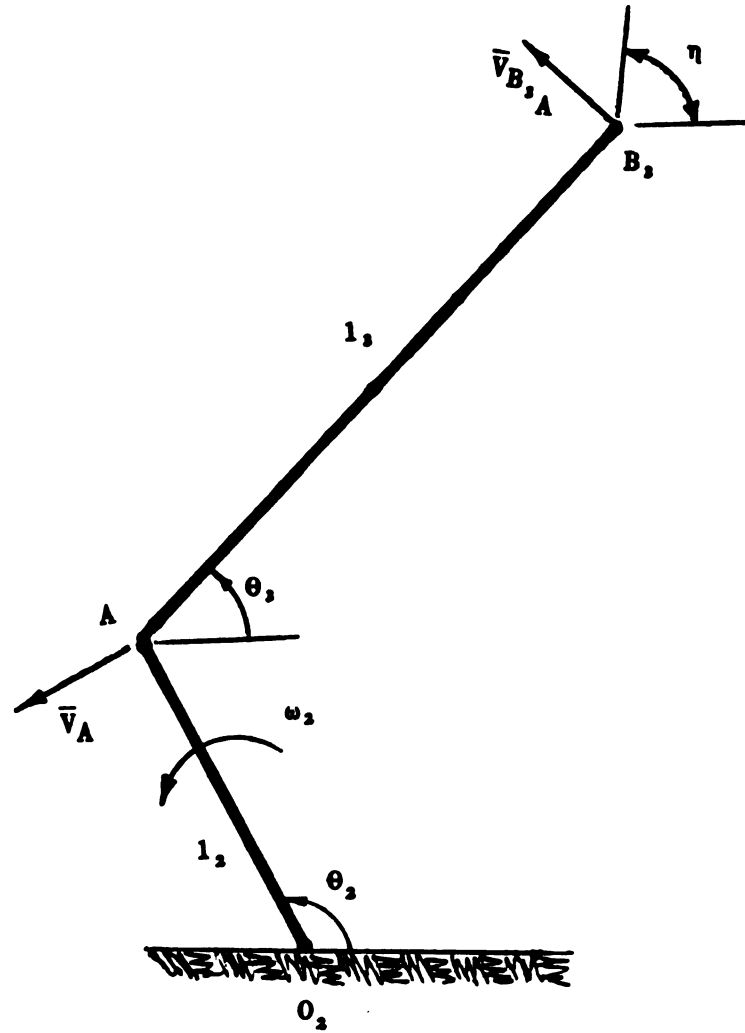
FIGURE 5.5. CRANK AND COUPLER PRIOR TO IMPACT
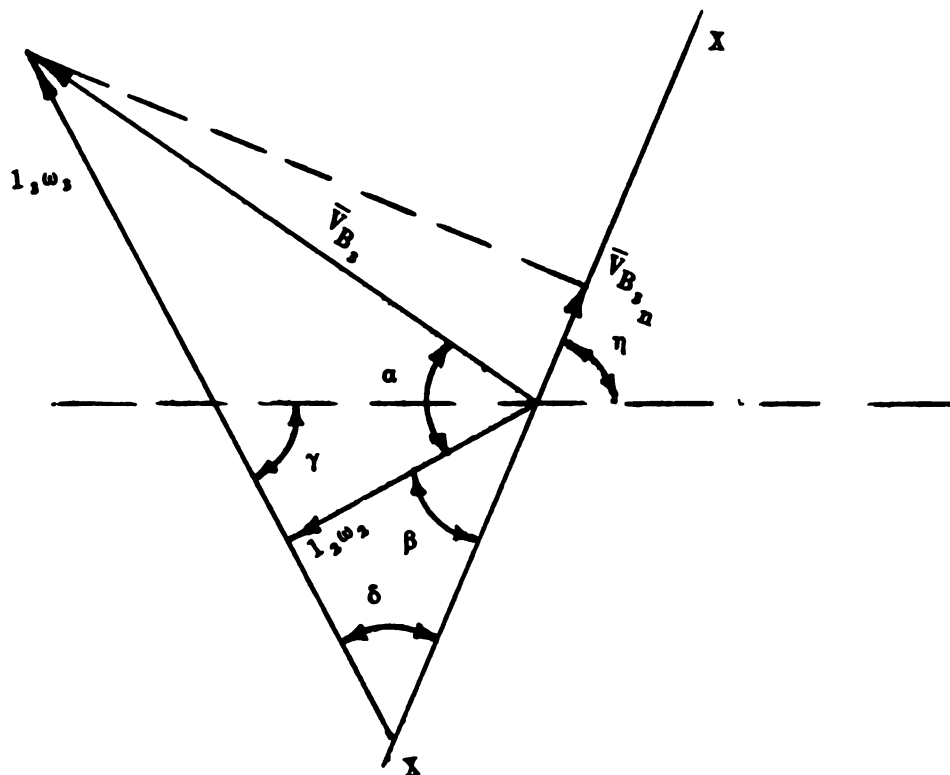
FIGURE 5.5. VECTOR REPRESENTATION OF VELOCITY $V_{B,n}$

Line X-X in Figure (5.5) represents the direction of the normal approach of the pin and the bushing. Thus

$$V_{B_{3_n}} = -l_2\omega_2\cos\beta + l_3\omega_3\cos\delta \qquad (5.2-2)$$

But,

$$\beta = \eta - \alpha$$

$$\alpha = \Theta_2 - \pi/2$$

or

$$\beta = \pi/2 + (\eta - \Theta_2) \qquad (5.2-3a)$$

$$\delta = \pi - (\gamma + \eta)$$

$$\gamma = \pi/2 - \Theta_3$$

or

$$\delta = \pi/2 + (\Theta_3 - \eta) \qquad (5.2-3b)$$

Substituting equations (5.2-3) into (5.2-2) and rearranging yields

$$V_{B_{3_n}} = l_2\omega_2\sin(\eta - \Theta_2) + l_3\omega_3\sin(\eta - \Theta_3) \qquad (5.2-4)$$

Equation (5.2-4) is an expression for the normal velocity of approach of the coupler end.

To find the corresponding equation for the rocker, reference is made to Figure (5.6) on the next page, which depicts the rocker at a given position prior to impact. It should be noted that, l_4, which is assumed as the rocker link with angular displacement Θ_4, spans between point O_4 and the center of the bushing, point C, and, ρ which is an imaginary line with angular displacement γ, extends from the pivot point O_4 to the point of contact of the pin and the bushing, B_4. α is the difference in the angular displacements of l_4 and ρ.

Figure (5.7) is a vector presentation of the absolute velocity of point B_4 at the instant of impact. It is directed perpendicular to ρ, and has a magnitude of $\rho\omega_4$. Line X-X reflects the direction of normal approach of the pin and the bushing, and line Y-Y is the direction of the imaginary line ρ. Hence

$$V_{B_{4_n}} = -V_{B_4}\cos\delta \qquad (5.2-5)$$

or

$$V_{B_{4_n}} = -\rho\omega_4\cos\delta \qquad (5.2-6)$$

But, from Figure (5.7)
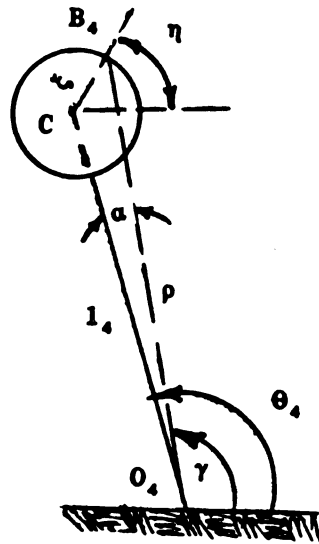
FIGURE 5.6. ROCKER PRIOR TO IMPACT
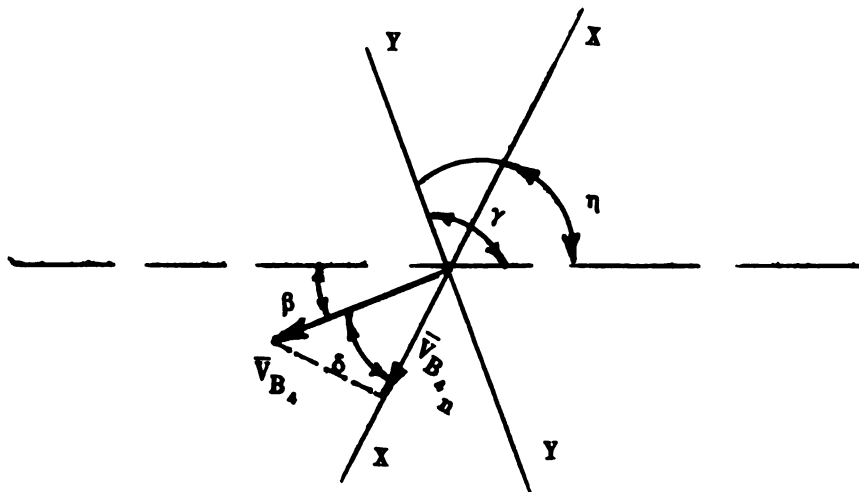
FIGURE 5.7. VECTOR REPRESENTATION OF $\bar{V}_{B_4}$

$$\delta = \pi/2 + (\eta - \gamma) \qquad (5.2\text{-}7a)$$

and

$$\gamma = \theta_4 - \alpha \qquad (5.2\text{-}7b)$$

then

$$\delta = \pi/2 + (\eta - \theta_4 + \alpha) \qquad (5.2\text{-}7c)$$

Substitution of (5.2-7c) into (5.2-6) and rearranging yields

$$V_{B_{4_n}} = \rho \omega_4 \sin(\eta - \theta_4 + \alpha) \qquad (5.2\text{-}8)$$

Angle α can be found using the law of cosines in triangle O_4CB_4, i.e.,

$$\zeta/\sin\alpha = \rho/\sin(\theta_4 - \eta)$$

or

$$\sin\alpha = (\zeta/\rho)\sin(\theta_4 - \eta) \qquad (5.2\text{-}9)$$

The magnitude of ρ can be found by writing the vector loop closure equation for the triangle O_4CB_4 (fig. 5.6), i.e.,

$$\bar{\rho} = \bar{l}_4 + \bar{\zeta} \qquad (5.2\text{-}10)$$

Decomposition of (5.2-10) into its real and imaginary parts yields

$$\rho \sin\alpha = 1_4 \sin\theta_4 + \zeta \sin\eta \qquad (5.2\text{-}11a)$$

$$\rho \cos\alpha = 1_4 \cos\theta_4 + \zeta \cos\eta \qquad (5.2\text{-}11b)$$

Squaring and adding of the resulting expressions yields

$$\rho = [1_4{}^2 + \zeta^2 + 21_4 \zeta \cos(\eta - \theta_4)]^{1/2} \qquad (5.2\text{-}12)$$

Equation (5.2-6) combined with (5.2-9) and (5.2-12) yields an expression for the normal velocity of approach of the rocker. Substitution of equations (5.2-4) and (5.2-6) into (5.2-1) gives

$$-[1_3 \sin(\eta - \theta_3)]\omega_3{}^+ + [\rho \sin(\eta - \theta_4 + \alpha)]\omega_4{}^+ =$$

$$[e1_3 \sin(\eta - \theta_3)]\omega_3 - [\rho e \sin(\eta - \theta_4 + \alpha)]\omega_4 +$$

$$[(1+e)1_2 \sin(\eta - \theta_2)]\omega_2$$

$$(5.2.13)$$

Equation (5.2-13) provides the third relation necessary for finding the unknown parameters in the impact mode.

5.3- Nature of Contact

The fourth amending equation which is required to find the unknowns is furnished by the nature of contact of the colliding surfaces. Three distinct types of contact can occur

i- The SMOOTH case, in which the contacting surfaces offer negligible frictional forces in the tangential direction.

ii- The ROUGH case, where the surfaces are badly worn, and no relative slip can occur in the tangential direction during impact.

iii- The STICK-SLIP case, in which the surfaces offer a Coulomb-type friction in the tangential direction. The coefficient of dry friction, μ_e, is assumed to be constant in this case. It is obvious that, the smooth and rough cases are special instances of the stick-slip case. In other words, when μ_e is set to zero, the result is the smooth case, and when μ_e is assumed extremely large, it becomes identical to the rough case.

The following notation will be employed to simplify the notations

$$\mu_3 = l_3 \sin(\eta - \theta_3) \qquad\qquad (5.3\text{-}1a)$$

$$\mu_4 = l_4 \sin(\eta - \theta_4) \qquad\qquad (5.3\text{-}1b)$$

$$\mu_5 = l_3 \sin(\eta - \theta_3) \qquad\qquad (5.3\text{-}1c)$$

$$\mu_6 = \rho \sin(\eta - \theta_4 + \alpha) \qquad\qquad (5.3\text{-}1d)$$

$$\mu_7 = l_4 \cos(\eta - \theta_3) \tag{5.3-1e}$$

$$\mu_8 = l_4 \cos(\eta - \theta_4 + \zeta) \tag{5.3-1f}$$

$$\mu_9 = l_3 \cos(\eta - \theta_3) \tag{5.3-1g}$$

$$\mu_{10} = \rho \cos(\eta - \theta_4 + a) \tag{5.3-1h}$$

Just before impact, all the parameters in equations (5.3-1) are known quantities. In terms of these notations, equations (5.1.2-11), (5.1.3-7), and (5.2-13) can be written in matrix form as following

$$
\begin{bmatrix}
I_{A_3} & 0 & \mu_9 & \mu_7 \\
0 & I_{O_4} & -\mu_4 & -\mu_8 \\
-\mu_9 & \mu_6 & 0 & 0
\end{bmatrix}
\begin{bmatrix}
\omega_3^+ \\
\omega_4^+ \\
F \\
f
\end{bmatrix}
=
\begin{bmatrix}
I_{A_3} & 0 & 0 \\
0 & I_{O_4} & 0 \\
e\mu_9 & -e\mu_6 & (1+e)\mu_9
\end{bmatrix}
\begin{bmatrix}
\omega_3 \\
\omega_4 \\
\omega_9
\end{bmatrix}
\tag{5.3-2}
$$

At this stage, the related equations of the types of contact will be investigated

5.3.1- The Smooth Case

Since in this type of contact frictional forces are negligible, the tangential force F_t, at the point of contact due to friction van-

ishes. Hence, equation (5.1.2-5) becomes

$$f = \int F_t \, dt = 0 \qquad (5.1.3-1)$$

Therefore, f can be eliminated from equation (5.3-2) and the resulting system of equations can be solved for the remaining unknowns. Note that, equation (5.3.1-1) implies that the tangential velocities remain unchanged in this case, i.e.,

$$V_{B_3,t}^{\;+} = V_{B_3,t}$$

and

$$V_{B_4,t}^{\;+} = V_{B_4,t}$$

5.3.2- The Rough Case

Since due to friction, there is no slipping or relative motion in the tangential direction, then

$$V_{B_3,t}^{\;+} = V_{B_4,t}^{\;+} \qquad (5.3.2-1)$$

By referring to Figure (5.5), one can write

$$V_{B_3}_t = l_2\omega_2\cos(\eta-\Theta_2)+l_3\omega_3\cos(\eta-\Theta_3)$$

(5.3.2-2a)

$$V_{B_4}_t = \rho\omega_4\cos(\eta-\Theta_4-\alpha)$$
(5.3.2-2b)

Combining equations (5.3.2-1) and (5.3.2-2) yields

$$[l_3\cos(\eta-\Theta_3)]\omega_3^+-[\rho\cos(\eta-\Theta_4-\alpha)]\omega_4^+=$$

$$-[l_2\cos(\eta-\Theta_2)]\omega_2$$
(5.3.2-3)

and using the notations of equations (5.3-1)

$$(\mu_7)\omega_3^+-(\mu_{10})\omega_4^+=-(\mu_9)\omega_2$$
(5.3.2-4)

The above equation is the fourth relation necessary to solve equation (5.3-2) for this type of contact

5.3.3- The Stick-Slip Case

In this case, due to Coulomb friction, sticking occurs if the tangential force, F_t, during impact is less than the frictional force,

i.e.,

$$F_t \leq \mu_e F_n \tag{5.3.3-1}$$

where μ_e is the Coulomb coefficient of friction. Integrating both sides of inequality (5.3.3-1) with respect to time yields

$$\int F_t dt \leq \mu_e \int F_n dt$$

or

$$f \leq \mu_e F \tag{5.3.3-2}$$

The system then behaves in an identical manner to that of the rough case, which was discussed in section 5.3.2.

Slipping is initiated once the inequality (5.3.3-2) is violated. At this stage, F_t, the tangential force assumes a constant value given by

$$f_t = \sigma \mu_e F_n \tag{5.3.3-3}$$

where

$$\sigma = \text{sign}(V_{B_{3_t}} - V_{B_{4_t}}) \tag{5.3.3-4}$$

Again, integration of equation (5.3.3-3) with respect to time will result in

$$f = \sigma\mu_e F \qquad (5.3.3-5)$$

5.4- Assemblage of the Equations of Motion

The matrix equation (5.3-2) can be combined with equations (5.3.1-1), (5.3.2-4), and (5.3.3-5) to yield the general equations of motion of the mechanism in the impact mode as follows

$$
\begin{bmatrix}
I_{A_3} & 0 & \mu_{11} & \mu_7 \\
0 & I_{O_4} & -\mu_{12} & -\mu_8 \\
-\mu_3 & -\mu_6 & 0 & 0 \\
\mu_7 & -\mu_{10} & 0 & 0
\end{bmatrix}
\begin{bmatrix}
\omega_3^+ \\
\omega_4^+ \\
F \\
f
\end{bmatrix}
=
\begin{bmatrix}
I_{A_3} & 0 & 0 \\
0 & I_{O_4} & 0 \\
e\mu_3 & -e\mu_6 & (1+e)\mu_5 \\
0 & 0 & -\mu_9
\end{bmatrix}
\begin{bmatrix}
\omega_3 \\
\omega_4 \\
\omega_2
\end{bmatrix}
$$

$$(5.4-1)$$

where for smooth or rough (stick) case

$$\mu_{11} = \mu_3$$

$$\mu_{12} = \mu_4$$

and, for slip case

$$\mu_{11}=\mu_3+\sigma\mu_6\mu_7$$

$$\mu_{12}=\mu_4+\sigma\mu_6\mu_8$$

Equation (5.4-1) includes all three types of nature of contact. With proper partitioning, it can be solved for each case as follows

1. For the smooth case and the slip case, one considers only the top 3 x 3 submatrix (solid line partitioning).

2. For the rough and stick cases, the entire matrix in equation (5.4-1) has to be considered. Even then, the solution is easily obtained by considering the 2 x 2 system of partitioning shown by the dotted lines. Due to the existence of a zero submatrix in the bottom right, it is possible to solve explicitly for ω_3^+ and ω_4^+. then, F and f can be given in terms of these two parameters.

Although in this study the only case considered will be the smooth type of contact, equation (5.4-1) is solved for each case, and their explicit forms are shown as follows

For the smooth and the slip cases

$$\omega_3^+=1/D_1\Big[[I_{A_3}\mu_6\mu_{12}-eI_{0_4}\mu_3\mu_{11}]\omega_3+[\mu_6\omega_4$$

$$-\mu_3\omega_3][(1+e)I_{0_4}\mu_{11}]\Big]$$

(5.4-2a)

$$\omega_4^+ = 1/D_1 \Big[[I_{O_4}\mu_3\mu_{11} - \theta I_{A_3}\mu_6\mu_{12}]\omega_4 + [\mu_3\omega_3$$

$$+\mu_5\omega_2][(1+\theta)I_{A_3}\mu_{12}]\Big]$$

$$(5.4-2b)$$

$$F = 1/D_1 [I_{A_3}I_{O_4}(1+\theta)(\mu_3\omega_3 - \mu_6\omega_4 + \mu_5\omega_2)]$$

$$(5.4-2c)$$

$$f = 0 \text{ (for smooth) }; \ \sigma\mu_\theta F \text{ (for slip)} \qquad (5.4-2d)$$

$$D_1 = I_{A_3}\mu_6\mu_{12} + I_{O_4}\mu_3\mu_{11} \qquad (5.4-2e)$$

For the rough and the stick cases

$$\omega_3^+ = 1/D_2 \Big[\theta\mu_{10}[\mu_6\omega_4 - \mu_3\omega_3] + [\{\mu_6\mu_9$$

$$-(1+\theta)\mu_5\mu_{10}]\omega_2\Big] \qquad (5.4-3a)$$

$$\omega_4^+ = 1/D_2 \Big[\theta\mu_{[7}[\mu_6\omega_4 - \mu_3\omega_3] + [\mu_3\mu_9 - (1+\theta)\mu_5\mu_{[7]}]\omega_2\Big]$$

$$(5.4-3b)$$

$$F = 1/D_3 [I_{A_3}\mu_8(\omega_3^+ - \omega_3) + I_{O_4}\mu_7(\omega_4^+ - \omega_4)] \qquad (5.4-3c)$$

$$f = -1/D_3 [I_{A_3}\mu_4(\omega_3^+ - \omega_3) + I_{O_4}\mu_3(\omega_4^+ - \omega_4)] \qquad (5.4-3d)$$

$$D_2 = \mu_3\mu_{10} - \mu_6\mu_7 \qquad (5.4-3e)$$

$$D_3 = \mu_4\mu_7 - \mu_3\mu_8 \qquad (5.4-3f)$$

The equations of motion developed in chapters three, four, and five furnish all of the required equations for the three modes of behavior, namely, the following, the free-flight, and the impact mode. The next chapter discusses the method of solution of these equations along with some results.

CHAPTER SIX

CORRELATION AND NUMERICAL SOLUTION OF
THE MODES OF BEHAVIOR

The preceding chapters, taken together, comprise a complete set of governing equations of motion of the mechanism under study. The task is now to tie these equations together, using appropriate boundary conditions, and then solve them numerically, which in turn necessitates the existence of a set of system parameters used as initial conditions.

The appendix represents the flow chart of a code, called SIMUL, used for the numerical solution of the equations. It is not practical, if not redundant, to explain every line of this code. However, its main framework and objectives will probably become clear in the remainder of this chapter.

6.1- Initial Conditions

The choice of initial conditions plays a significant role in the results of the simulation. For instance, for a given set of parameters and a prescribed upper bound value of the integration error, and for one full revolution of the crank, the outcome of the numerical solution is entirely different for the initial condition corresponding to a crank angular displacement of, say, zero degree than that corresponding to a crank angle of 20 degrees. This inconsistency in the results is due to several reasons. The assumed configuration of the mechanism corresponding to the value of the crank angle chosen as being the 'start-up' position might not be the true configuration. Obviously, at any instant of time, due to the small size of the clearance, the angular displacements of the links of the mechanism (crank, coupler, and rocker) are practically the same as their counterparts corresponding to the nominal mechanism. However, as mentioned in section (3.4), when selecting appropriate initial conditions, the angular displacement of the 'clearance link' is taken to be that of the corresponding bearing reaction in the nominal mechanism. So, now the question is that how accurately does the direction of the 'nominal bearing force' approximate that of the clearance link in the mechanism under study at initial conditions ? A method of such approximation has been proposed by Earles and Wu [3] - explained in section 3.4 - which relies on the determination of the dead-center-point (d.c.p.), which is too specialized and cannot be extended to any mechanism such as the one under investigation. Since there is no universally accept-

ed method of selection of the start-up time, the optimum path seems to be a trial-and-error approach.

Although during the the first few cycles of the simulation, the influence of the choice of initial conditions on the response of the system is quite pronounced, this dependency on the start-up position tends to diminish as the solution is advanced into higher number of cycles (about 10 or 20 cycles). In other words, as pointed out by Mansour et. al. [7], the response of the system during the numerical solution begins with a 'transient' phase which continues to converge to a 'quasi-steady' phase after a few simulated revolutions of the crank. In the transient phase the response does not behave periodic and has no tendency to follow a consistent path. But, in the quasi-steady phase, the response tends to become periodic whose funda- mental wavelength often spans over a number of crank revolutions.

Hence, any angular displacement of the crank can be taken as initial conditions, so far as the quasi-steady response is concerned. Once the solution is initiated, it can be carried on to this phase, and the results can readily be studied. However, more critical than the choice of the initial conditions is the efficiency and accuracy limits dictated by the type of the digital computer utilized to carry on the task of numerical solution of the equations. The computer used in this work was a PRIME 750 which has an accuracy of maximum of 14 significant digits, depending on the case under study, in the double precision mode. But, as will be apparent, the accuracy needed to

solve the equations of motion at hand requires a machine with far greater accuracy than the PRIME's. Also, due to the round-up and truncation errors, at some points the degree of accuracy tends to fall below the specified maximum, thus magnifying the problem. In other words, the choice of initial conditions was governed by the PRIME system to solve the system of equations with reasonable speed and accuracy.

There were only a few values of the crank angular displacement that seemed likely for the PRIME to use them as initial conditions and iterate the solution through one full crank revolution. The other values would either cause an overflow problem with subsequent halt of the solution or, totally erroneous and divergent results.

The final note that should be mentioned is that due to length of time involved, all the numerical solutions shown hereafter are for the first cycle of solution or, the first crank revolution. Carrying the solution into higher crank revolutions using the PRIME, if possible at all, would require unacceptable amount of computer time.

6.2- Method of Solution

It would be helpful to take a quick glance at the appendix, which contains the main flow chart of the code (SIMUL) along with an alphabetical listing of all of the related subroutines and functions developed for the numerical solution of the equations. The primary

thrust of the main code is to manipulate and correlate the parameters computed by the subroutines, and also, perform the task of storing the data and shifting the 'flow-direction' of the computation to appropriate points and places.

Once the code is compiled and started, all of the desired parameters corresponding to the nominal mechanism are computed. This is done prior to the numerical solution of the equations. These parameters are stored aside for further comparison with the final results.

After determining the instant of time used as the time of initial condition, along with a few other auxiliary parameters, the numerical solution is initiated. This task is performed using a numerical integration package called HPCG. It is not overemphasized to state that this package is the heart of the computer code used for the numerical solution. For in this subroutine all of the required iterations and integrations are carried out. Hence, it is obvious that, the overall efficiency of the whole program is primarily dictated by the efficiency of the numerical integration package used. In other words, the more efficient the method adapted in the package, the more accurate and reliable are the final results.

Another limiting factor, again, is the capabilities of the computer at hand. This implies that, as the accuracy of the package, and consequently that of the final result is increased, there is a thres-

hold beyond which either there is no further improvement in the results or, in the worse case, the round-up and truncation errors dominate the results significantly and introduce a substantial level of 'ditgital noise' into the final results. For instance, a numerical integration package was used first which was quite powerful in terms of solving the equations occuring in this work. This code was developed by the Lawrence Livermore Laboratory, California, called LSODI (The Livermore Solver For Ordinary Differential Equations In Linearly Implicit Form). Two methods of integration could be used to solve any problem depending on its type. The first one was for sets of equations with stiff characteristics (sparse eigenvalues), which adapted the backward differentiation formulae to integrate the equations numerically. The second method which was essentially the implicit Adams method, was suitable for sets of equations that did not show stiff characteristics.

Unfortunately, such a package could not be compiled and handled by the PRIME system due to the occurence of overflow problems caused by the round-up errors generated in the system. Thus, replacement of the LSODI package with another one was unavoidable, and LSODI was substituted by the HPCG to carry out the task. This package (HPCG) is intended to solve a set of first order ordinary differential equations with prescribed initial conditions. Integration of the equations is done by means of the Hamming's modified corrector-predictor method, which uses four preceding points for computation of a new vector of the dependent variables. A fourth order Runge-Kutta method, as sug-

gested by Ralston [85,86], is used for adjustment of the initial increment, and for computation of the starting values.

To help give a better insight into the differences between the former package (LSODI) and the HPCG, it should be stated that, the example problem (along with answers) illustrated in the commentary section of the LSODI package was solved using the HPCG subroutine. Two major differences were observed.

1. The time required for the HPCG to solve the problem through the whole integration interval was computed to be in the neighborhood of several hours, whereas the same problem presumably would be carried out in a matter of minutes using LSODI. Obviously, when running the example problem on the HPCG the execution was halted due to the large extent of time required.

2. The answers obtained at the specified points of the integration interval were compared with the ones given by the LSODI. It was noted that all of the results obtained using HPCG resembled those found using LSODI only up to the third significant digit.

The apparent conclusion which can be drawn from these observations is that, the existence of 'digital noise' in the final results can be attributed primarily to the generation of round-up and truncation errors in the PRIME system, and partly to the approximation errors within HPCG during the iteration process.

Returning to the set of equations in this study; once the initial time is specified, the code is written such that it automatically assumes this instant of time to be in the following mode. This, in turn, implies that equation (3.3-7) is iterated using the parameters known at the initial condition, i.e.,

$$[A]\{ X \}=\{ B \}$$

where matrix [A] and vectors { X } and { B } are described in equations (3.3-8).

The iteration in HPCG is advanced until the contact-loss criteria (section 3.5) is met. At this point, the code exits from the HPCG and the above equation is replaced by equations (4.1-20) and (4.2-1), which are the governing equations of motion of the free-flight mode. The iteration is performed based on initial conditions corresponding to the values of parameters in the following mode just prior to contact-loss. As soon as the criteria for the termination of the free-flight mode, inequality (4.4-5), is met, the iteration is paused.

Utilizing the values of the parameters at the end of the free-flight interval, the impact mode is initiated and, equations (5.4-2) are solved for the unknowns, namely, the angular velocities of the coupler and rocker after impact. These two new parameters, along with the other known ones, constitute an 'updated' set of initial conditions for either the following mode or, the free-flight mode,

depending on the particular point of impact in the bearing and, other system parameters such as links' angular displacements, velocities, etc. The solution, therefore, is carried on in this manner over the desired time interval.

One of the major difficulties in obtaining the final results of the numerical solution was the time required to solve the equations with a prescribed upper bound value of the absolute error of integration. This problem is distinctly pronounced when high degrees of accuracy are desired. For instance, if the value of the maximum absolute error was prescribed to be 0.001, it would require an integration time step as small as one corresponding to a crank angular displacement of about 10^{-4} degrees per step to bypass the occurence of overflow. This would mean that, at least 3.6×10^6 iterations are required to solve the equations over one crank revolution only. As an experiment, such conditions were generated on the PRIME and, it was observed that after 17 continuous hours of CPU time spent in solving the equations on the system, the iteration had advanced only about 5 degrees of crank angular displacement relative to the initial condition. Obviously, the execution of the code was terminated since it required approximately 1200 hours to iterate through one full crank revolution at the same pace.

Thus, with a few trials, a much coarser mesh in terms of the time step was used in order to yield the final results in a reasonable length of time, i.e., from two to ten hours depending on the size of

the mesh and the acurracy required. This, of course, implied a compromise on the initially intended degree of accuracy required. It is noteworthy to mention that, Mansour et. al. [6] solved a similar problem (all the equations except those of the following mode) on an IBM 370/165 and, the time required to iterate the equations up to as high as ten crank revolutions was reported to be less than 15 seconds including the compilation time. Admitting that, in this work a third (following) mode is coupled with the other two, and also that all the dimensions used here are different than those used by Mansour, this comparison still gives an idea as to the advantage of using fast and efficient computers.

With all of the aforementioned difficulties involved which could not be eliminated altogether, the results in this work were obtained for the first crank revolution. This implies that, only the start-up cycle was simulated which possesses the severest response in terms of the vibrations and oscillations in the parameters due to the existence of the bearing clearance. The previously mentioned limiting factors made it impossible to study the response of the system in the higher cycles. Also, as described in chapters two and five, the coupler-rocker bearing that has a finite clearance is assumed to be frictionless (Coulomb coefficient of friction is zero) and, the coefficient of restitution at impact equals unity (no energy dissipation due to impact). Once introduced into the system, these two latter assumptions imply that, there is no dissipation of energy into the surroundings from the coupler-rocker bearing at any instant of time

during the simulated motion.

6.3- Numerical Results

Table (6.1) is a compilation of all of the relevant information concerning the physical and dynamic dimensions of the mechanism used for the simulation, which is a model of the four bar linkage serving as the experimental rig. As previously mentioned in chapters two and five, the Coulomb coefficient of friction is assumed to be zero, implying that, there is no friction between the pin and the bushing of the coupler-rocker bearing.

Two complete sets of simulation results are presented here. All of the dimensional characteristics of these two simulations are the same except that, the coefficient of restitution at impact is assumed to be unity in one case and, 0.50 in another. The former implies that, there is no type of energy dissipation into the surroundings at the time of impact, while the latter allows for some absorption of the energy of impact by the colliding surfaces and, yielding it to the surroundings through heat transfer or acoustic generation or, other means of system-surroundings interaction.

In order to achieve a better understanding of the results of the simulation, each curve is superimposed on its nominal counterpart. However, in some of these plots, which will be presented on subsequent pages, the scale of the plot is largely dominated by the simulation

TABLE (6.1)
SPECIFICATIONS OF THE SIMULATION MECHANISM

link	length (size) (mm)	center of gravity (mm)	mass (kg)	mass moment of inertia (kg.mm^2)
Crank	64.0	9.0	0.6095	2645.0
Coupler	309.0	185.0	0.2439	2950.0
Rocker	312.0	134.0	0.2334	3176.0
Ground	387.0	----	----	----
Clearance	0.2540	----	----	----

Crank angular velocity : 36.6519 rad/sec (350 RPM)

Crank angular acceleration : 0.0 rad/sec^2

Coefficient of restitution : 1.0

Coulomb coefficient of friction : 0.0

Gravitational acceleration : 9814.5 mm/sec^2

result and, the behavior of the superimposed nominal plot cannot be readily recognized. For this reason, Figures (6.1) to (6.9) illustrate the behavior of all of the studied parameters of the system for the nominal (clearance free) mechanism. Note that, in chapter eight a selected number of the simulation results will be compared to the experimental results which will be brought in chapter seven.

Figures (6.10a) and (6.10b) are the coupler angular displacements corresponding to coefficients of restitution of 1.0 and 0.50, respectively. Figures (6.11a) and (6.11b) are the analogous plots for the rocker link of the mechanism. As expected, there are no significant differences between the angular displacements of the simulation mechanism (called the 'base' mechanism hereafter) and, those of the nominal mechanism. This is primarily due to the fact that, the size of the clearance in the coupler-rocker bearing of the base mechanism is small enough (0.010 inches or 0.2540 millimeters) to have negligible effect on the 'geometrical' configuration of the system.

Figures (6.12a) and (6.12b) are the angular velocities of the coupler, with e=1.0 and e=0.50, respectively. Although the effect of the presence of clearance is quite pronounced on these plots, the influence of the magnitude of the coefficient of restitution cannot be clearly sensed. Note that, in Figure (6.12b), there is a rather severe disturbance in the coupler angular velocity of the base mechanism occuring at crank angle of about 20 degrees and, spanning over approximately four degrees of crank angular displacement. It is the
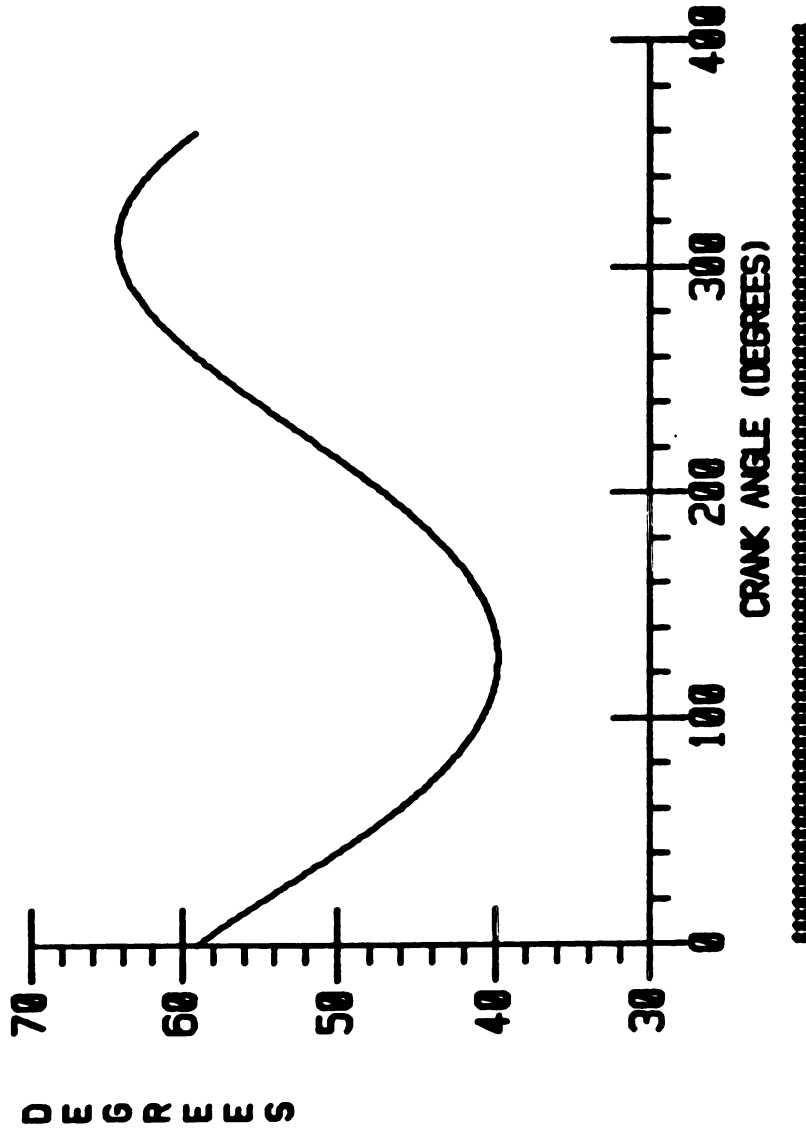
FIGURE 6.1. COUPLER ANGULAR DISPLACEMENT
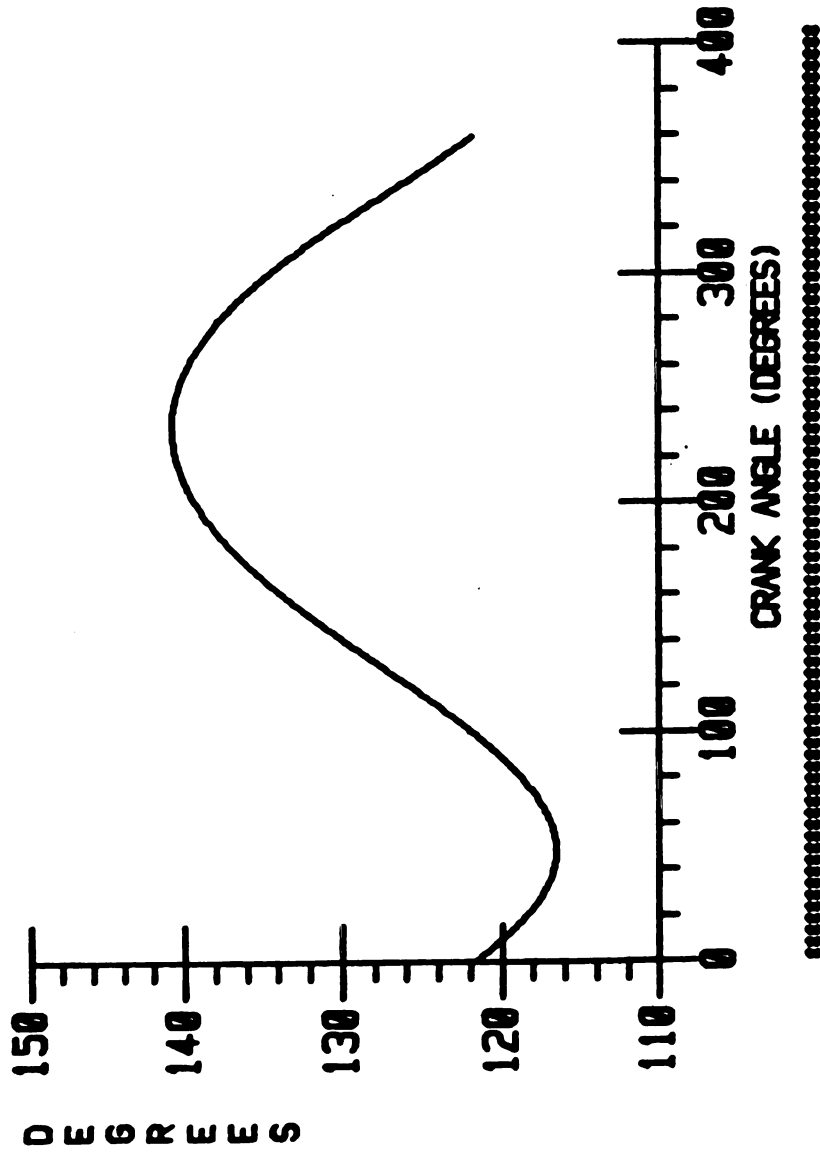
350 RPM, NOMINAL MECHANISM

FIGURE 6.2. ROCKER ANGULAR DISPLACEMENT
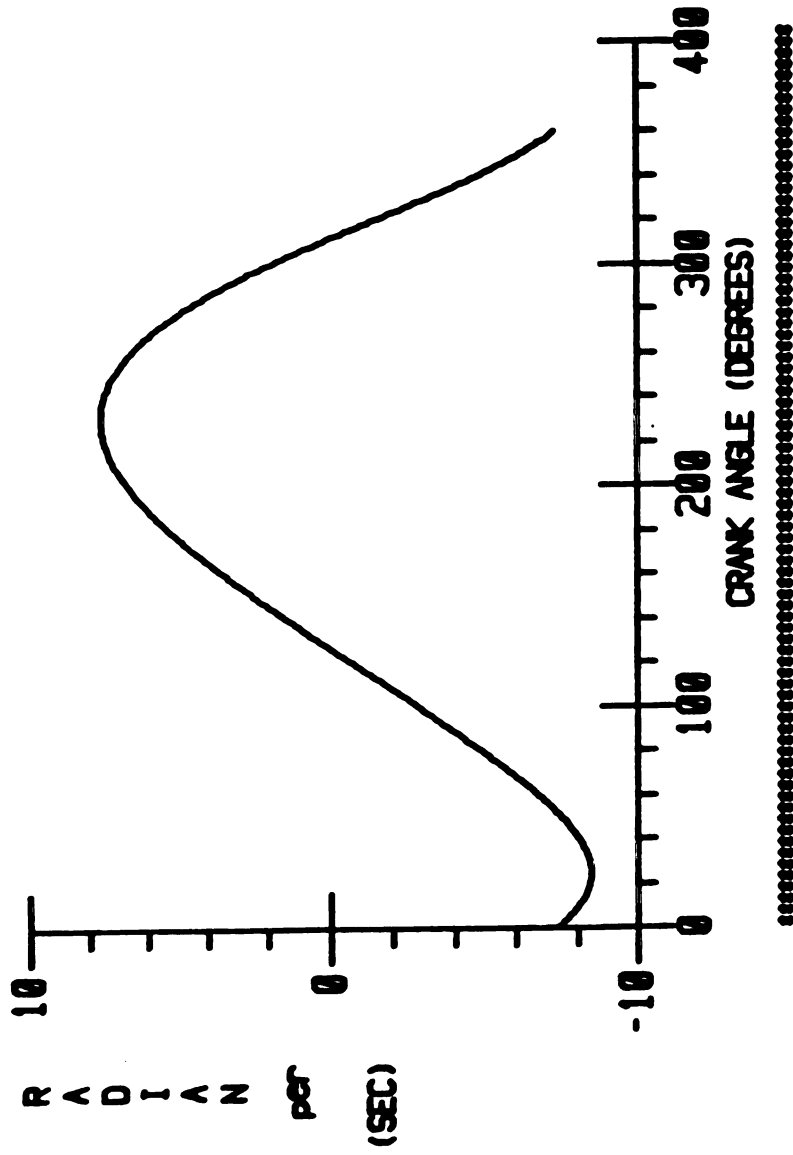
350 RPM. NOMINAL MECHANISM

FIGURE 6.3. COUPLER ANGULAR VELOCITY
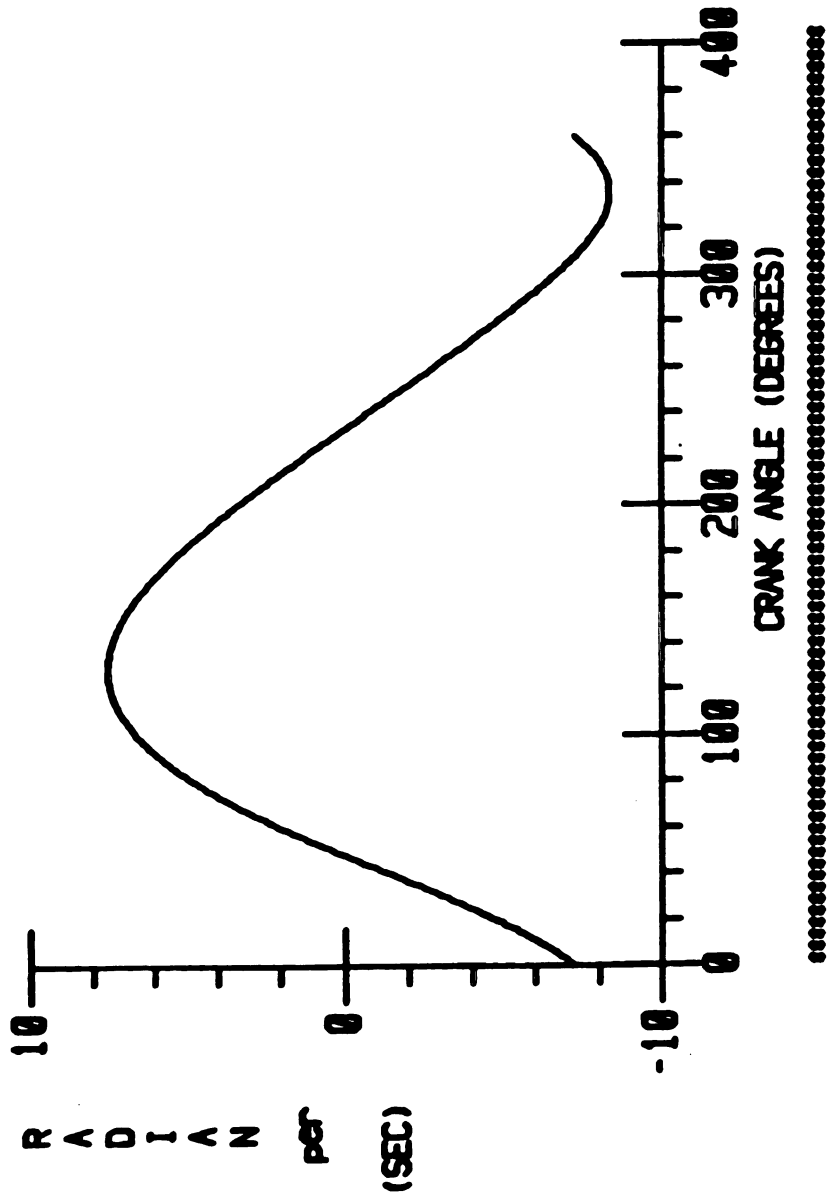
350 RPM, NOMINAL MECHANISM

FIGURE 6.4. ROCKER ANGULAR VELOCITY

108
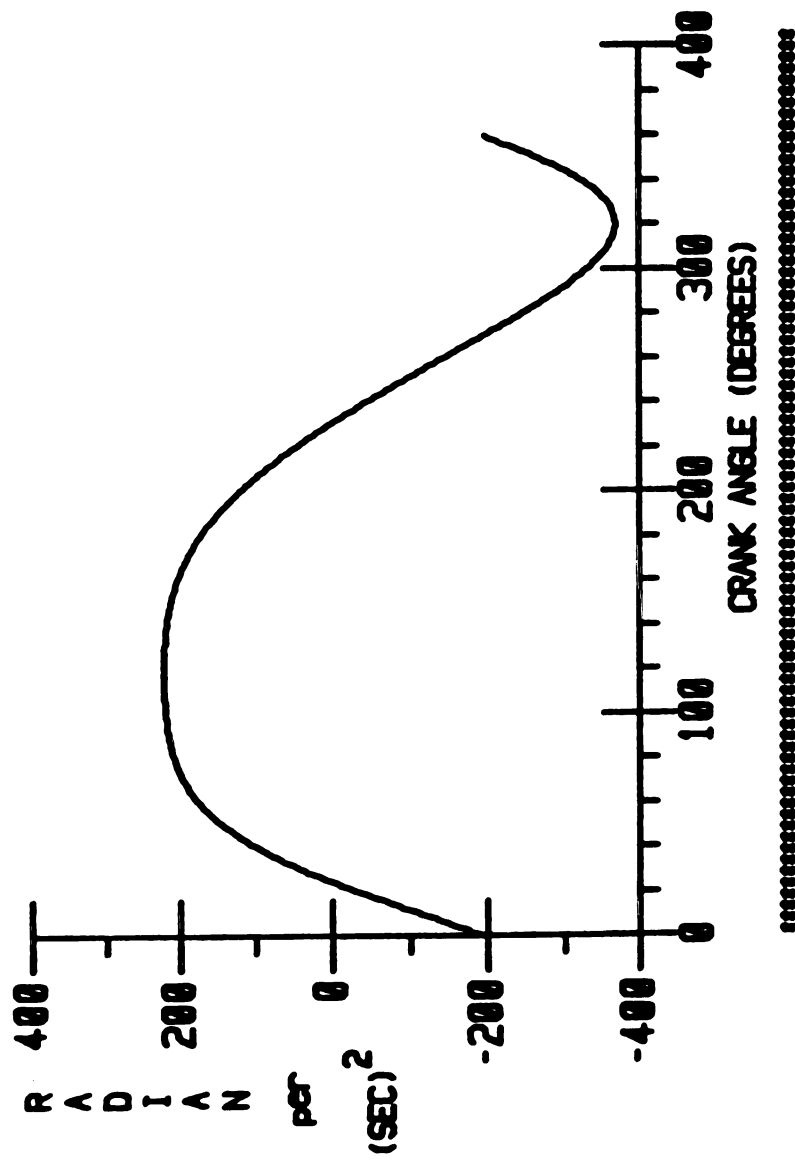
FIGURE 6.5. COUPLER ANGULAR ACCELERATION
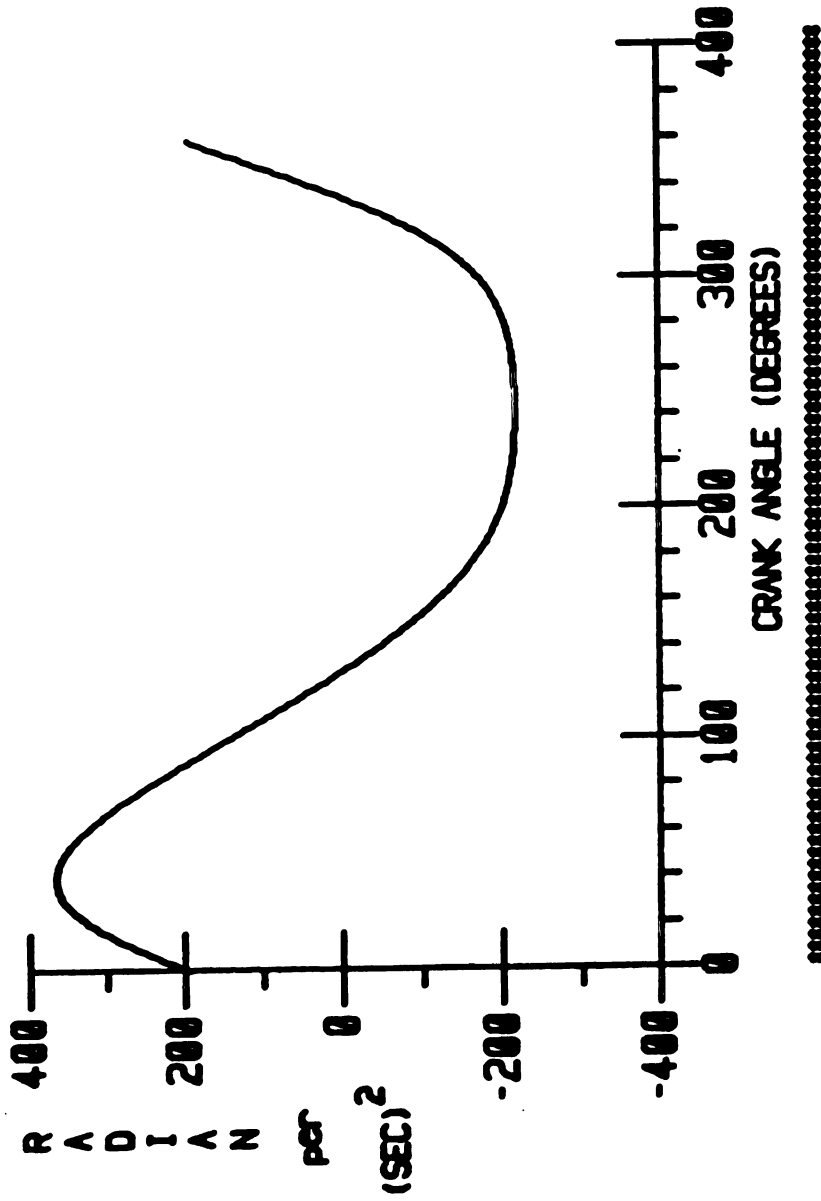
350 RPM, NOMINAL MECHANISM

FIGURE 6.6. ROCKER ANGULAR ACCELERATION
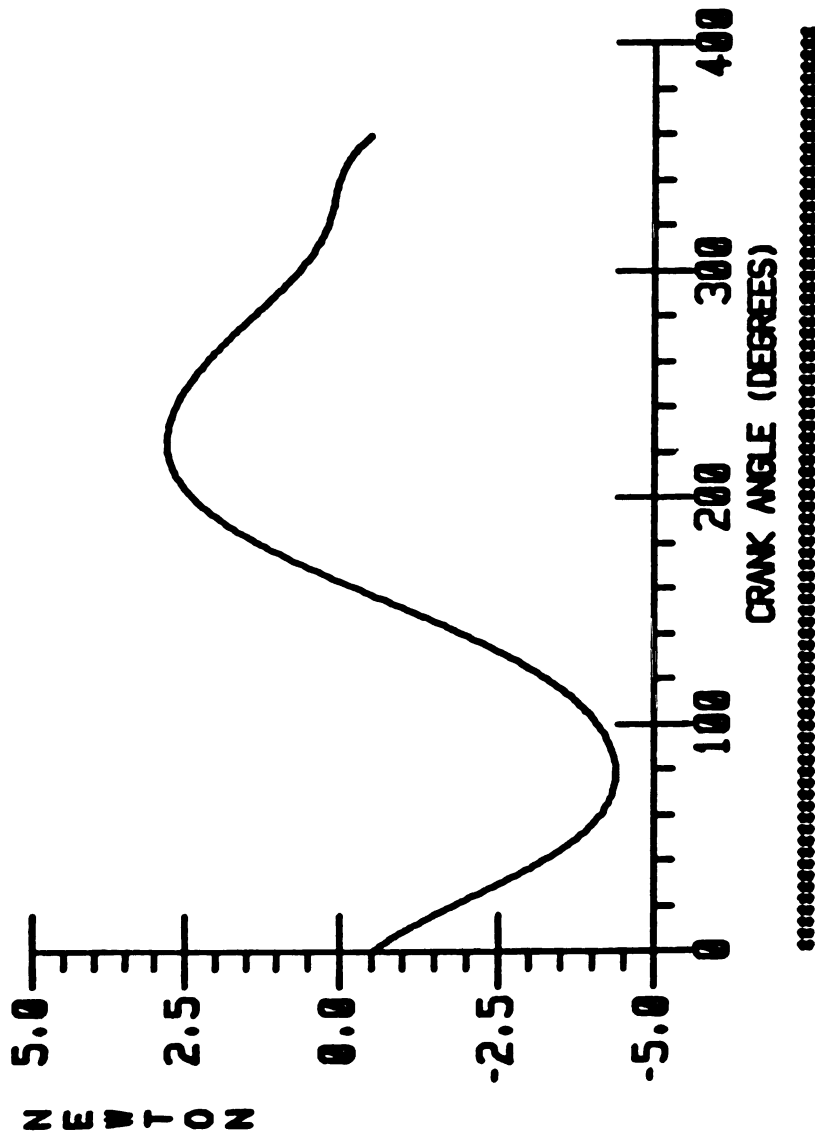
350 RPM. NOMINAL MECHANISM

FIGURE 6.7. C-R BEARING REACTION; X-COMPONENT

CRANK ANGLE (DEGREES)
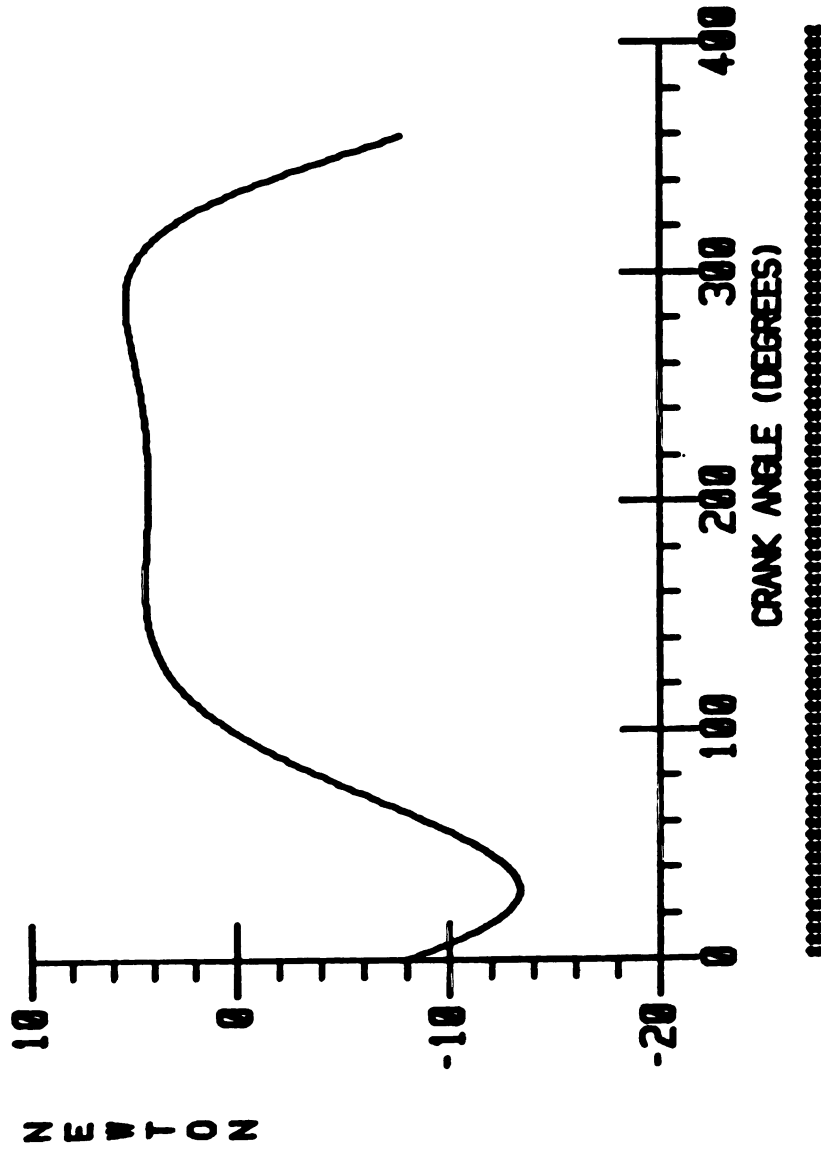
350 RPM. NOMINAL MECHANISM.

FIGURE 6.8. C-R BEARING REACTION; Y-COMPONENT
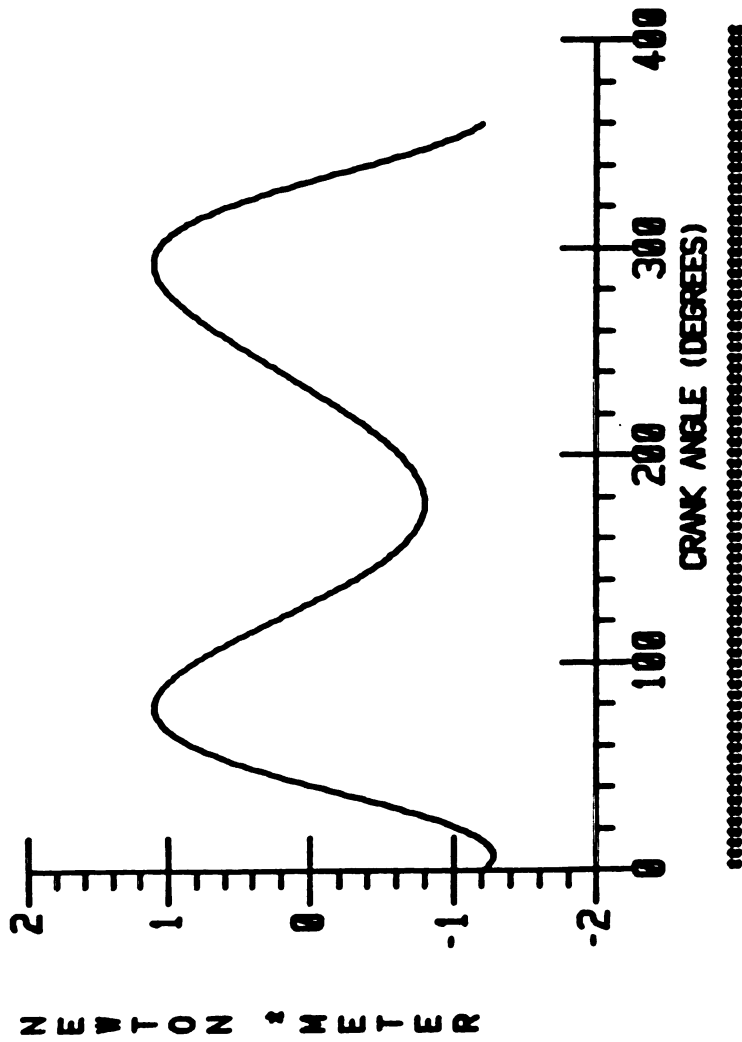
350 RPM. NOMINAL MECHANISM.

FIGURE 6.9. CRANK TORQUE
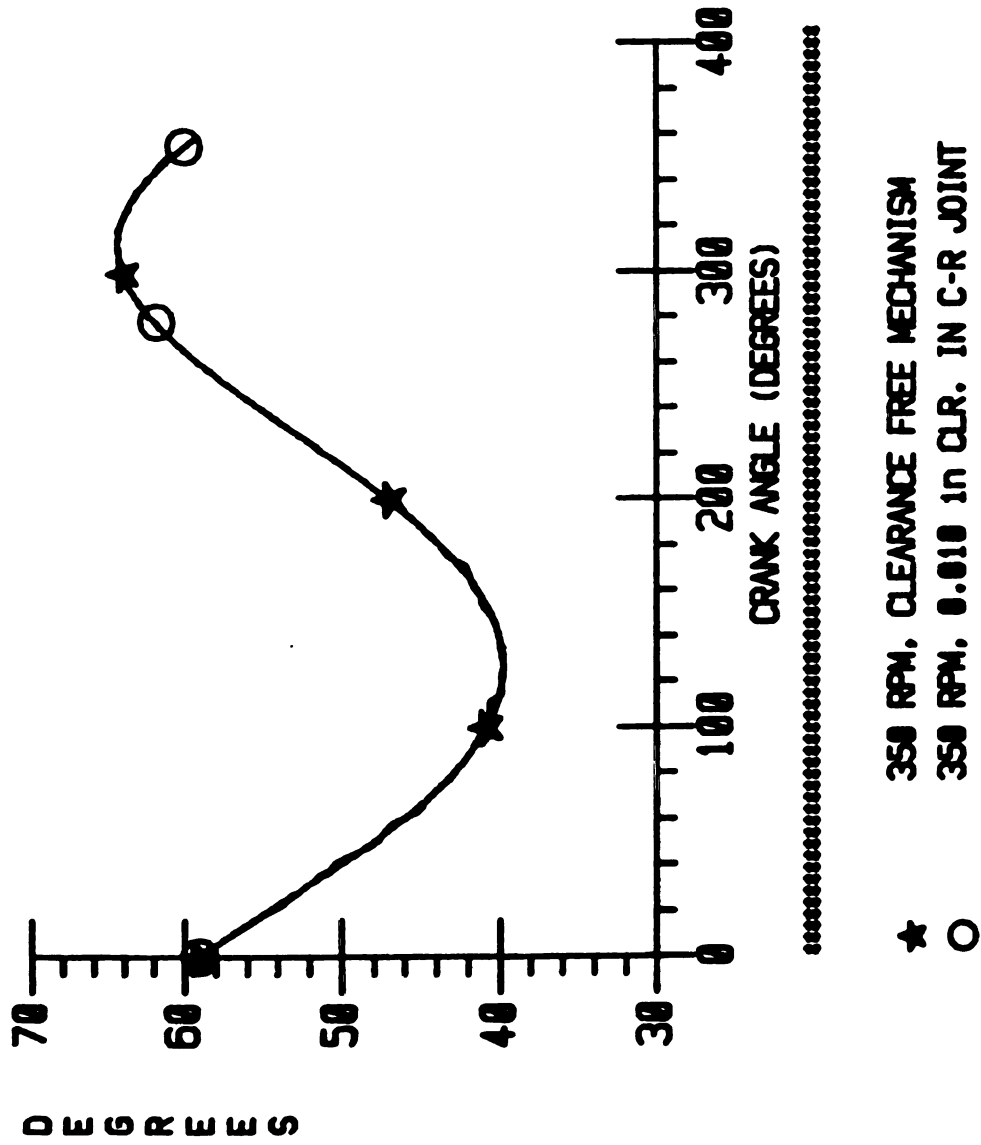
FIGURE 6.10a.   COUPLER ANGULAR DISPLACEMENT (e=1.0)

114

CRANK ANGLE (DEGREES)

★ 350 RPM. CLEARANCE FREE MECHANISM

O 350 RPM. 0.010 in CLR. IN C-R JOINT
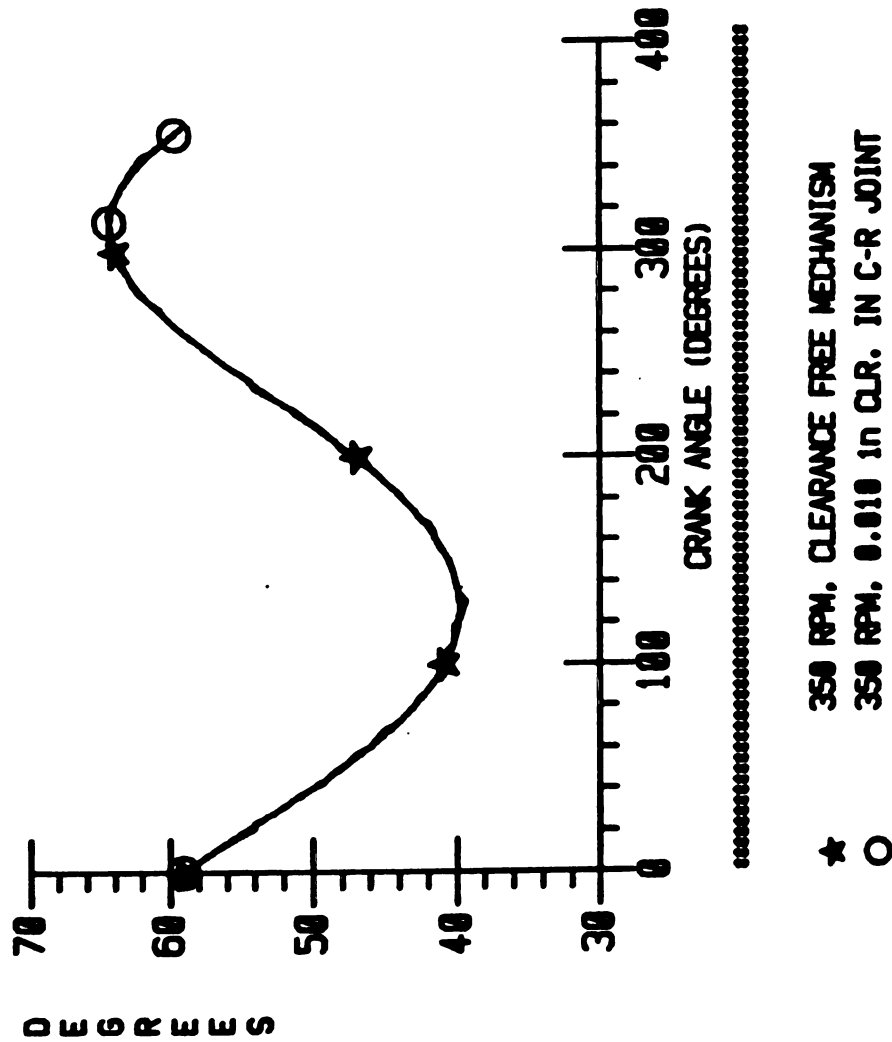
FIGURE 6.10b. COUPLER ANGULAR DISPLACEMENT (e=0.50)
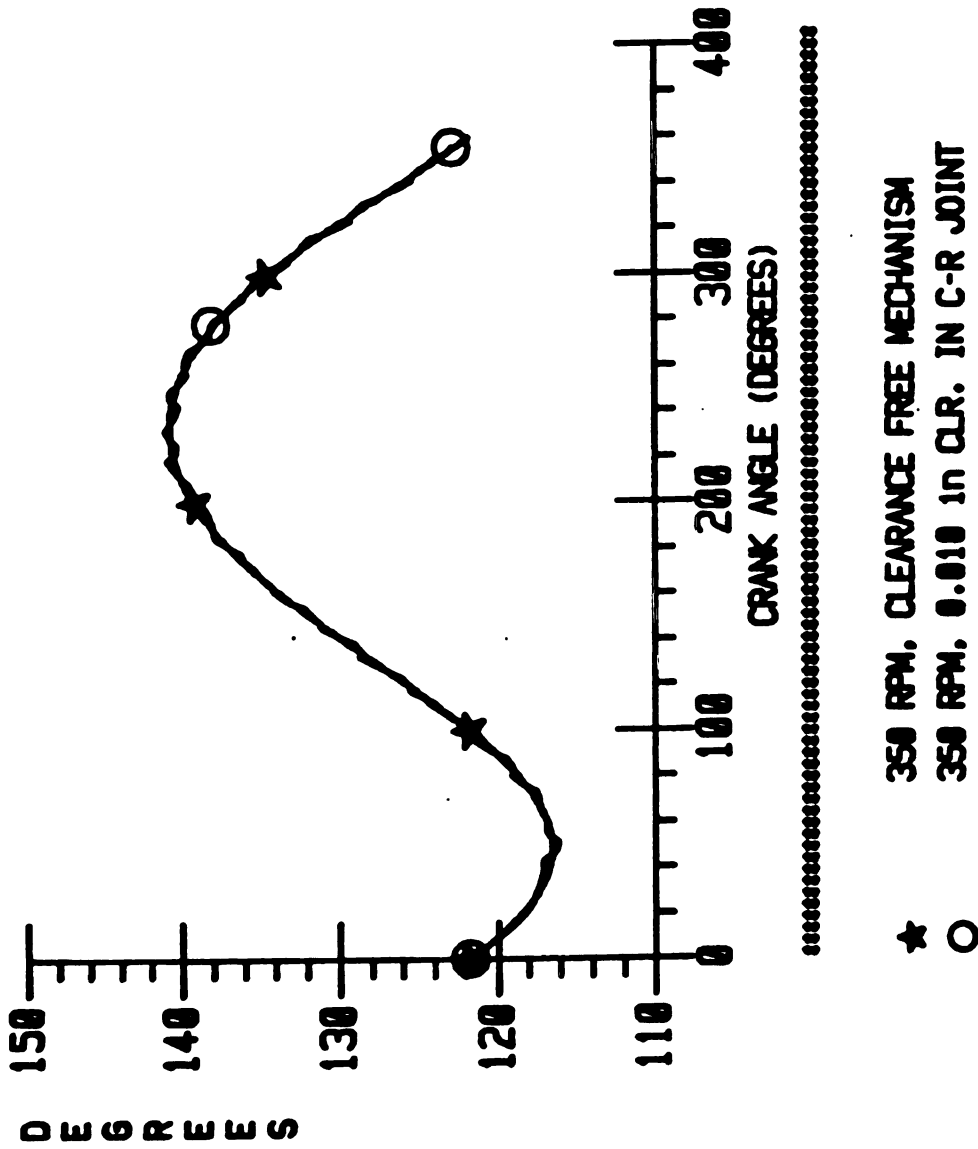
FIGURE 6.11a. ROCKER ANGULAR DISPLACEMENT (e=1.0)
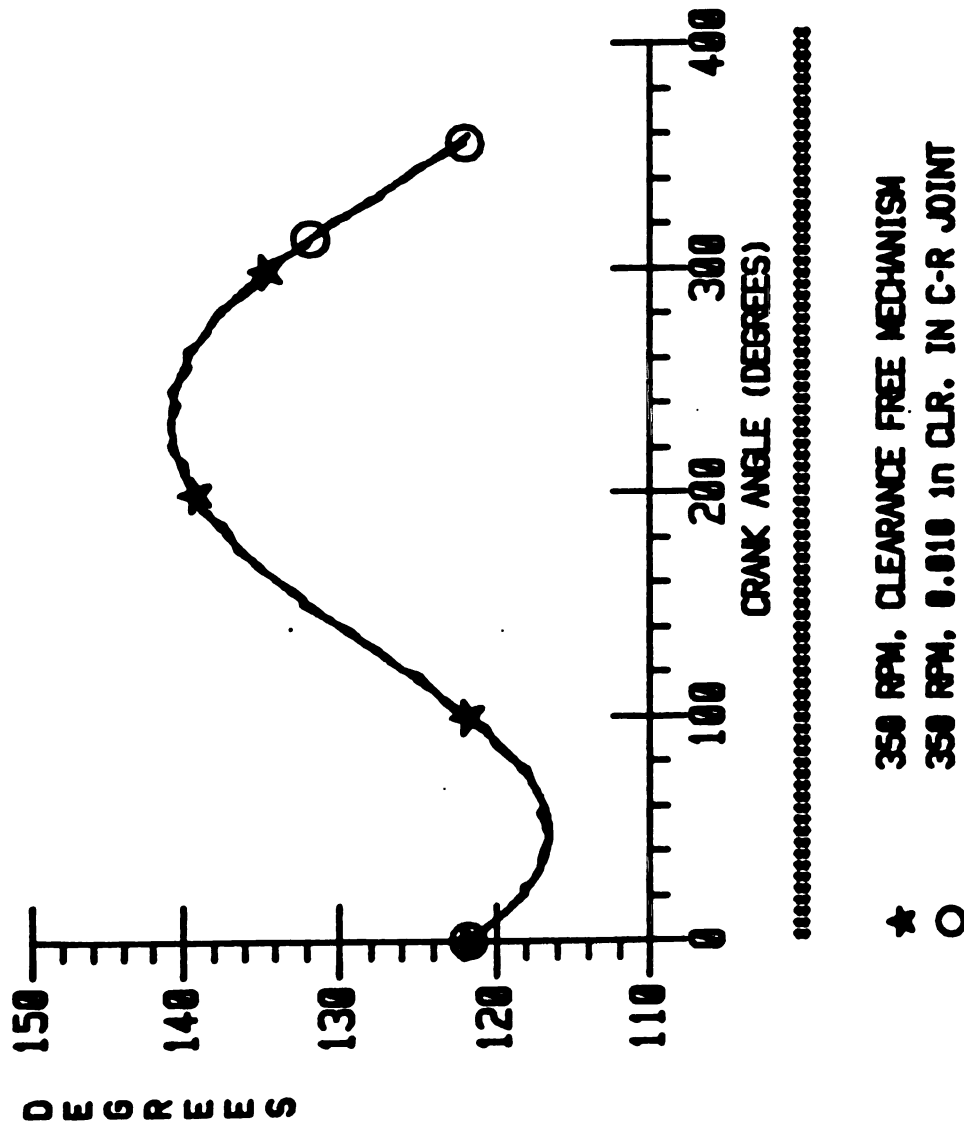
FIGURE 6.11b. ROCKER ANGULAR DISPLACEMENT (e=0.50)
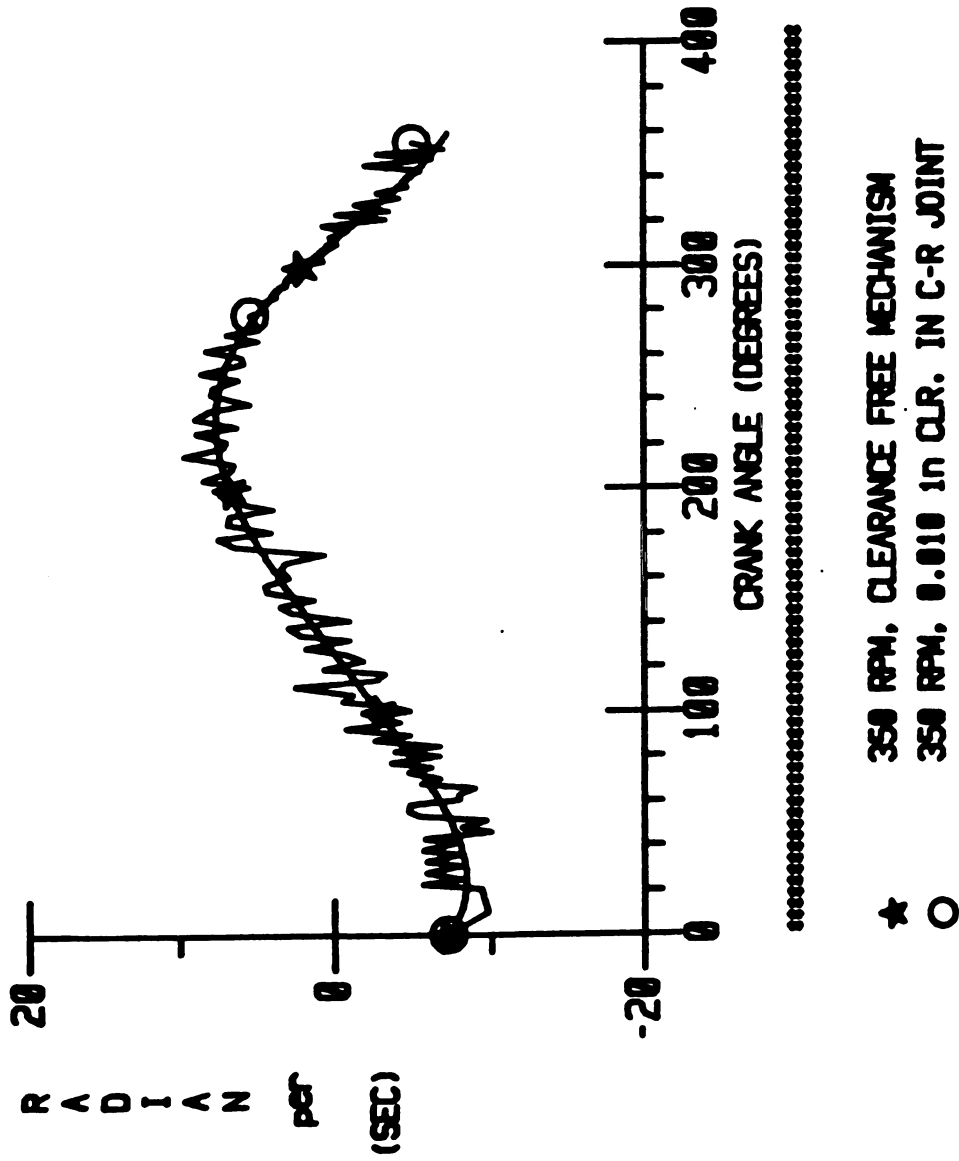
FIGURE 6.12a. COUPLER ANGULAR VELOCITY (e=1.0)

118
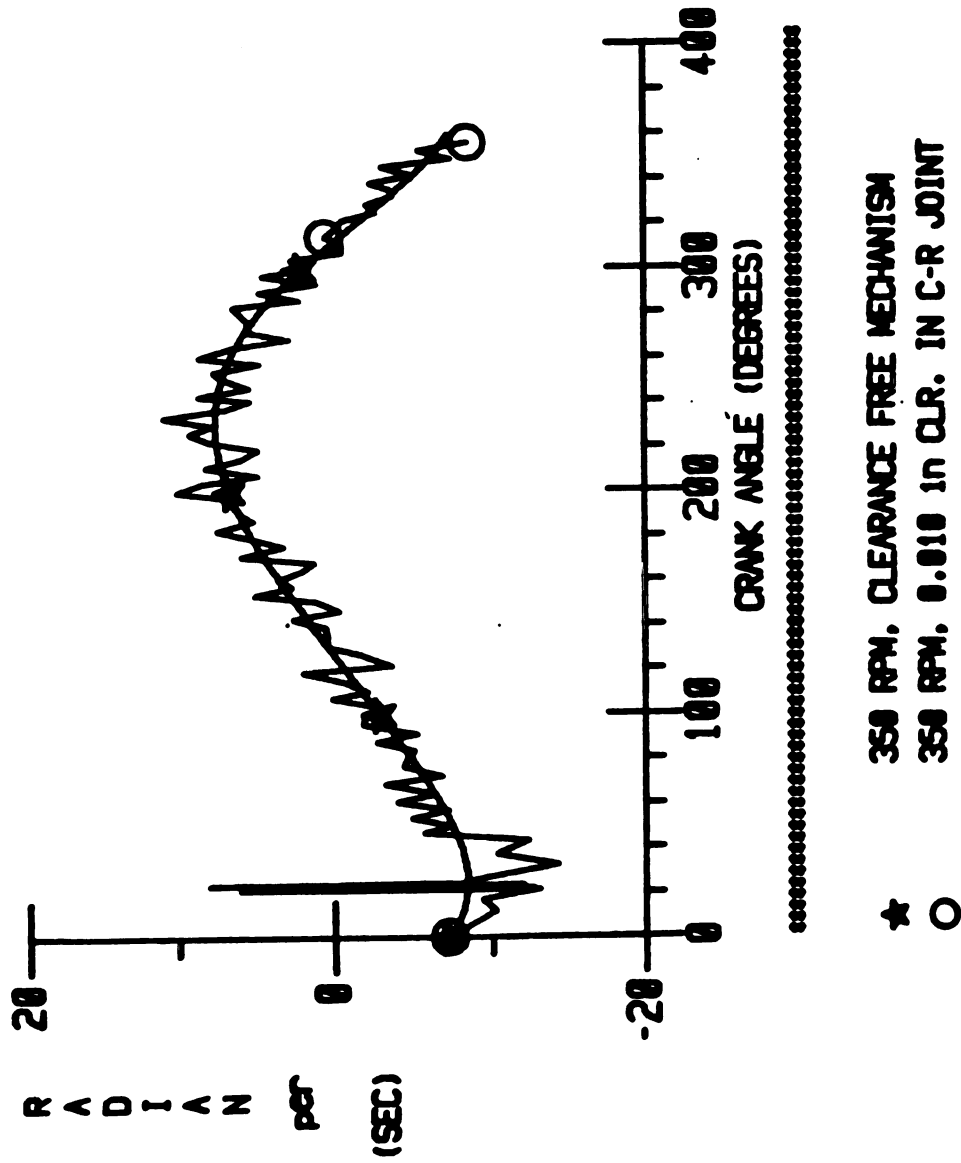
FIGURE 6.12b. COUPLER ANGULAR VELOCITY (e=0.50)

author's opinion that two possibilities exist

1. This disturbance, which attenuates after a few time-steps, is the result of a digital noise generated during the iteration and integration of the equations of motion.

2. It is the response of the mechanism based on the solution of the equations of motion. In this case, the term 'disturbance' could not be applied to this portion of the plot since it is now a part of the response. However, as previously mentioned, all of these simulations are for the start-up cycle with severest response. This could in part be due to the existense of any inaccuracies in the initial values of the parameters selected at the start of the iteration of equations, namely, initial conditions. In other words, this would imply that, such a severe response could occur in the process of numerically 'forcing' the results to trace a path in the neighborhood of their nominal counterpart. The reader should also note that, at this point one of the major reasons for the occurence of the overflow conditions during the simulation becomes more clear. That is, the overflow occurs primarily in this stage while attempting to reach a compromise between any inaccuracies in the values of the initial conditions and, the true response of the system. Obviously, the precision of the computing machine can often dictate the outcome of the simulation process in terms of either integrating the equations successfully through the prescribed time interval or, introducing enough error into the results as to cause the whole iteration process to halt at some point within the time interval.

With the above two possibilities in mind, one can claim that, this small portion of the response (Figure 6.12b) can be isolated from the remainder of the plot with no loss of accuracy and generality in the results. Such a phenomena can also be observed in Figure (6.12a) which occurs in the neighborhood of crank angle of 10 degrees. However, in this case, it is not as severe as in the former case. The reader should bear in mind that, these so-called disturbances are propagated to the other system parameters. Thus, any plot presented in subsequent which bears this type of behavior, will be studied with that specific portion of the response isolated from the remainder of the plot.

Figures (6.13a) and (6.13b) are the angular velocities of the rocker link for e=1.0 and e=0.50, respectively. Eliminating the disturbances on the plots, there seems to be no significant difference between the two angular velocity curves. Figures (6.14a) and (6.14b) depict the angular accelerations of the coupler. Note that, there is a clear distinction in the acceleration responses for different values of coefficient of restitution. As can be seen, the coupler angular acceleration for e=1.0 (Figure 6.14a) is, on the average, twice that of the one for e=0.50 (Figure 6.14b). This can be attributed to the fact that, when e=0.50, a portion of the impact energy is absorbed by the coupler-rocker bearing components, while in the case when e=1.0 (Figure 6.14a), the energy of the impact is theoretically conserved. Figures (6.15a) and (6.15b) illustrate the corresponding plots for the rocker link.
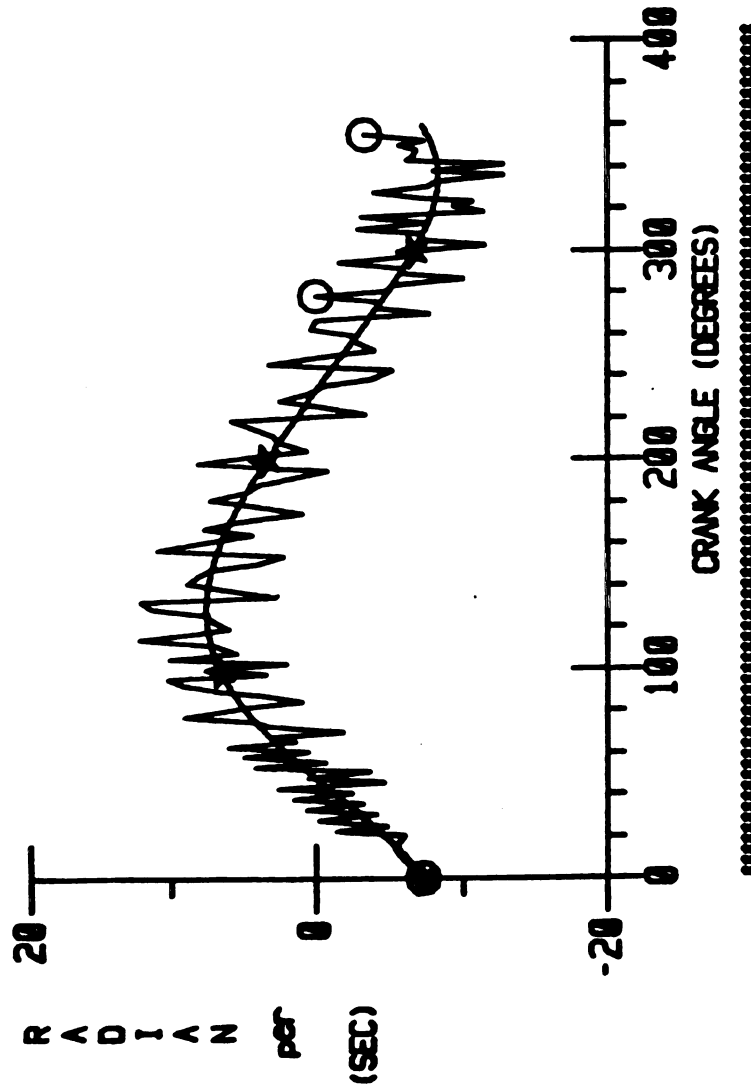
350 RPM, CLEARANCE FREE MECHANISM

350RPM, 0.010 in CLR. IN C-R JOINT

FIGURE 6.13a.   ROCKER ANGULAR VELOCITY (e=1.0)
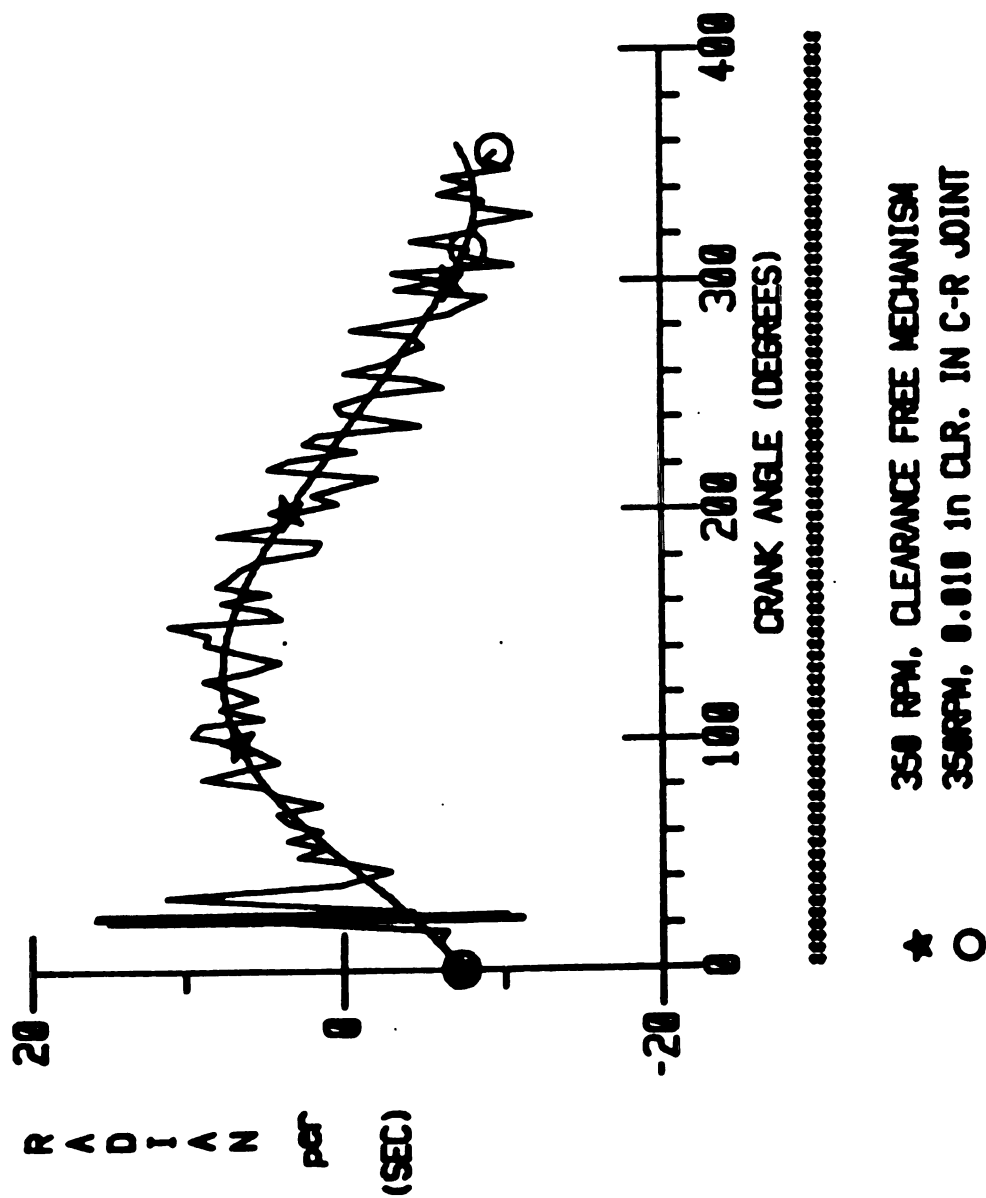
FIGURE 6.13b. ROCKER ANGULAR VELOCITY (e=0.50)

X10⁴

R
A
D
I
A
N
per
(SEC)²

CRANK ANGLE (DEGREES)
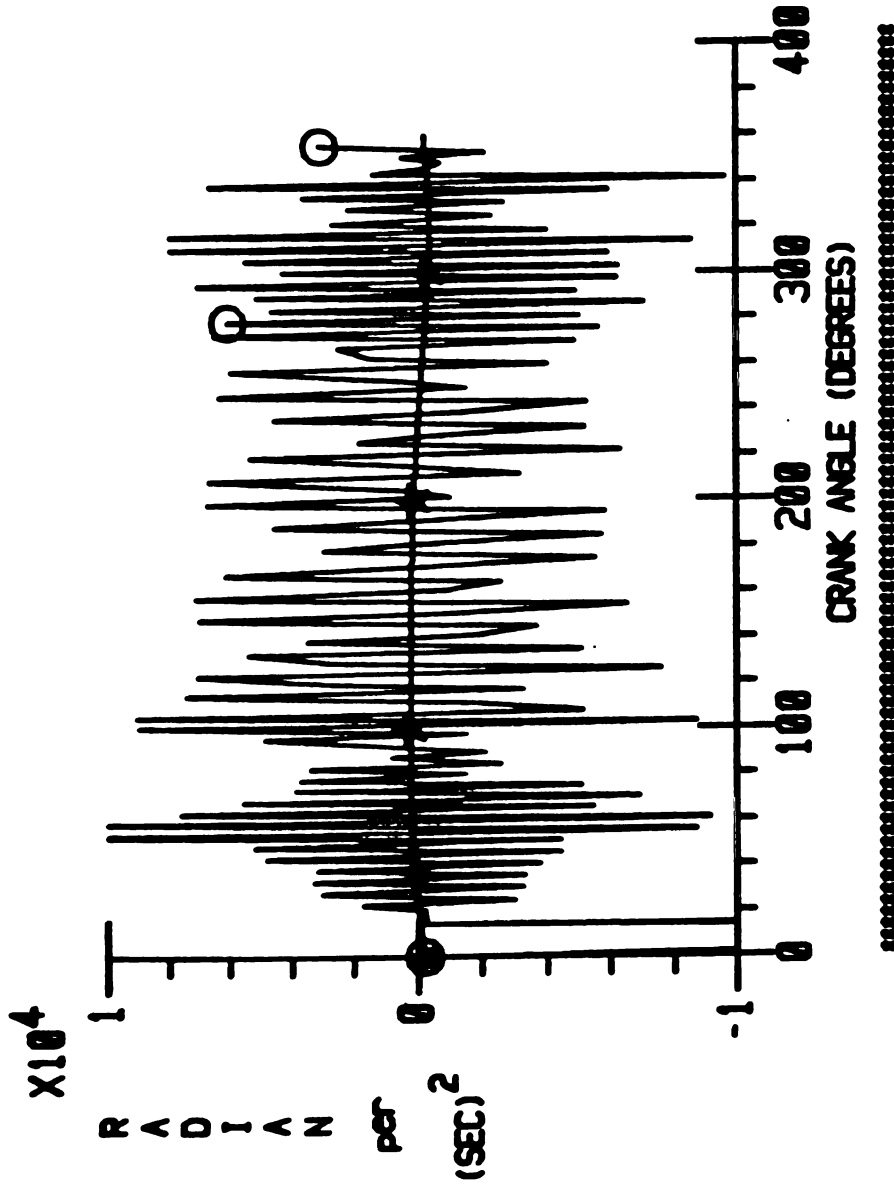
★ 350 RPM, CLEARANCE FREE MECHANISM
O 350 RPM, 0.010 in CLR. IN C-R JOINT

FIGURE 6.14a. COUPLER ANGULAR ACCELERATION (e=1.0)

124

FIGURE 6.14b.   COUPLER ANGULAR ACCELERATION (e=0.50)
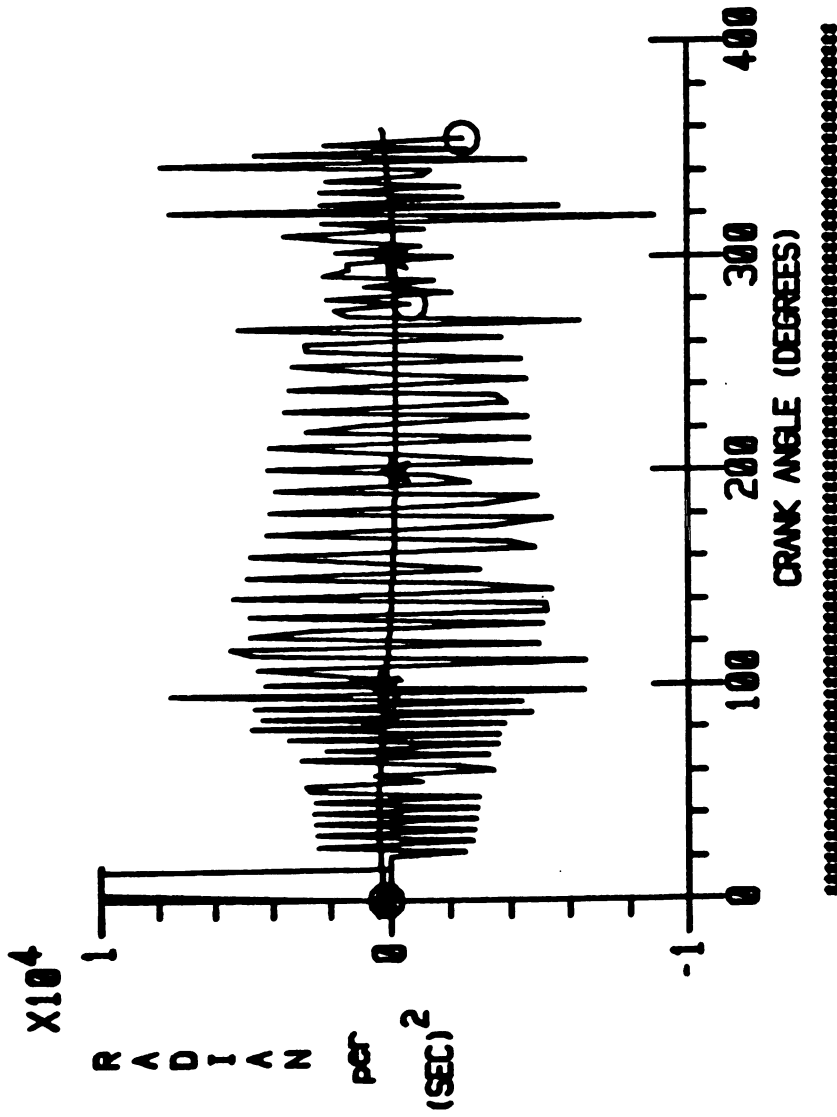
FIGURE 6.15a. ROCKER ANGULAR ACCELERATION (e=1.0)
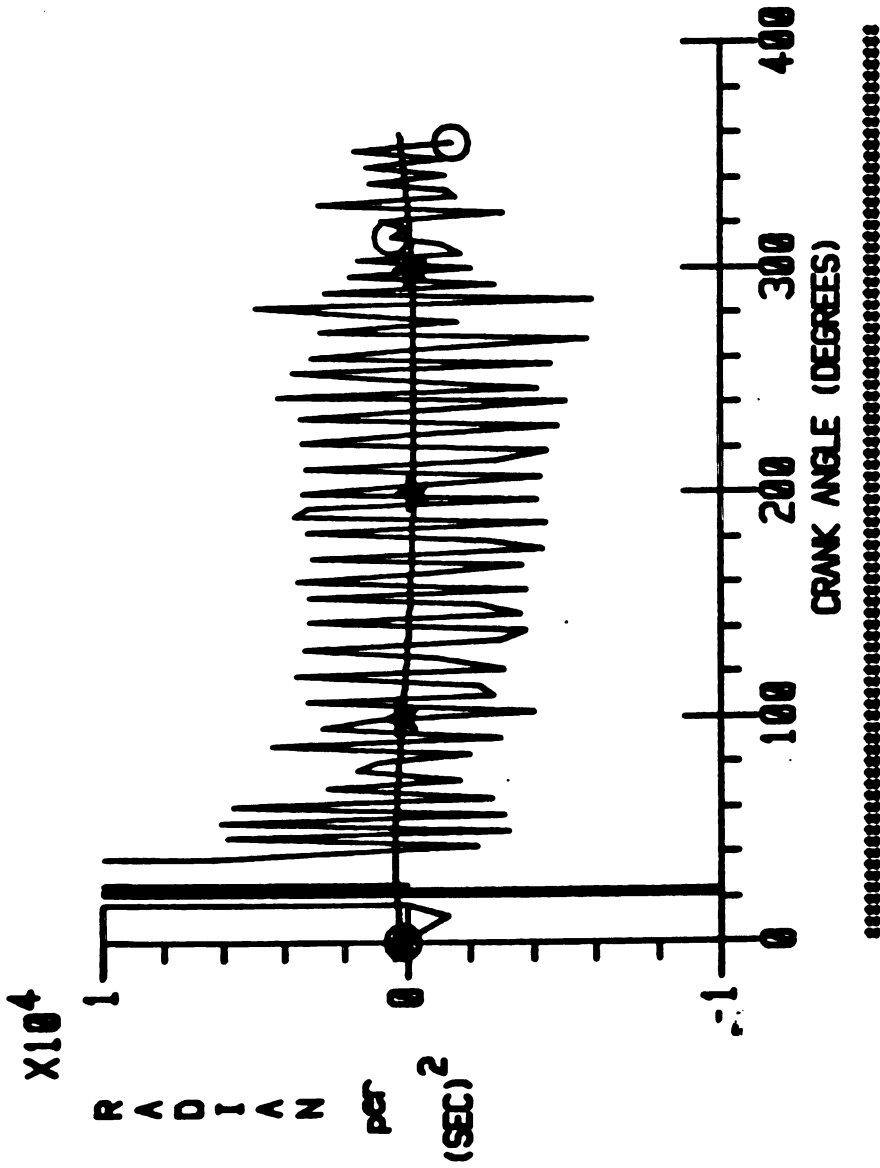
FIGURE 6.15b. ROCKER ANGULAR ACCELERATION (e=0.50)
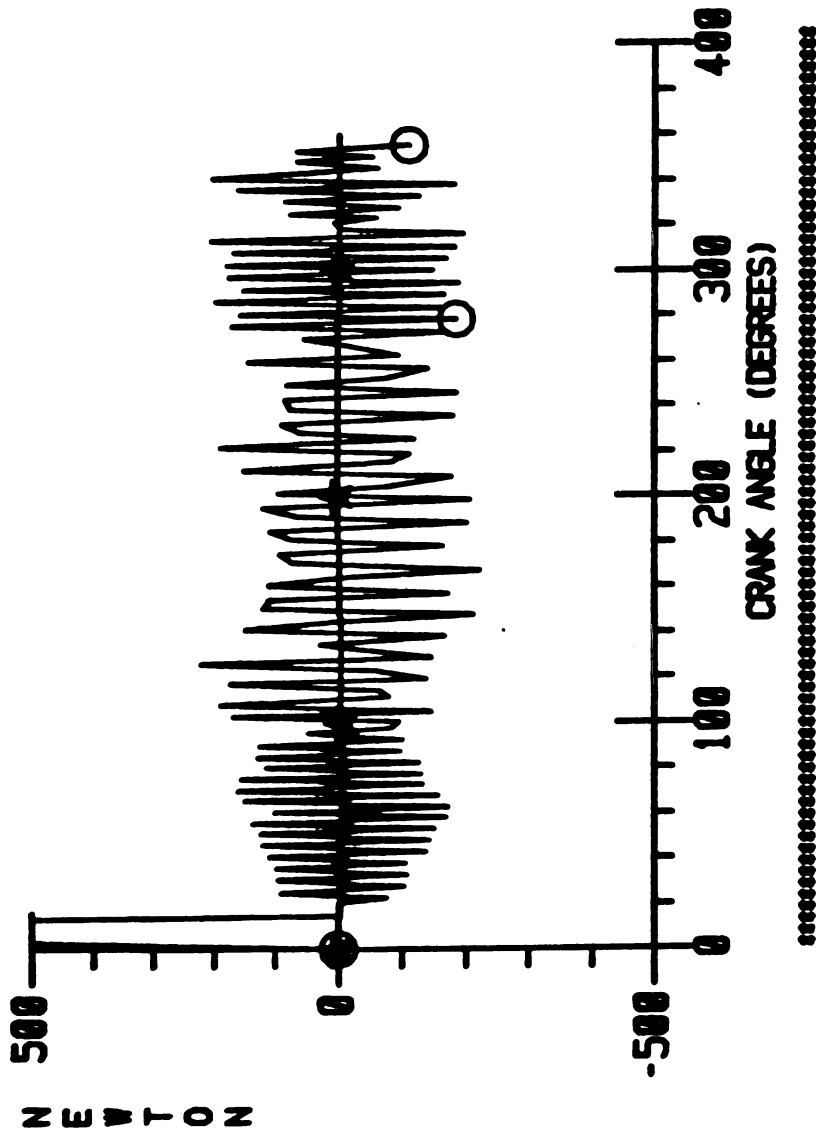
350 RPM. CLEARANCE FREE MECHANISM

350 RPM. 0.010 in CLR. IN C-R JOINT

FIGURE 6.16a.   C-R BEARING REACTION; X-COMPONENT (e=1.0)
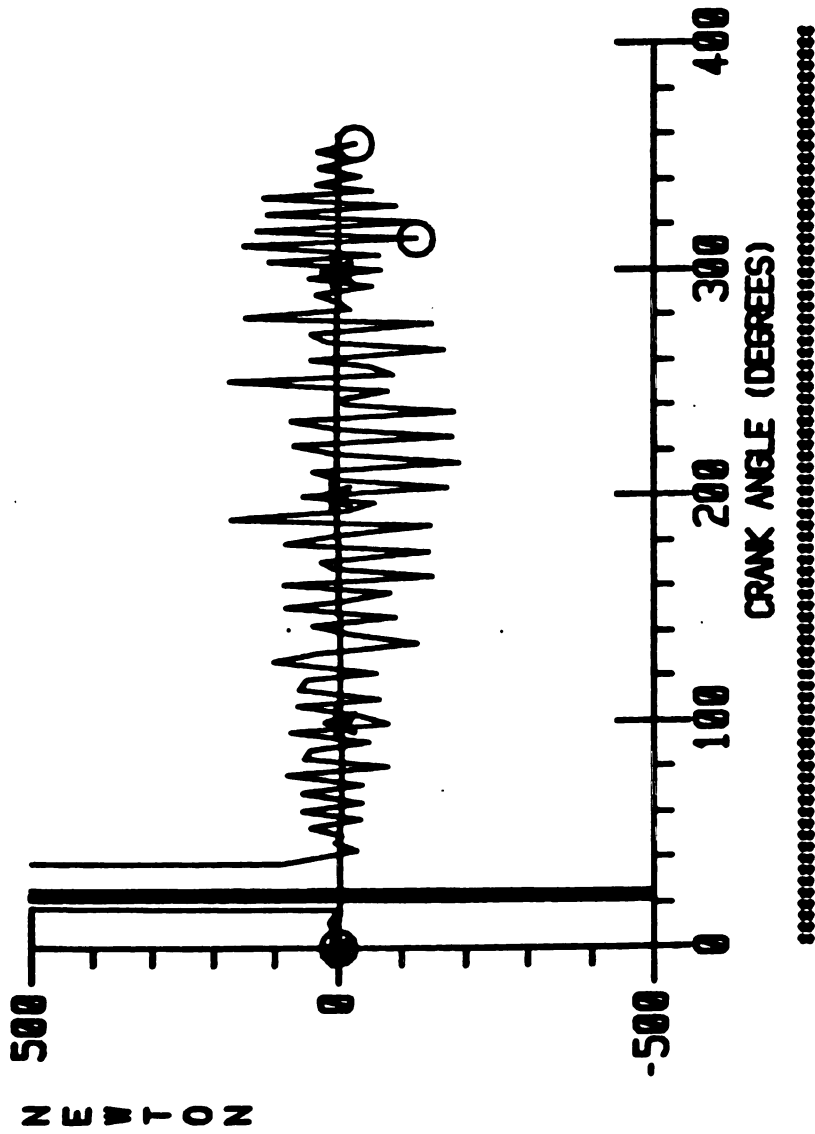
FIGURE 6.16b. C-R BEARING REACTION; X-COMPONENT (e=0.50)

500 —

0 —

-500 —

NEWTON

CRANK ANGLE (DEGREES)

350 RPM, CLEARANCE FREE MECHANISM

350 RPM, 0.010 in CLR. IN C-R JOINT
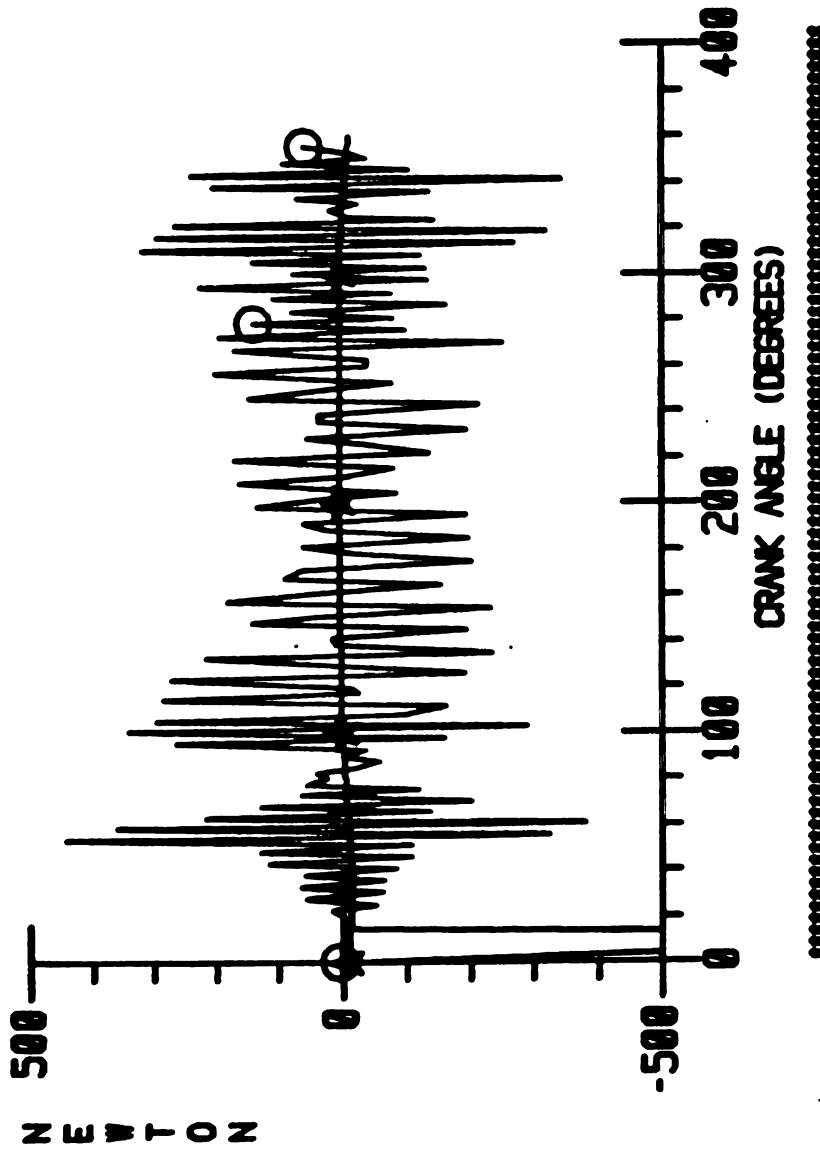
FIGURE 6.17a. C-R BEARING REACTION; Y-COMPONENT (e=1.0)
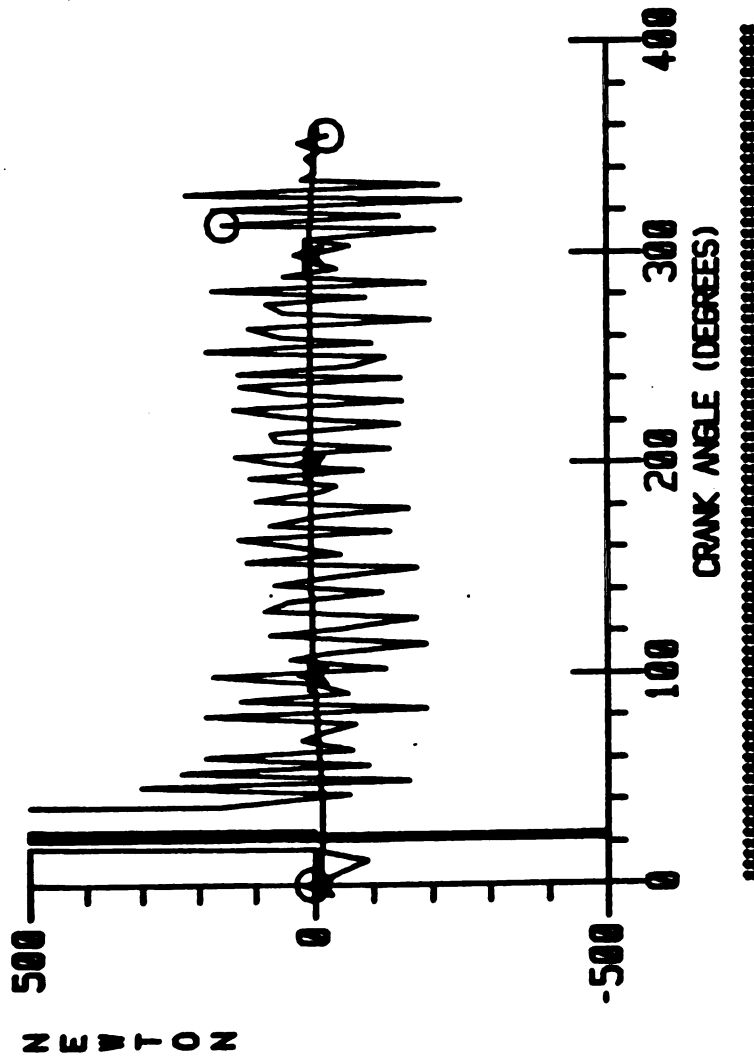
FIGURE 6.17b.   C-R BEARING REACTION: Y-COMPONENT (e=0.50)
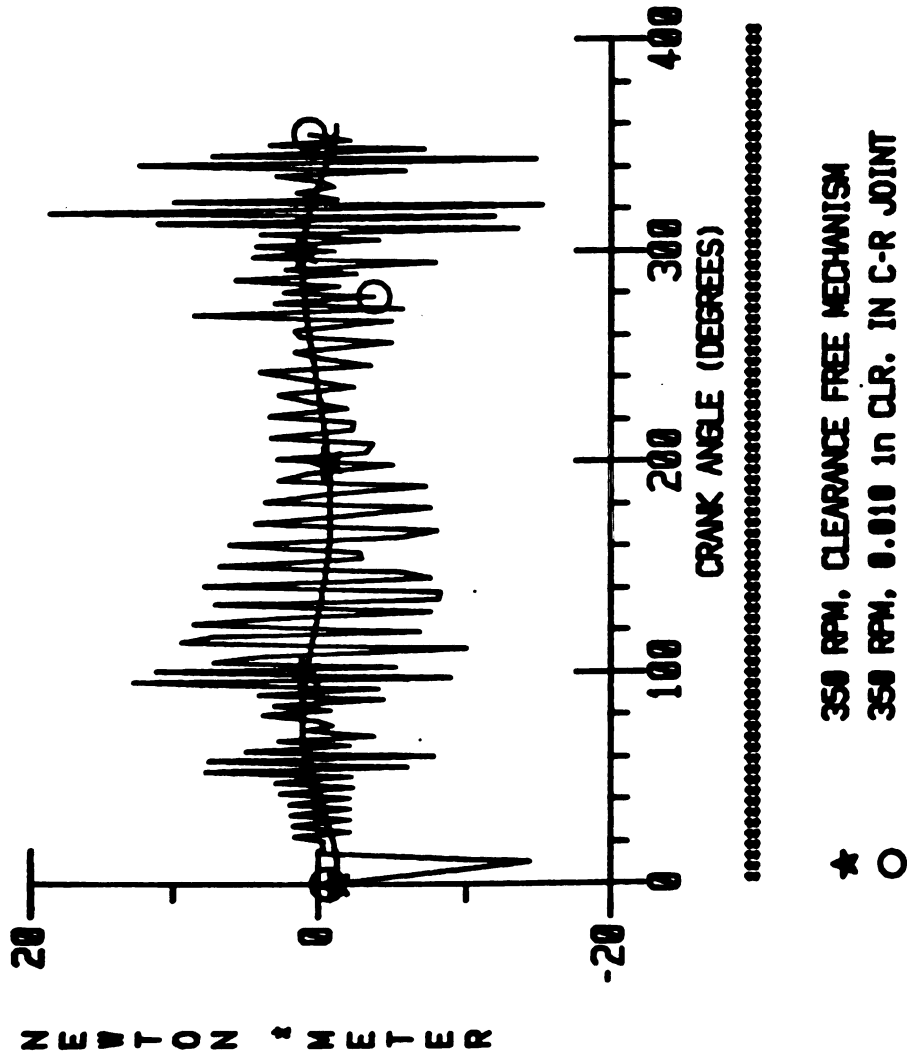
FIGURE 6.18s. CRANK TORQUE (e=1.0)

132
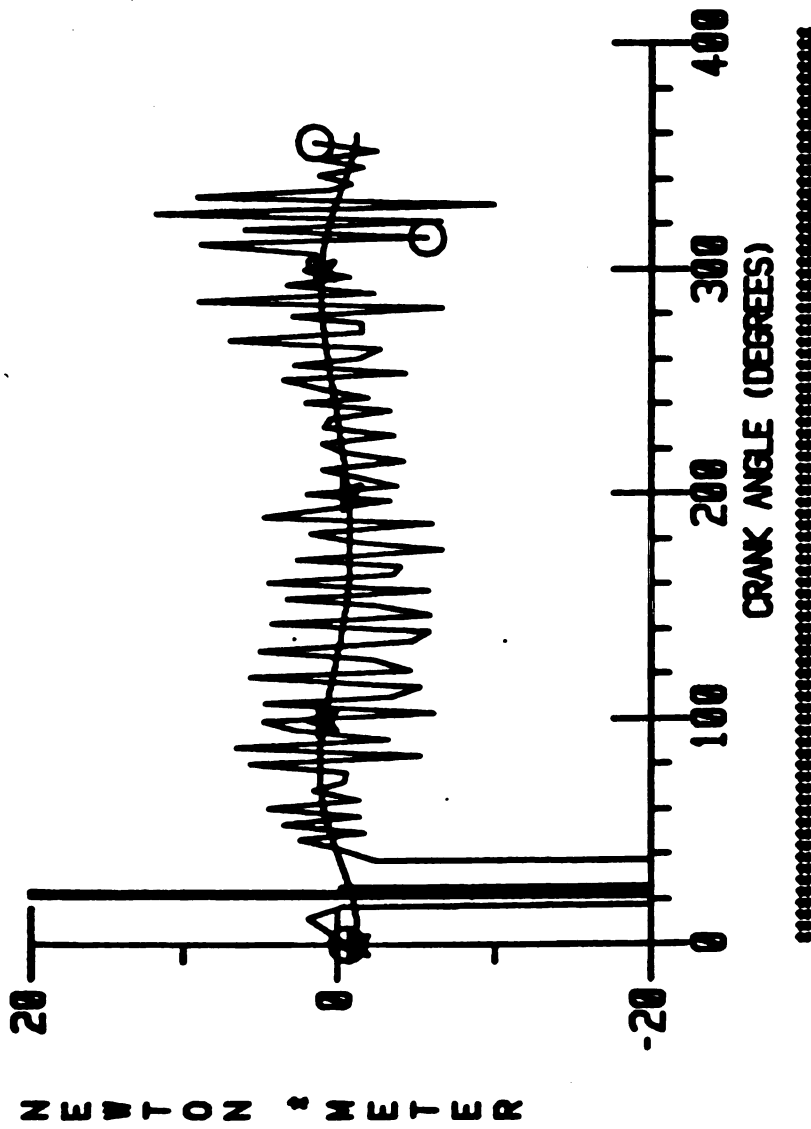
FIGURE 6.18b. CRANK TORQUE (e=0.50)

Figures (6.16) and (6.17) present the X- and Y- components of the coupler-rocker bearing, respectively. Each figure consists of two plots. One for when e=1.0 and, the other for e=0.50. Figures (6.18a) and (6.18b) show the analogous plots of the crank torque for different values of the coefficient of restitution. In all of the latter six plots the effect of magnitude of the coefficient of restitution can be observed.

The reader should note again that, a portion of these plots will be studied further in chapter eight in an effort to correlate the analytical and experimental results. Other sets of plots, such as describing the effect of clearance size on the general response of the system or, other (preferrably smaller) values of the coefficient of restitution could not be obtained due to the frequent occurence of overflow conditions, and/or the extent of time required to simulate the system through one full crank revolution successfully. This is primarily due to the fact that, for instance, as the clearance size is reduced, more precision is required to solve the equations of motion and, simultaneously, detect the occurence of contact-loss or impact time promptly.

The next chapter describes the experimental apparatus and also the instrumentation along with subsequent experimental results. This provides the basis for further comparison of the analytical and experimental results.

CHAPTER SEVEN

EXPERIMENTAL INSTRUMENTATION AND RESULTS

Figure (7.1a) is a photograph of a four bar linkage which furnished the expeimental data and, Figure (7.1b) shows the relevant instrumentation for signal conditioning and recording of the data. A detailed description of the method of data acquisition is also presented.

7.1- Experimental Apparatus

The experimental mechanism (Figure 7.1a) was mounted on a large cast iron table which was bolted to the floor of the laboratory. While the length of the crank link was fixed, the rig was designed such that it could operate with varying lengths of the coupler and rocker links. The two common link lengths used were 16 cm and 30 cm.
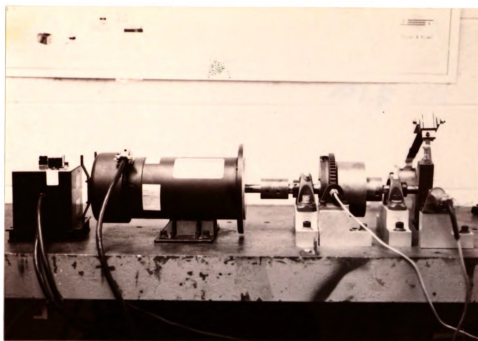
FIGURE 7.1a. PHOTOGRAPH OF THE EXPERIMENTAL RIG

FIGURE 7.1b. PHOTOGRAPH OF THE INSTRUMENTATION

The links were prepared to form coupler and rocker links in practically identical dimensions. At the end of each link two clearance holes were drilled in order to secure them to the bearings. These accomodated socket screws which clamped each link to the bearing housing and, permitted the experimental four bar linkage to be constructed. The links were bolted to the aluminum bearing housings by two socket screws at either end.

The crank-ground, crank-coupler and, rocker-ground joints were all matched pairs of FAG R3 DB R12 ball bearings of 0.25 inches in bore. Each of these bearings was preloaded using a Dresser torque limiting screw driver with ±1.0 in-lbf preloading. This procedure was to ensure that bearing clearance was eliminated. Inaccurate preloading of these bearings would introduce additional clearance into the system or otherwise, produce large frictional forces in these bearings. Either of these conditions would invalidate the assumptions made in chapter two. The coupler-rocker bearing (Figure 7.2), however, which was the joint designed to possess a finite clearance, was a simple pin-and-bushing journal bearing. The bushing was made of oil impregnated brass and, the pin was made of steel. The bearing was designed in a such a manner that the pin could easily be removed, thus making it possible to incorporate a varying range of clearnce sizes into the bearing by simply changing the pin with a one having a different diameter. The range of clearances that could be incorporated into the bearing was from 0.0010 to 0.010 inches with a tolerance of ±0.0005 inches.
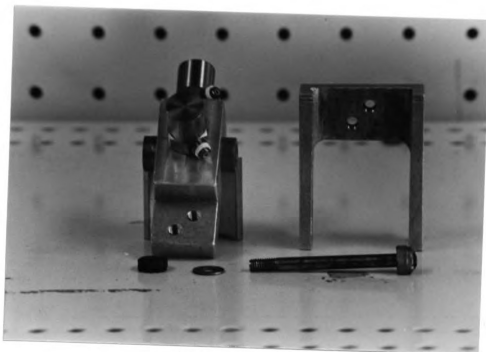
(a)- DISASSEMBLED

(b)- ASSEMBLED
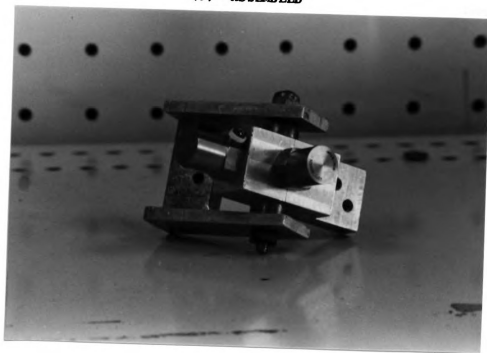
FIGURE 7.2. COUPLER-ROCKER BEARING

A 0.75 hp variable speed DC motor (Dayton 2Z846) powered the crank through a 0.625 inch diameter shaft supported by a cast iron pillow box bearing. A 4.0 inch diameter flywheel was keyed to the shaft, so as to provide a large inertia to ensure minimum fluctuations in the crank angular velocity once a desired crank frequency had been established.

7.2- Instrumentation

A schematic of the the instrumentation employed in the experimental study is shown in Figure (7.3). The rated speed of the electric motor was measured to three decimal places by an HP 5314A universal counter which was activated by a digital-magnetic pickup, model 58423 - Electro Corporation. These devices allowed the operator to adjust the speed controller of the motor in order to achieve the desired crank angular velocity.

The experimental results, shown in subsequent sections, present the variation of coupler and rocker angular velocities and accelerations with respect to the crank angular displacement. These measurements were obtained using a 4371 Bruel and Kjaer accelerometer with delta-shear piezoelectric type of sensor. Figure (7.4) shows the coupler-rocker bearing with two accelerometers mounted for obtaining the data for the coupler link. In order to obtain the same data for the rocker link, the bearing housing is rotated 180 degrees relative to the two links.
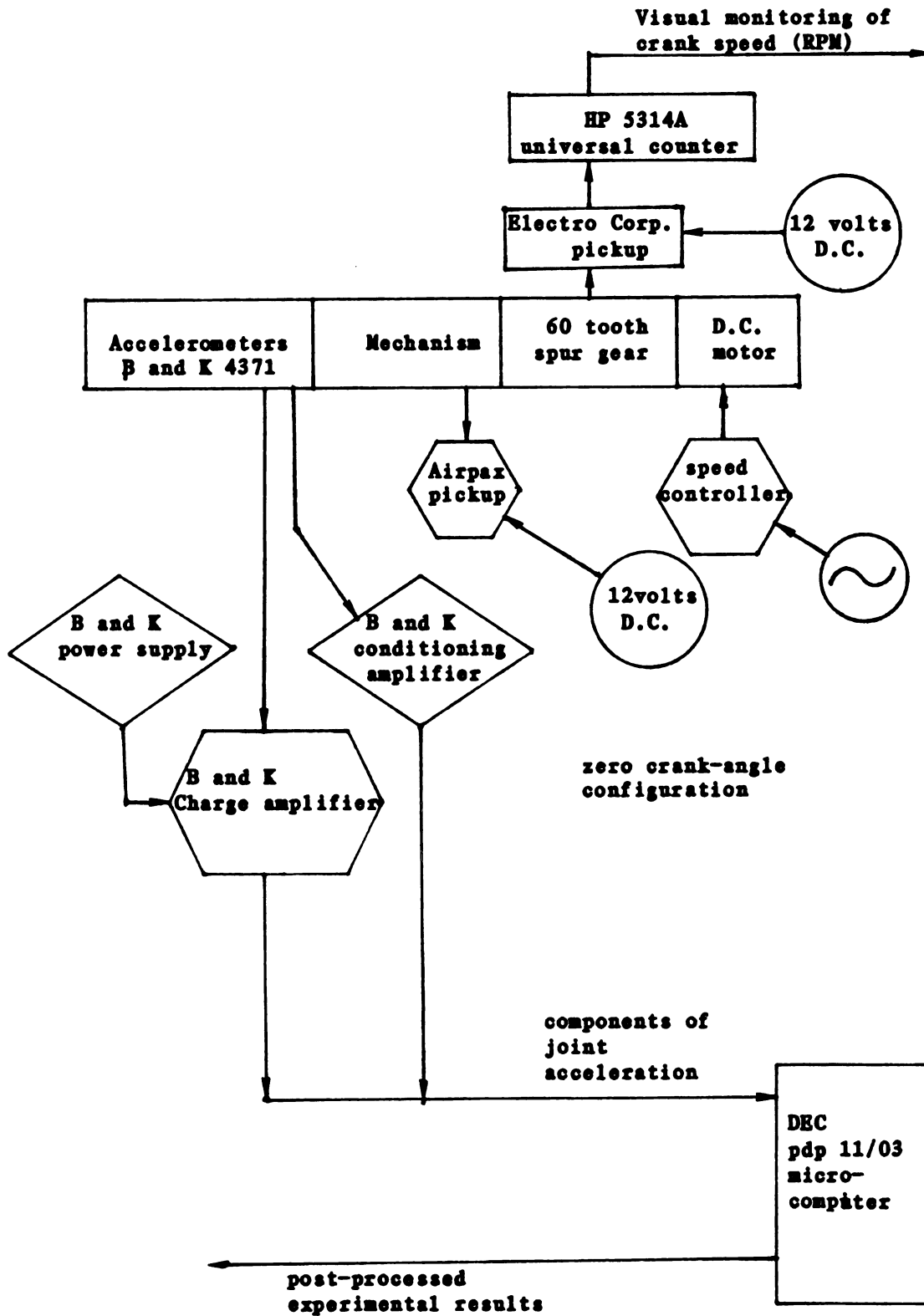
FIGURE 7.3 — SCHEMATIC OF THE INSTRUMENTATION
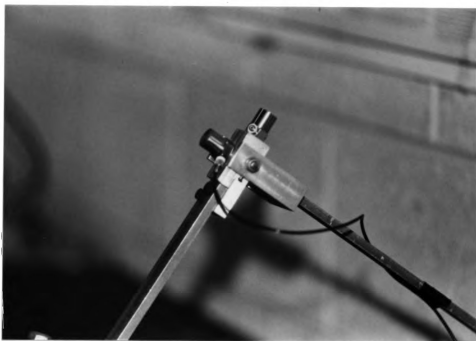
FIGURE 7.4. COUPLER-ROCKER BEARING MOUNTED ON THE MECHANISM

The signal from the accelerometer is sent to a conditioning amplifier of type 2635 Bruel and Kjaer with built-in low-pass filter of variable cutoff frequency. The amplifier can also be adjusted for different gains of amplification ranging from 0.1 to 1000. In addition, the conditioner is capable of simulating a band-pass filter of variable bandwidths. Finally, it is equipped with an integrator, thus enabling one to measure the time-integral of the accelerometer's signal.

The two accelerometers shown in Figure (7.4) measure the normal and tangential components of the absolute acceleration (velocity/displacement) of the four bar linkage at the point of mounting (coupler's end in this figure) with respect to the link. To find the angular acceleration of the links (coupler or rocker), expressions must be found which relate these components of the absolute acceleration to the angular accelration of the link.

7.2.1- Angular Acceleration and Velocity of the Coupler

Figure (7.5) is a two-dimensional view of the mechanism with an accelerometer mounted on the coupler-rocker bearing in order to measure the component of the absolute accelration of the coupler in the direction normal to the link. Using the law of relative reference frames, the following expression for the accelerations can be written

142
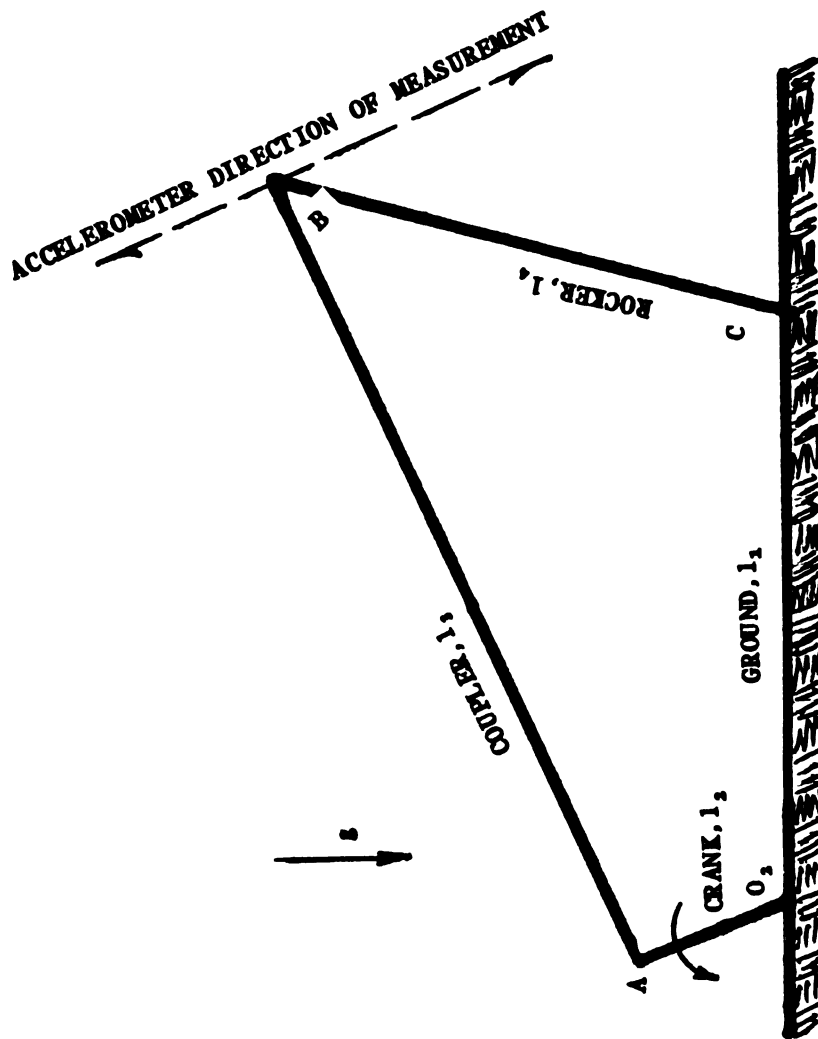
FIGURE 7.5. 2-D VIEW OF THE EXPERIMENTAL RIG

$$\bar{a}_B = \bar{a}_A + \bar{a}_{B/A} \qquad (7.2.1-1)$$

where the equation is in vector form, and $\bar{a}_{B/A}$ is the acceleration of point B relative to point A.

The terms on the right hand side of equation (7.2.1-1) can be written in their normal and tangential components with respect to their corresponding links as follows

$$\bar{a}_A = \bar{a}_{A_n} + \bar{a}_{A_t} \qquad (7.2.1-2a)$$

where

$$a_{A_n} = 1_2 \omega_2^{2}$$

$$a_{A_t} = 0$$

and also

$$\bar{a}_{B/A} = (\bar{a}_{B/A})_n + (\bar{a}_{B/A})_t \qquad (7.2.1-2b)$$

where

$$(a_{B/A})_n = 1_3 \omega_3^{2}$$

$$(a_{B/A})_t = 1_3 \alpha_3$$

A graphical representation of equation (7.2.1-1) with the help of equations (7.2.1-2) is shown in Figure (7.6). From this figure the following expressions can be derived

$$a_{B_x} = -1_2\omega_2^2\cos\Theta_2 - 1_3\omega_3^2\cos\Theta_3 - 1_3\alpha_3\sin\Theta_3 \qquad (7.2.1-3a)$$

$$a_{B_y} = -1_2\omega_2^2\sin\Theta_2 - 1_3\omega_3^2\sin\Theta_3 + 1_3\alpha_3\cos\Theta_3 \qquad (7.2.1-3b)$$

thus the tangential component of equations (7.2.1-3) can be expressed as

$$(a_{B_x})_t = a_{B_x}\sin\Theta_3 \qquad (7.2.1-4a)$$

$$(a_{B_y})_t = a_{B_y}\cos\Theta_3 \qquad (7.2.1-4b)$$

but

$$(a_B)_t = (a_{B_x})_t - (a_{B_y})_t \qquad (7.2.1-5)$$

Hence, substitution of equations (7.2.1-3) and (7.2.1-4) into equation (7.2.1-5) and carrying out a few algabraic steps yields the desired expression of the angular acceleration of the coupler link in terms of the measured tangential component of the absolute acceleration of the coupler link in the tangential direction, i.e.,

$$\alpha_3 = 1.0/1_3\left[1_2\omega_2^2\sin(\Theta_2 - \Theta_3) - (a_B)_t\right] \qquad (7.2.1-6)$$
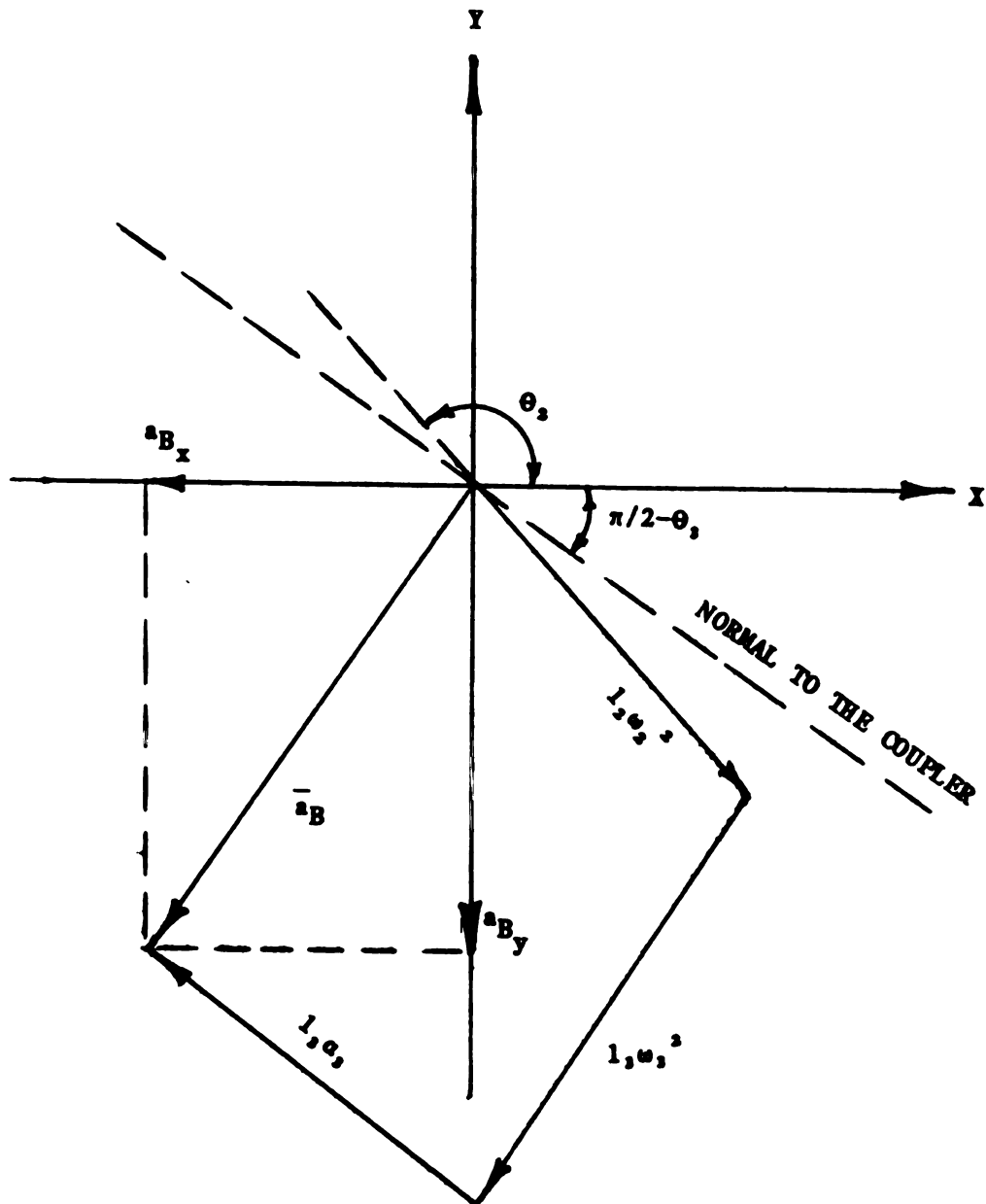
FIGURE 7.6. GRAPHIC REPRESENTATION OF EQUATION (7.2.1-1)

The angular velocity of the coupler can be found in an analogous manner to the above procedure. However, due to some difficulties, which was mainly attributed to the characteristic behavior and response of the integrating circuit components of the signal conditioner/amplifier used, the computation of the conversion factor needed to obtain the correct values of the angular velocities was not advantageous due to the extent of time and the laborious calculations involved. Thus, another method was used to determine the angular velocity of the coupler link. This alternate method is an adaptation of the simple trapezoidal rule whose thorough description can be found in any numerical analysis text such as [88]. Nevertheless, the salient features of this method will be presented here.

Suppose $f(x)$, a continuous function over interval [a,b], is to be integrated. i.e.,

$$I = \int f(x)dx$$

where the limits of integration are from x=a to x=b. The area under the curve $f(x)$ between a and b can be divided into n equal intervals. The boundaries of the resulting trapezoids are X_0, X_1, ... , X_n on one side and, $f(x_1)$, $f(x_2)$, ... , $f(x_n)$ on the other side. It can be readily noted that, the above integral, I, can be approximated by the total area of the n trapezoids, i.e.,

$$I=w/2\left[f(x_0)+2f(x_1)+2f(x_2)+\ldots+2f(x_{n-1})+f(x_n)\right]$$

(7.2.1-8)

where w is the length of the subintervals or,

$$w=(b-a)/n$$

In our case, the function to be integrated is defined at equally-spaced, discrete points, thus fixing the number of subintervals. This is due to the fact that the signal is sampled at a certain rate implying that the accuracy is directly proportional to the sampling rate.

7.2.2- Angular Acceleration and Velocity of the Rocker

Figure (7.7) is similar to Figure (7.5) except that, the accelerometer is mounted to measure the component of the absolute acceleration or velocity of the rocker tangent to the link. It can be observed that the angular acceleration (velocity) of the rocker link can be obtained by simply dividing the experimentally measured value of the acceleration (velocity) by the length of the rocker link, i.e.,

$$\alpha_4 = a_{Bt}/l_4$$

(7.2.2-1)

and

$$\omega_4 = V_{Bt}/l_4$$

(7.2.2-2)

148
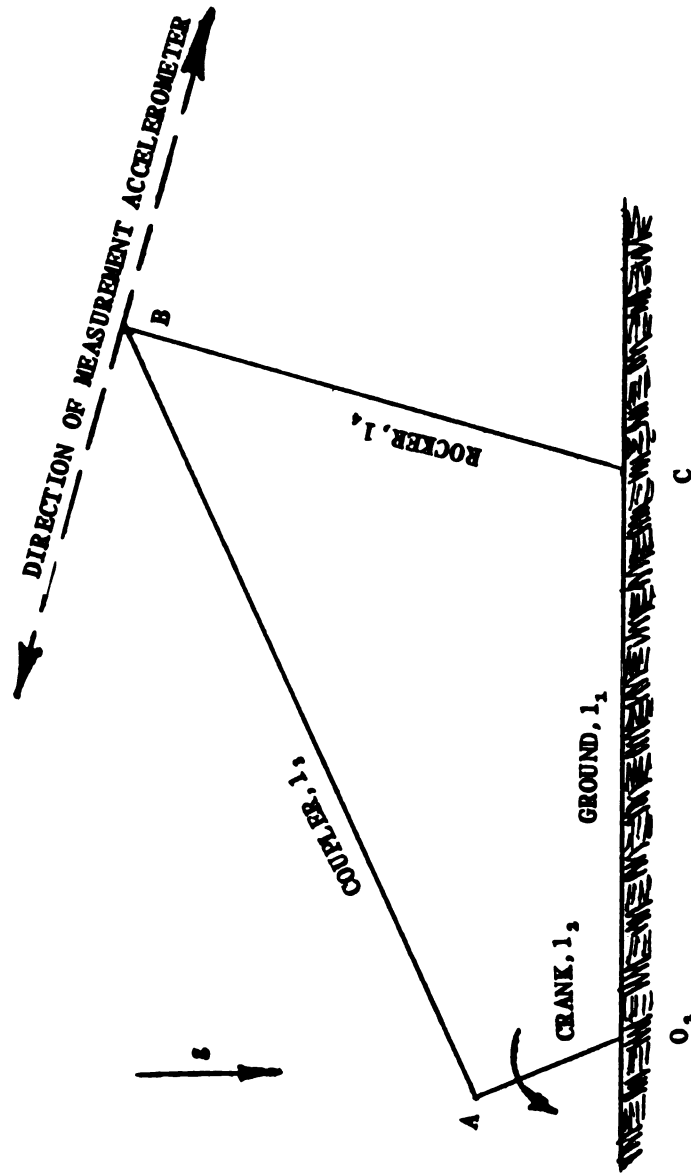
FIGURE 7.7. 2-D VIEW OF THE MECHANISM

In order to relate the accelerometer signal to the configuration of the experimental mechanism, another transducer arrangement was established. A zero velocity digital pickup, an Airpax 14-0001, was located so as to sense the bolt head mounted at the end of the crank when the four bar linkage was in the reference position of zero-degree crank angular displacement.

Thus the mechanism configuration signal and also, the conditioned and amplified output from the accelerometer were fed to the oscillo-scope for real-time visual monitoring of the response. In addition to obtaining photographs using a C-5C camera attachment for the oscillo-scope, the signal could also be fed to a digital data acquisition system (DEC PDP-11/03 microcomputer with 5 Mb storage on hard disk).

The BNC cables from the experimental apparatus were connected to an input-output module. This device has 16 analog-digital conversion channels, 4 digital-analog channels and, Schmitt triggers one and two. Using the code developed for acquisition of data, the response of the mechanism was recorded from the zero crank angle position through 360 degrees. The sampling of the data was initiated by firing of the Schmitt trigger two.

Once the data was sampled and stored, some further conditioning was carried out on the results. In almost all of the experiments, the signal had some degree of noise embedded within it, even after passing through the conditioning amplifier previously mentioned. There are

various sources that could contribute to the generation of the noise. For instance, if the environment is 'polluted' by electromagnetic fields generated by nearby radar and satellite stations or fluorescent lighting, the effect can be picked up at practically any point along the instrumentation, such as the accelerometer itself, the cables and connections and, any unshielded section of the circuitry or, poor grounding, and so forth.

Nevertheless, the severity of the noise in the sampled signal can be alleviated by simulating a digital band-pass filter, which is merely a code incorporating the Fast Fourier Transform (FFT) algorithm. The filtering is done by transforming the data from time-domain into frequency-domain, thus yielding the power spectrum of the signal. Figure (7.9) illustrates one such spectrum. At this stage, the signal can be studied and analyzed at different and discrete frequencies depending on the frequency resolution of the FFT routine, which in turn is dictated by the sampling rate. In this manner, the frequencies associated with noise can be identified and eliminated by 'fading' the amplitude of the signal at those particular frequencies. Once the noise is attenuated, the result, which is in the frequency-domain, is transformed back into the time-domain using the same FFT routine in reverse order.

Since the sampling rate is about 2.7 KHz, the maximum frequency available to work with in the frequency-domain is in the neighborhood of 1.3 KHz. In other words, in order to avoid aliasing (overlapping
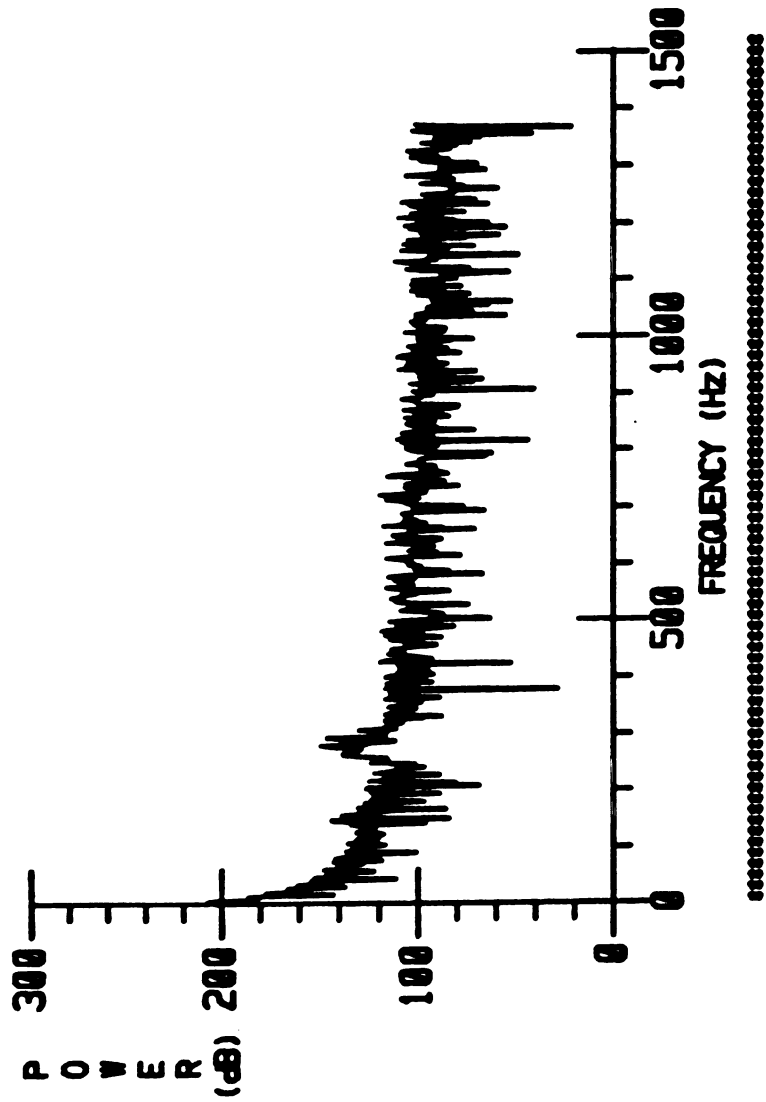
350 RPM, 0.010 in CLR IN C-R JOINT

FIGURE 7.8.   A TYPICAL POWER SPECTRUM

of two successive periods of the signal), the Nyquist rate (minimum allowable sampling rate) should be at least twice the maximum frequency desired [87].

It should be noted that, the windowing function adapted in the FFT routine is the simplest type, namely, the rectangular windowing function. This function has the disadvantage of introducing some additional degree of noise in the frequency-domain. However, once transformed back into the time-domain, all of these secondary generated noises are offset and hence, the net result of the noise associated with the type of the windowing function is zero. If a more accurate or, less noisy power spectrum is desired, windowing functions of higher order such as Kazier's function may be used [87].

7.3- Experimental Results

Table (7.1) is a duplicate of table (6.1) along with some additional information, such as the working range of the motor driving the crank link and, so forth. Although the motor was capable of driving the crank with angular velocities in excess of 2000 RPM, the highest speed used for the experiments was about 350 RPM. This was merely a precautionary step in order to avoid damaging the setup due to the exertion of large magnitudes of forces and impulses acting upon some parts of the system with relatively low strength such as the pin of the coupler-rocker bearing.

TABLE (7.1)
SPECIFICATIONS OF THE EXPERIMENTAL MECHANISM

link	length (size) (mm)	center of gravity (mm)	mass (kg)	mass moment of inertia (kg.mm^2)
Crank	64.0	9.0	0.6095	2645.0
Coupler	309.0	185.0	0.2439	2950.0
Rocker	312.0	134.0	0.2334	3176.0
Ground	387.0	——	——	——

Clearance size : 0.02540-0.2540 mm   (0.0010-0.010 inches)

Crank angular velocity : 0-2500 RPM

Crank angular acceleration : 0.0 rad/sec^2

Gravitational acceleration : 9814.5 mm/sec^2

Two different types of effects will be investigated in this experimental phase of the work. First, the effect of varying the angular velocity of the crank for a fixed clearance size will be studied. To perform this task, comparison will be made between the angular acceleration of the coupler link at 250, 300 and, 350 RPM. This test is carried out for four different clearance sizes of 0.0010, 0.0040, 0.0070 and, 0.010 inches.

In the second phase of the study, the effect of the variation of the clearance size is investigated for a fixed crank RPM. This set of experiments is performed for three different crank angular velocities of 250, 300 and, 350 RPM. Analogous experiments are carried out for the rocker link.

Figures (7.9a) to (7.9d) show the coupler angular acceleration at 350 RPM with four different clearance sizes. Note that, superposition of all of the experimental results are avoided in order to prevent loss of clarity of individual plots since the responses differ from each other by relatively small amounts.

A note is in order at this point. Mansour et. al. [7] introduced a design-oriented concept in order to be able to describe the severity of the response of the system due to the occurence of frequent impacts in the bearing of the mechanism possessing a finite clearance. Recalling from chapter five that F represents the magnitude of the tangential impulse at impact, it would be reasonable to
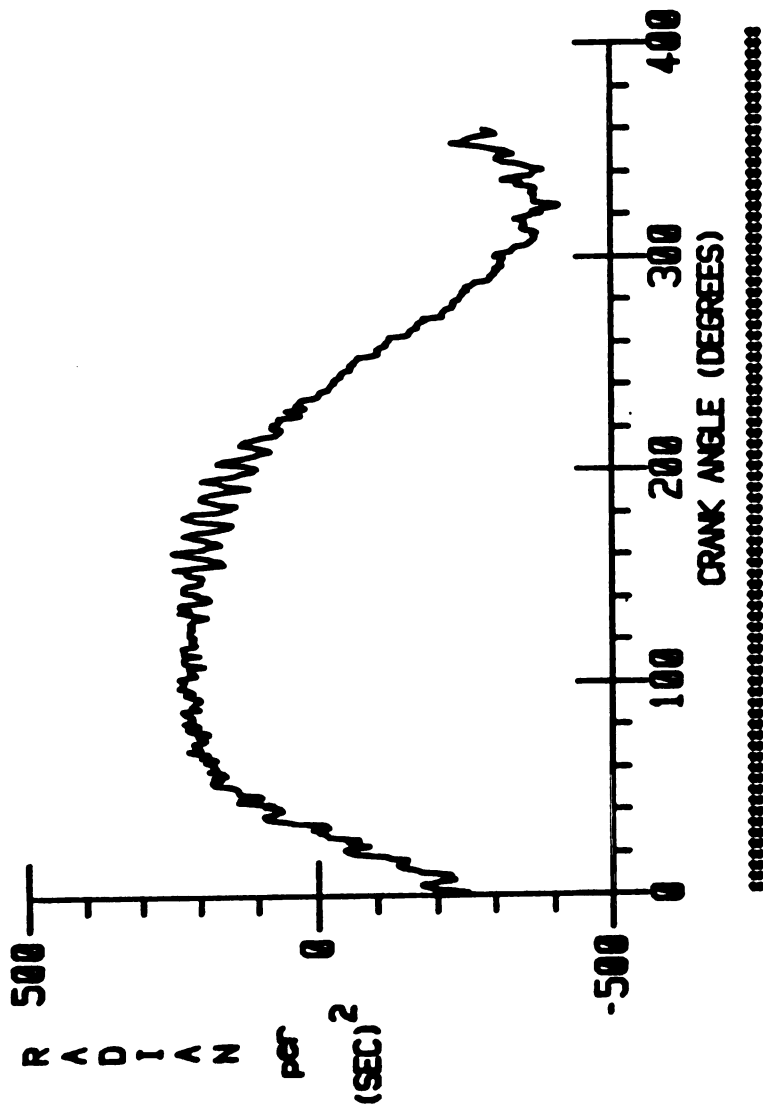
350 RPM. 0.0010 in CLR IN C-R JOINT

FIGURE 7.9a.   COUPLER ANGULAR ACCELERATION
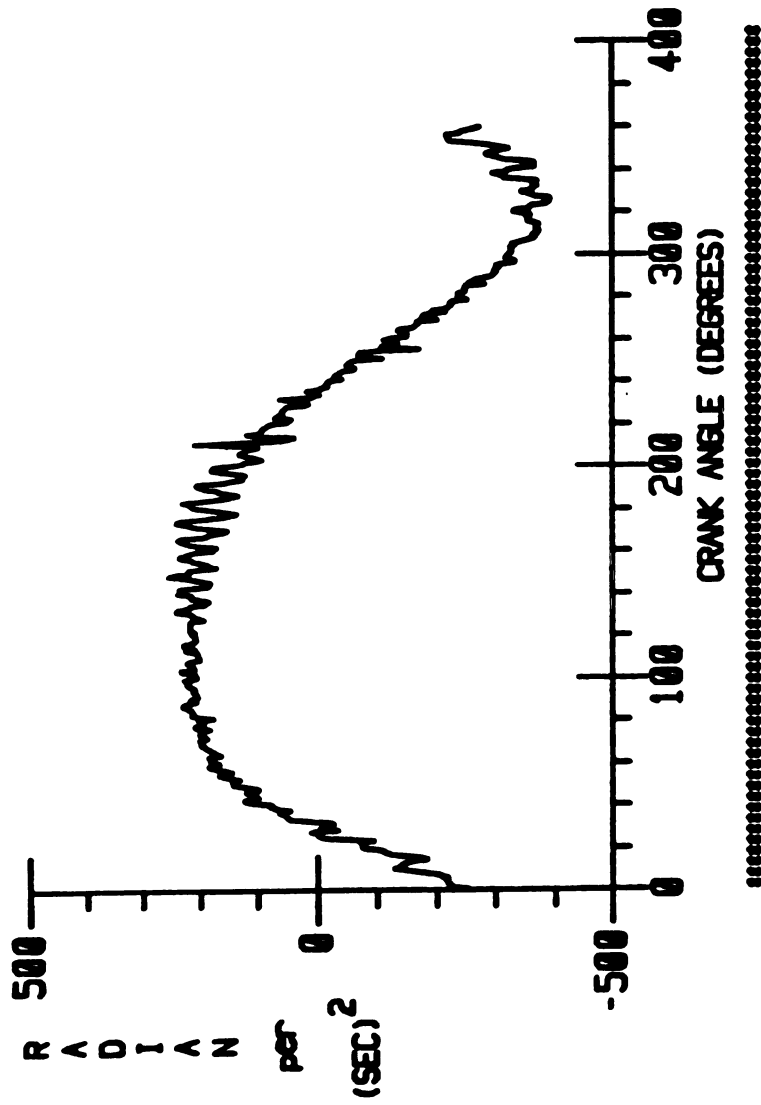
FIGURE 7.9 b.   COUPLER ANGULAR ACCELERATION

350 RPM, 0.0070 in CLR IN C-R JOINT

FIGURE 7.9.c.   COUPLER ANGULAR ACCELERATION

350 RPM, 0.010 in CLR IN C-R JOINT

FIGURE 7.9d.   COUPLER ANGULAR ACCELERATION

assume that, a useful way of describing the effect of presence of bearing clearance in a mechanism is to express that in terms of the summation of all of the tangential impulses for one crank revolution, namely, $\sum F$. This criterion can be improved further if an index number is deviced which would be the ratio of the $\sum F$ over the total number of impacts, n, for that specific cycle of revolution. If such an index is called I_n then by definition

$$I_n = \sum F / n$$

The advantage of using such terminology is that, the severity and sensitivity of the response of the system to the presence of clearance in a bearing of the mechanism can be described with a single number. It is quite helpful to present two of the plots that Mansour et. al. [7] developed in their work. Although these plots are based on a computer simulation of a model which only adapted the free-flight and impact modes for modeling, they can be correlated to some extent to the experimental results presented in the following. Such a correlation is merely for a better understanding of the experimental results by being able to observe the effect of, for instance, variation of the crank angular velocity on a single plot.

Figure (7.10) depicts the effect of the variation of the clearance size and, Figure (7.11) shows the effect of the variation of the crank speed. The numerical values on the axes of the plots are of no
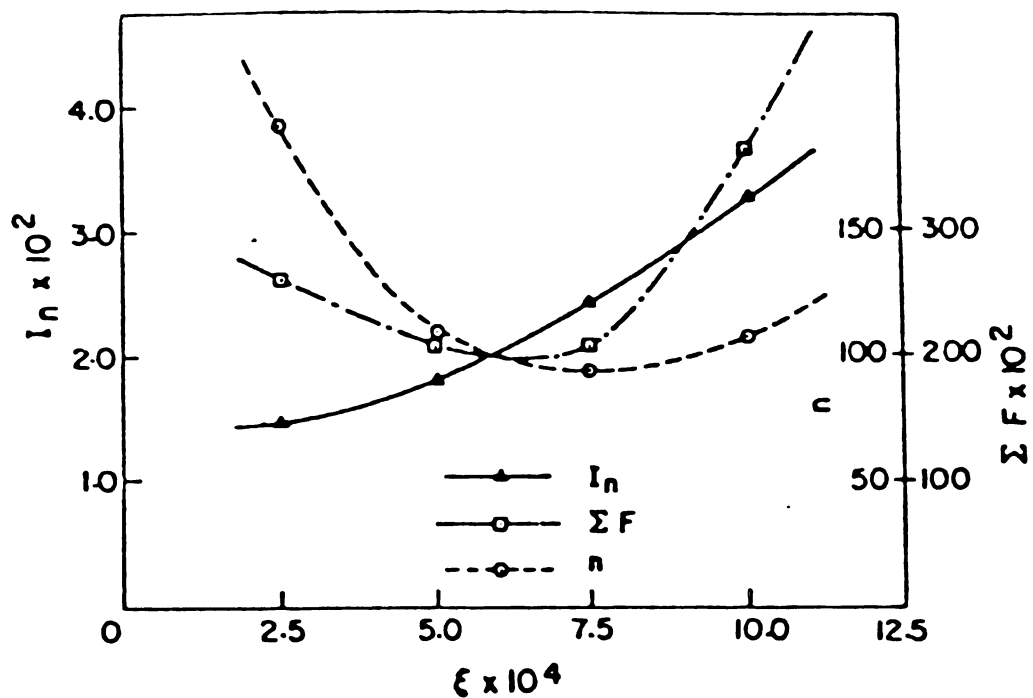
FIGURE 7.10. EFFECT OF VARIATION OF ξ ALONE
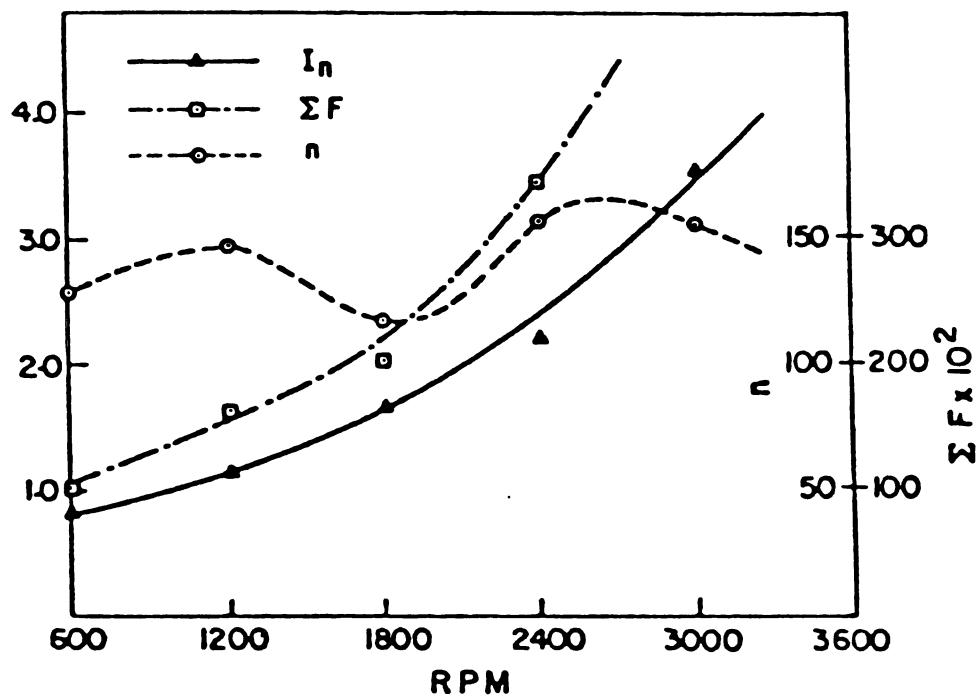
FIGURE 7.11. EFFECT OF VARIATION OF THE RPM ALONE

primary value here and, emphasis should be given mainly to the 'shape' of the individual plots.

Referring to Figures (7.9), it may be observed that, the severity of the amplitudes of oscillations of the coupler angular acceleration diminishes slightly as the clearance is increased from 0.0010 to 0.010 inches. Such a behavior can also be observed on the $\sum F$ curve of Figure (7.10) corresponding to the portion of the plot whose slope is negative. Similar results of Figures (7.9) are shown for the rocker link in Figures (7.12).

Figures (7.13) illustrate another case of variation of the clearance size for a crank angular acceleration of 250 RPM. In this case, as the clearance size increases, so does the severity of the fluctuations or $\sum F$, corresponding to the positive-slope portion of the $\sum F$ curve of Figure (7.10). On the other hand, Figures (7.14) show the same comparison while the crank was running at 300 rpm. As can be seen, the oscillations amplitudes decrease as the clearance size is increased from 0.0010 to 0.0040 inches (Figures 7.14a and 7.14b) and then remain relatively the same for a clearance of 0.0070 inches (Figure 7.14c) and, then again, it starts to increase for 0.010 inches (Figure 7.14d). Such a behavior can be related to the $\sum F$ curve of Figure (7.10) with cases corresponding to Figures (7.14a) and (7.14b) being on the negative-slope portion of the curve and, those of Figures (7.14c) and (7.14d) on the positive-slope portion of the curve.

162
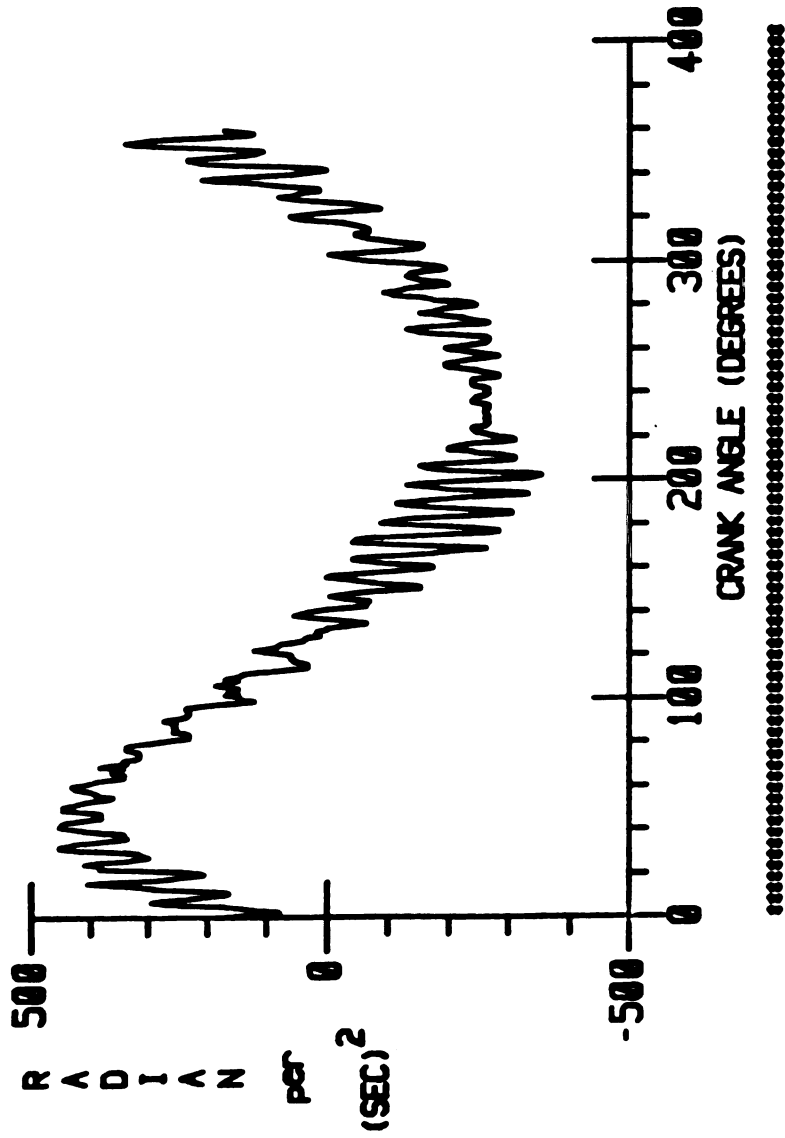
350 RPM, 0.0010 in CLR IN C-R JOINT

FIGURE 7.12a. ROCKER ANGULAR ACCELERATION
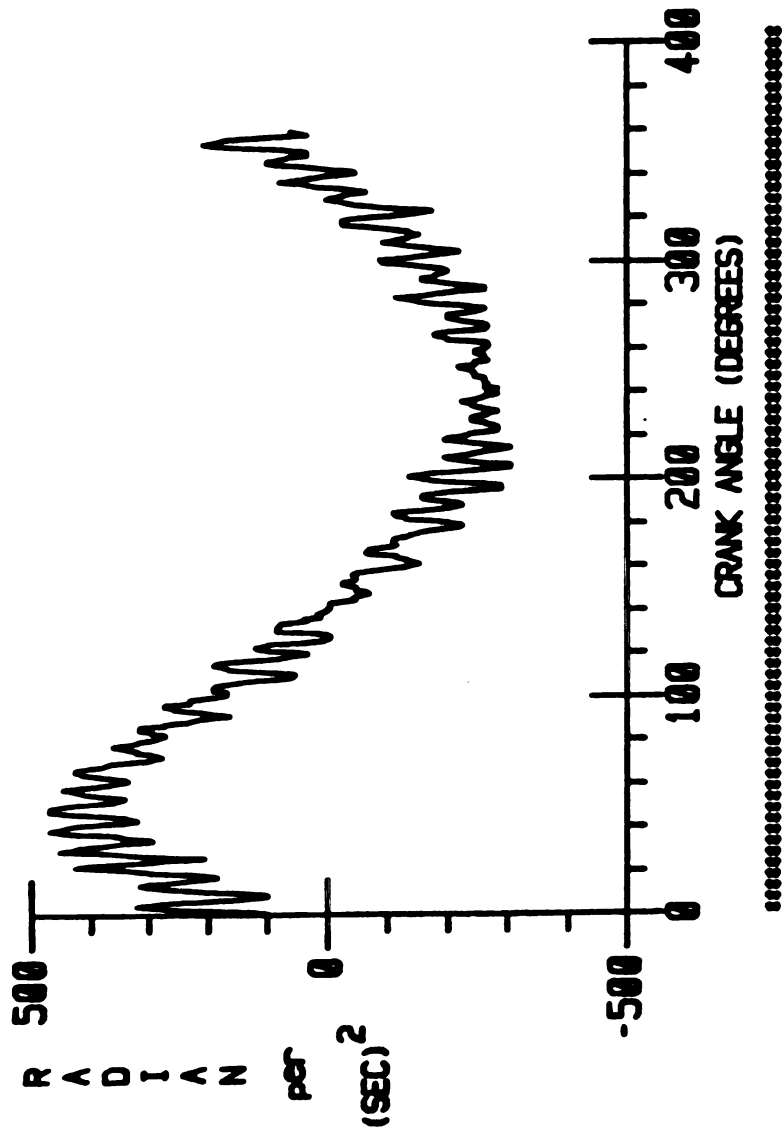
350 RPM. 0.0040 in CLR IN C-R JOINT

FIGURE 7.12b. ROCKER ANGULAR ACCELERATION

350 RPM, 0.0070 in CLR IN C-R JOINT

CRANK ANGLE (DEGREES)
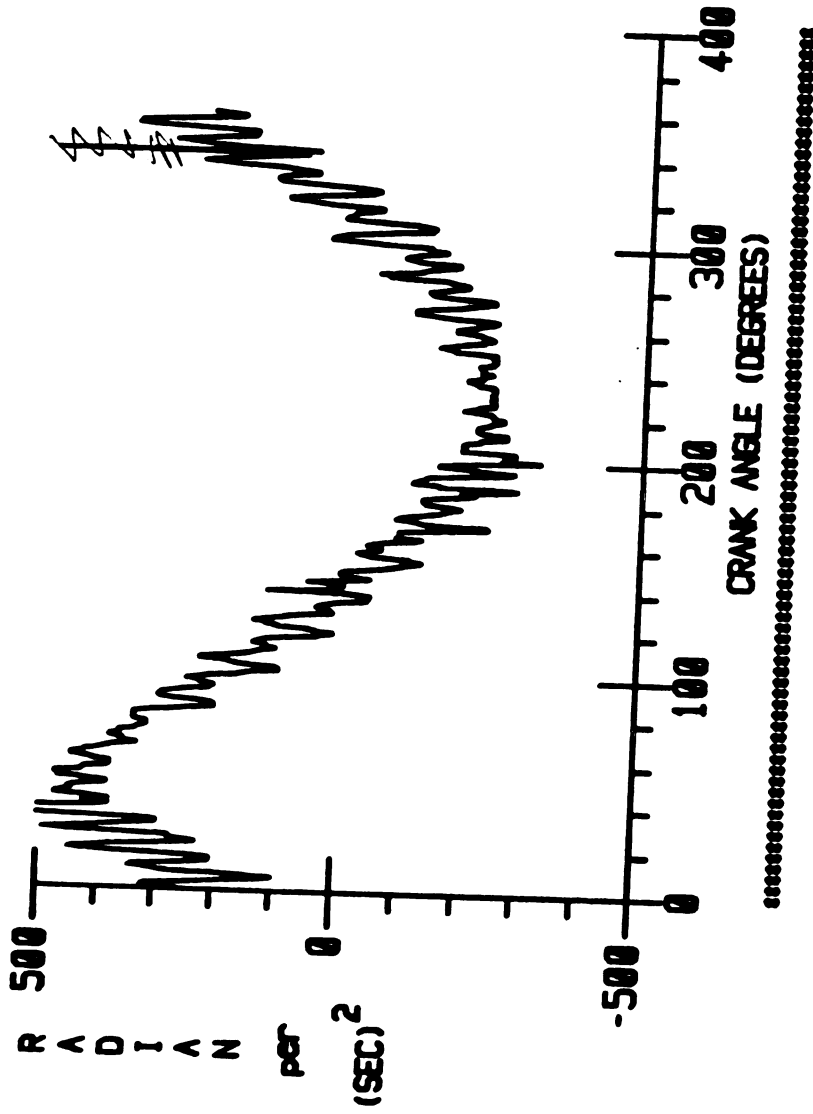
FIGURE 7.12: c.   ROCKER ANGULAR ACCELERATION

350 RPM. 8.010 in CLR in C-R JOINT

FIGURE 7.124.   ROCKER ANGULAR ACCELERATION

166
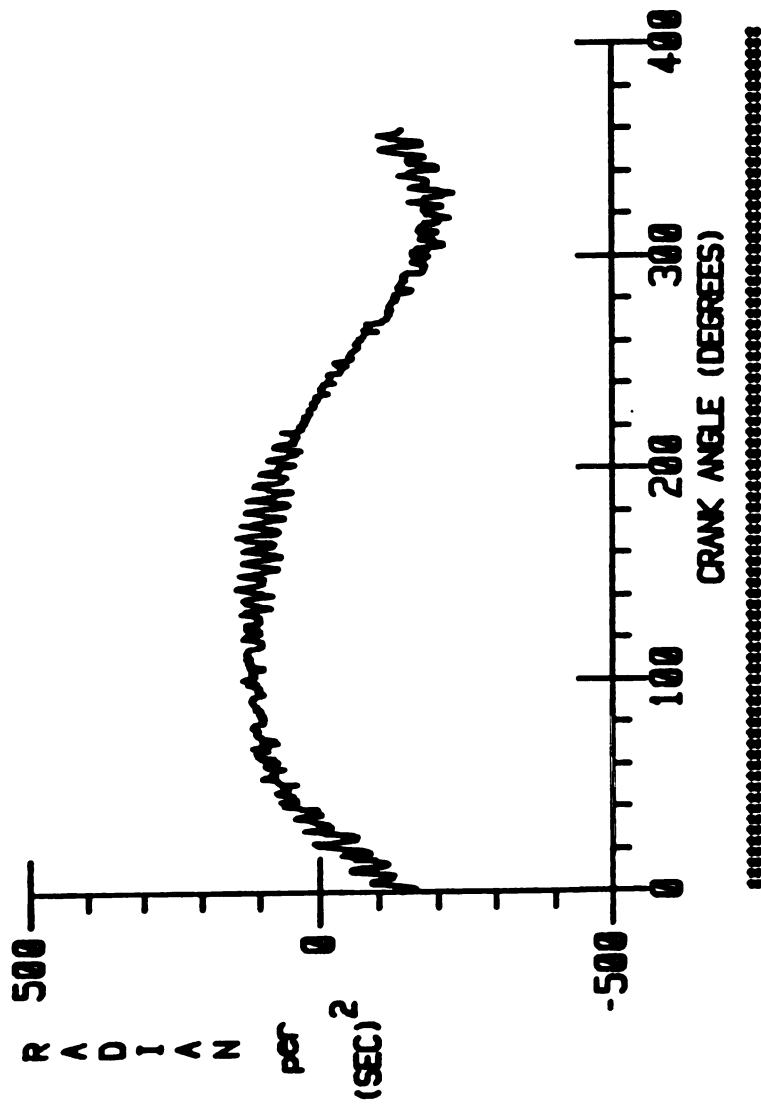
250 RPM, 0.0010 in CLR IN C-R JOINT

FIGURE 7.13a. COUPLER ANGULAR ACCELERATION
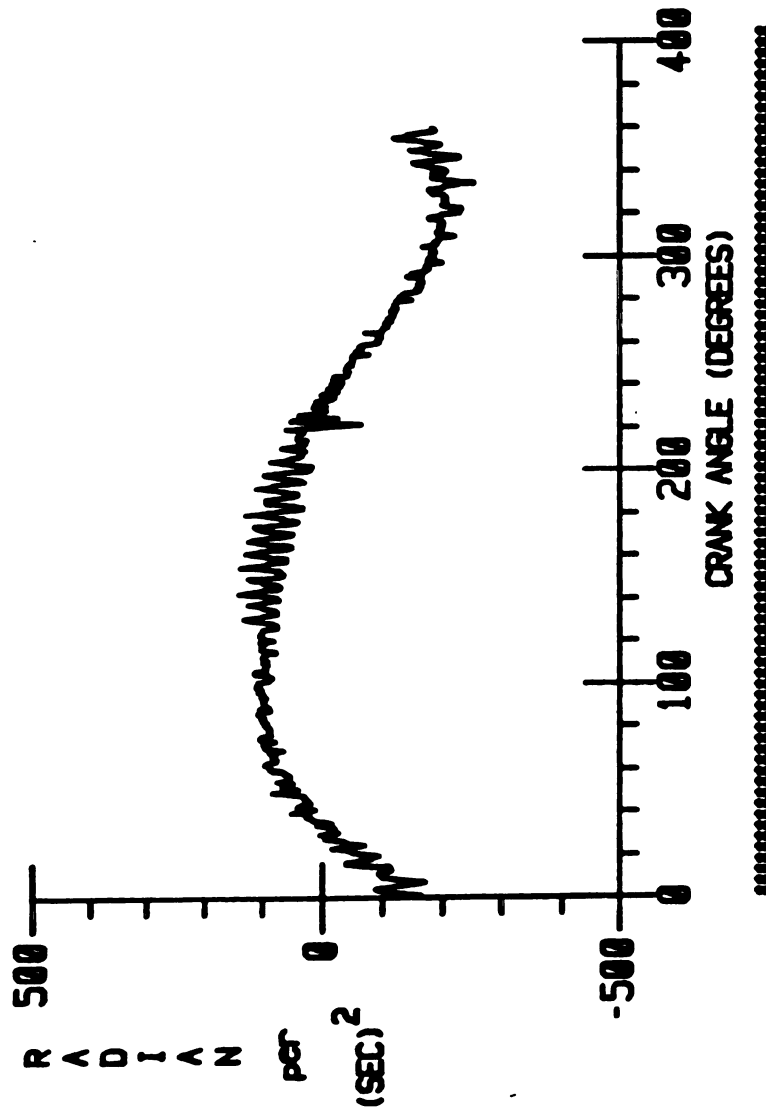
250 RPM, 0.0040 in CLR IN C-R JOINT

FIGURE 7.13b. COUPLER ANGULAR ACCELERATION
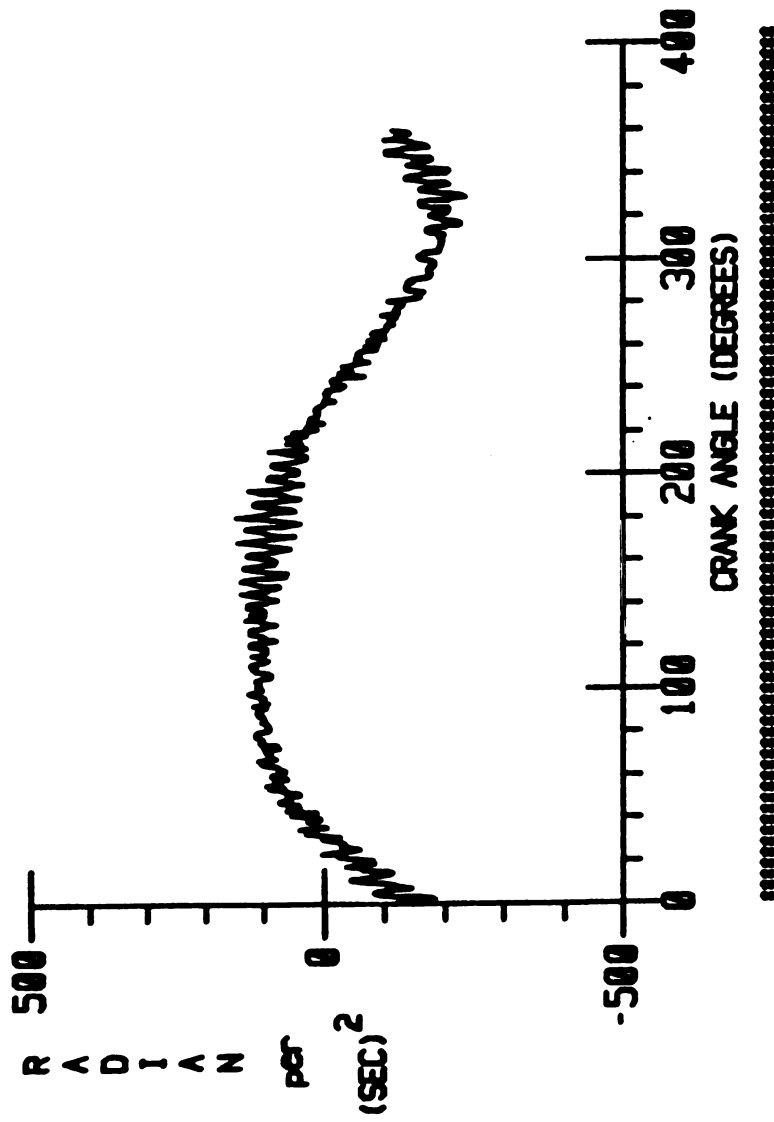
250 RPM, 0.0070 in CLR IN C-R JOINT

FIGURE 7.13c. COUPLER ANGULAR ACCELERATION
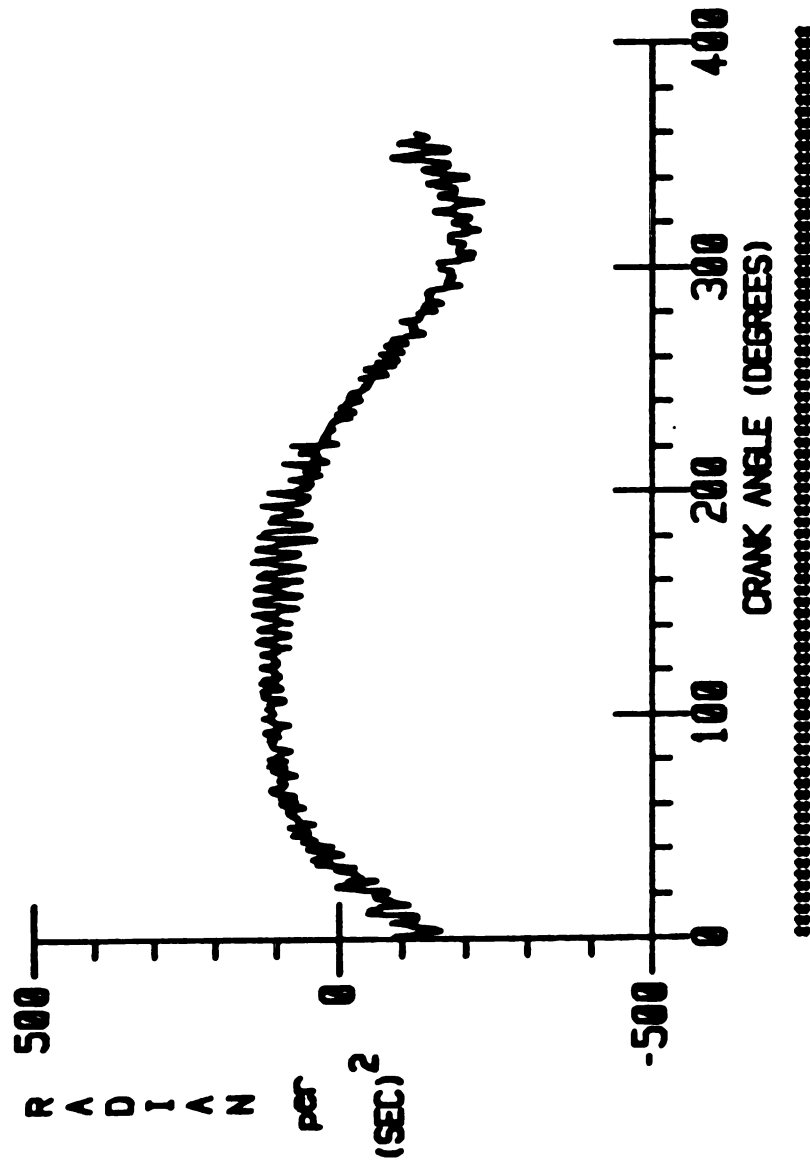
250 RPM, 0.010 in CLR IN C-R JOINT

FIGURE 7.13d. COUPLER ANGULAR ACCELERATION
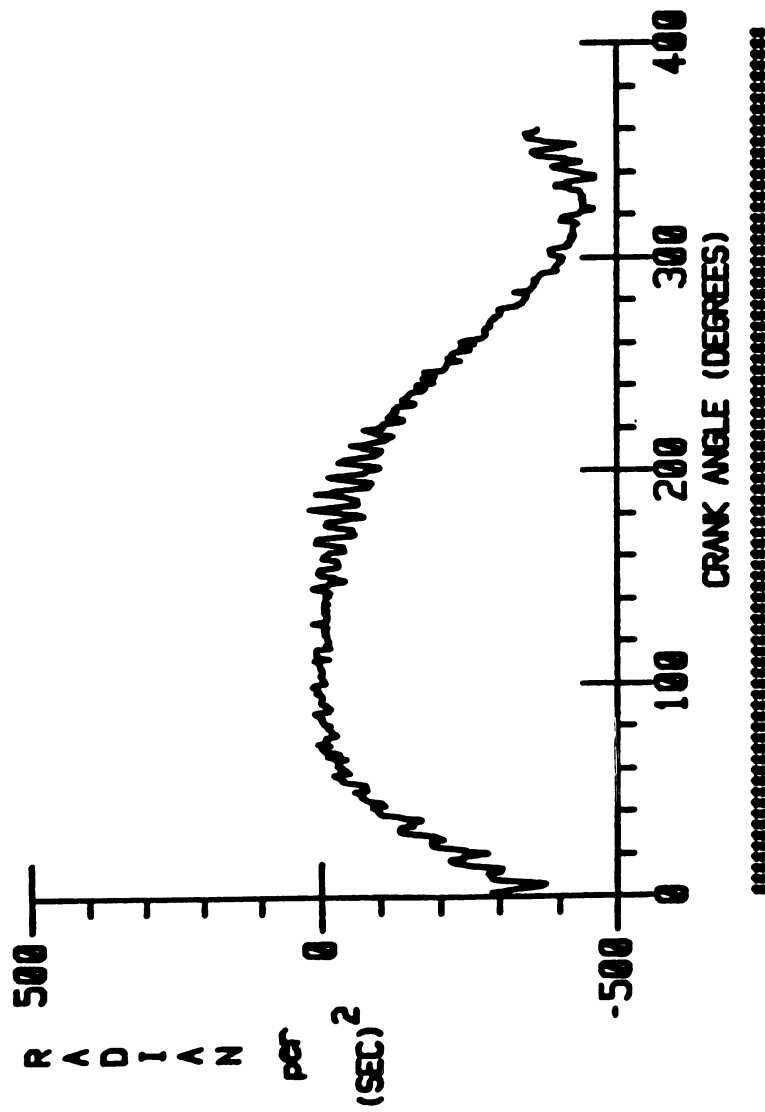
300 RPM, 0.0010 in CLR IN C-R JOINT

FIGURE 7.14a. COUPLER ANGULAR ACCELERATION

171
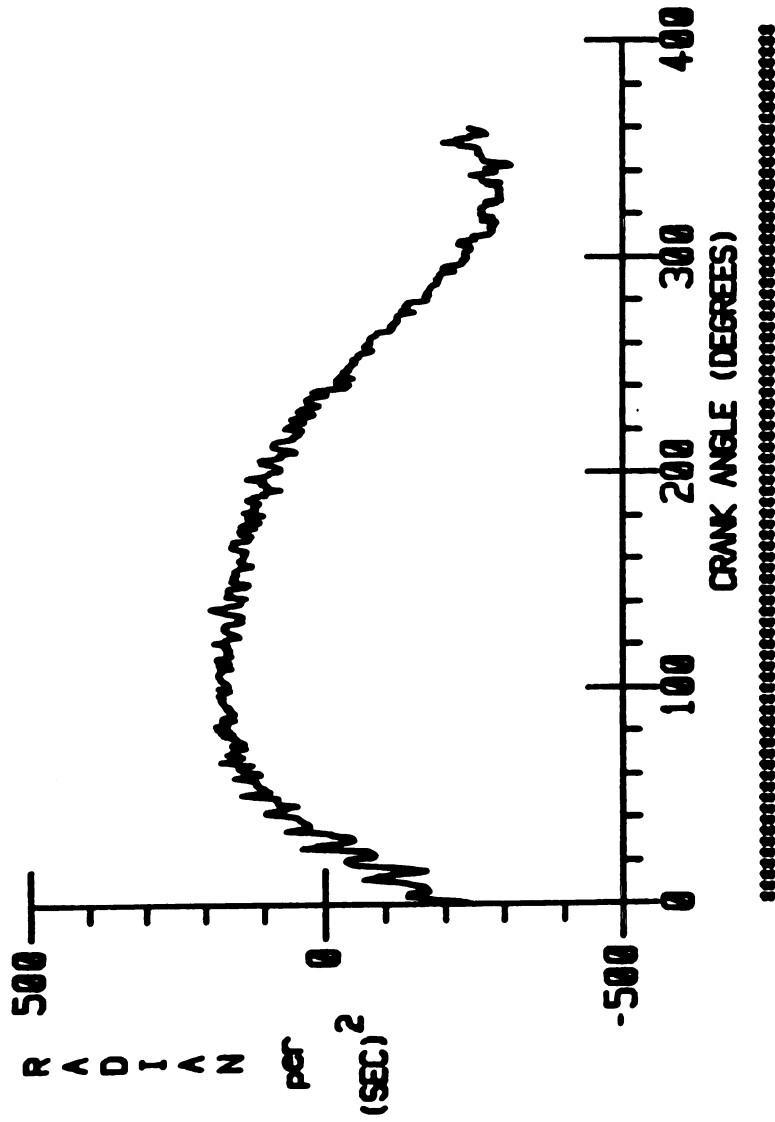
300 RPM, 0.0040 in CLR IN C-R JOINT

FIGURE 7.14b. COUPLER ANGULAR ACCELERATION
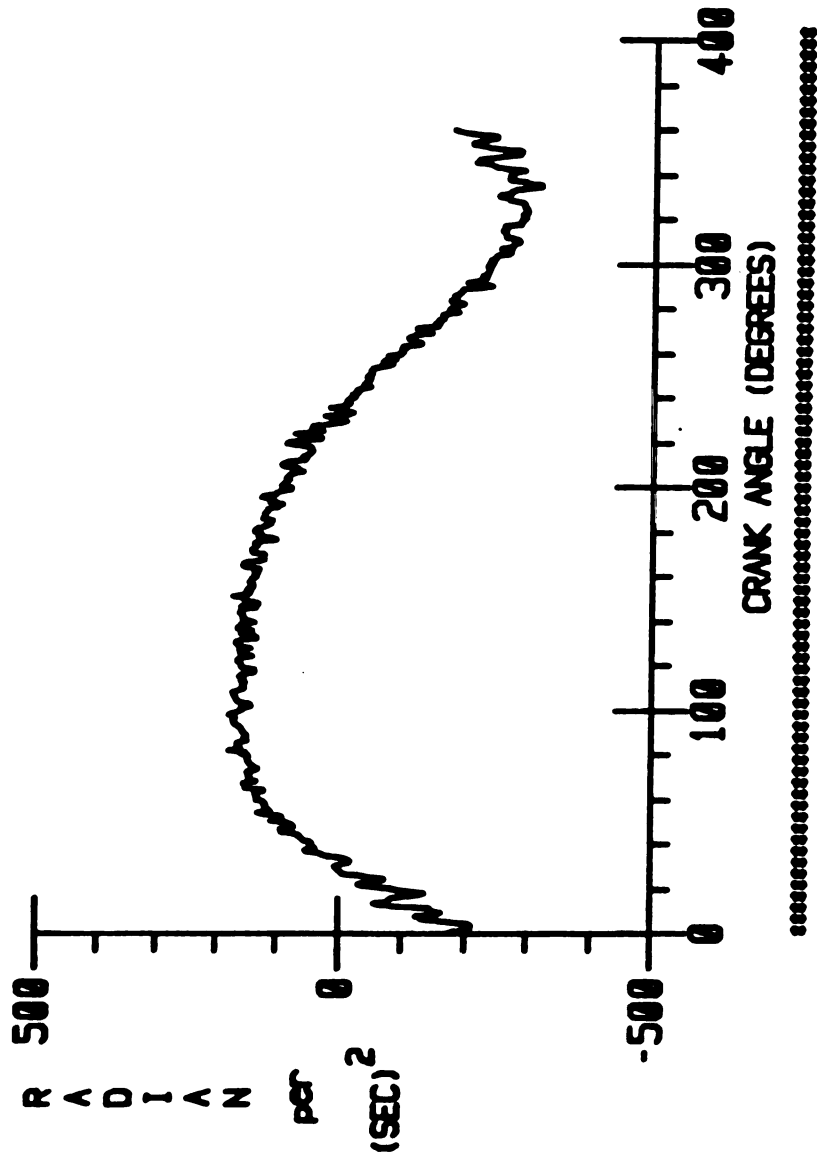
300 RPM, 0.0070 in CLR IN C-R JOINT

COUPLER ANGULAR ACCELERATION
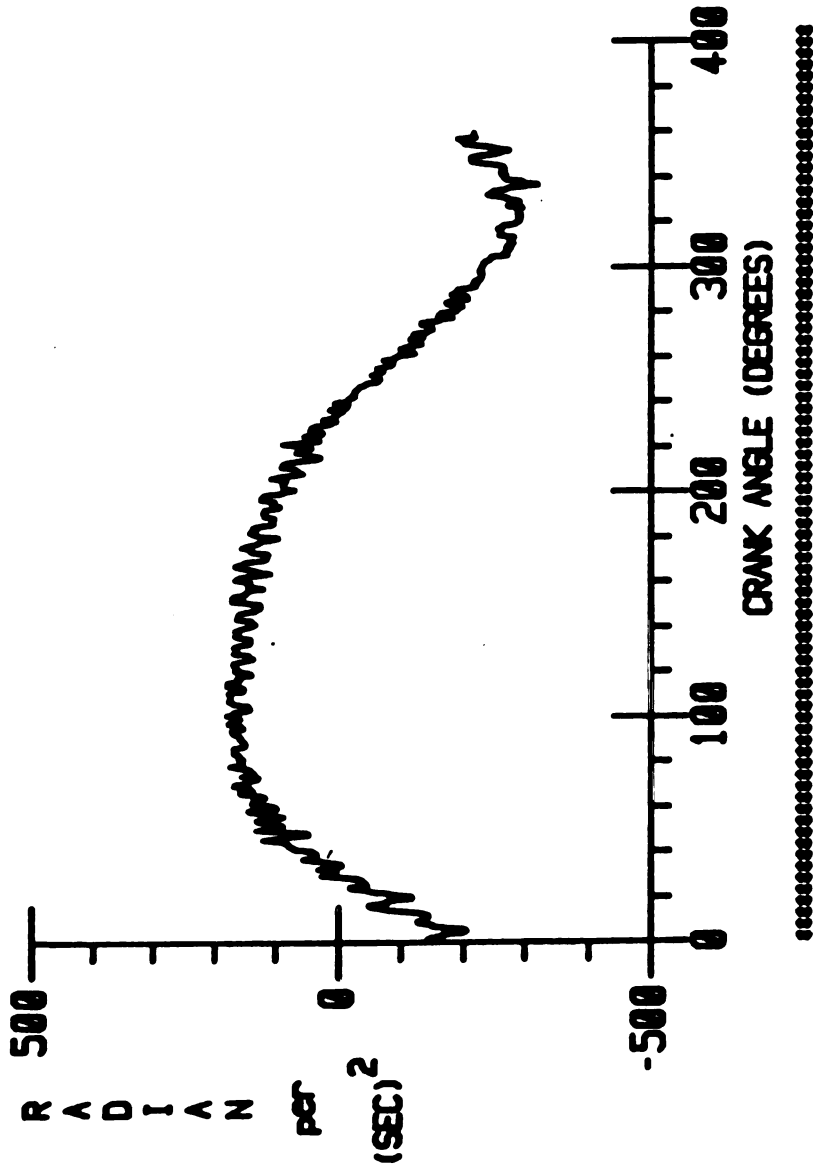
FIGURE 7.14c.

300 RPM, 0.010 in CLR IN C-R JOINT

FIGURE 7.14d.   COUPLER ANGULAR ACCELERATION

174
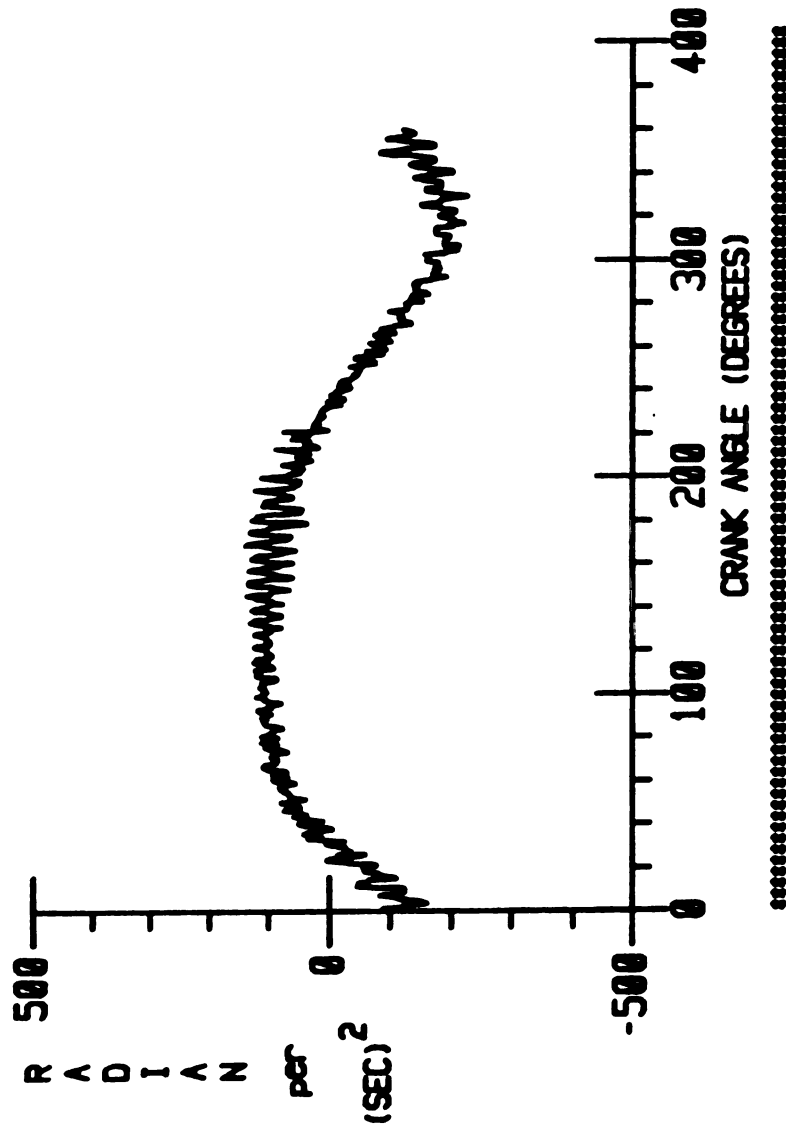
250 RPM, 0.010 in CLR IN C-R JOINT

FIGURE 7.15a. COUPLER ANGULAR ACCELERATION
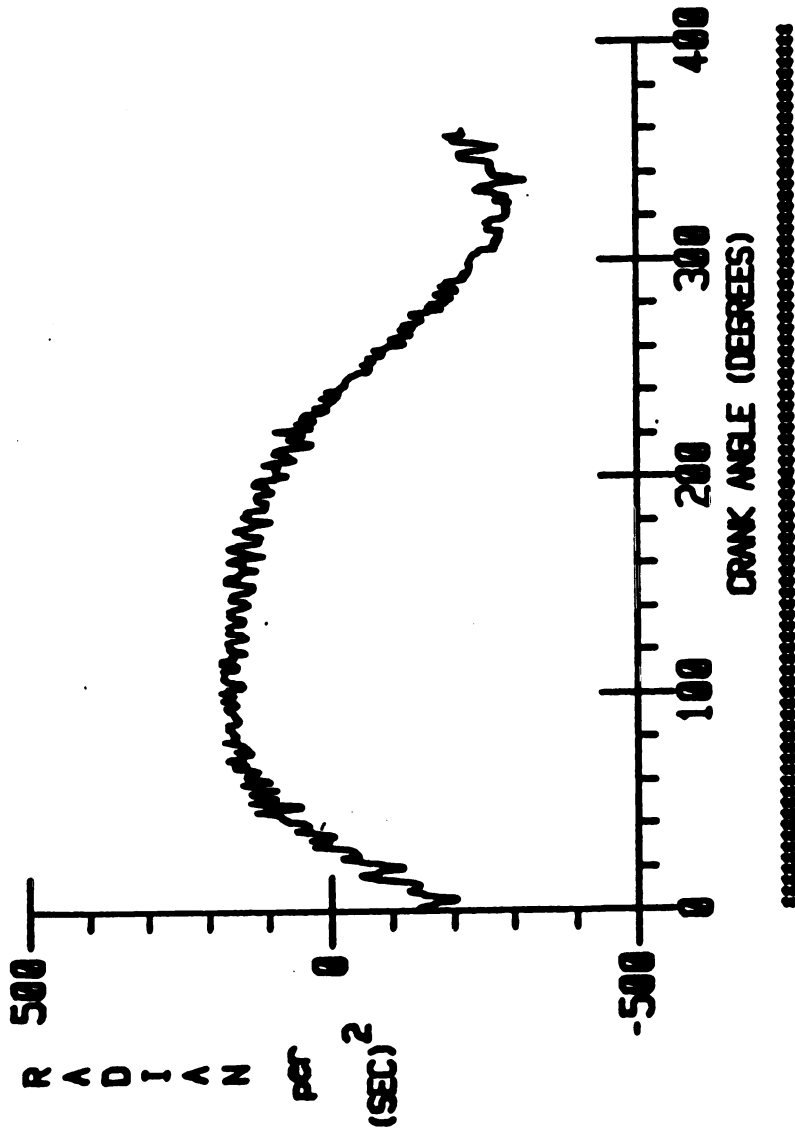
300 RPM, 0.010 in CLR IN C-R JOINT

FIGURE 7.15b. COUPLER ANGULAR ACCELERATION
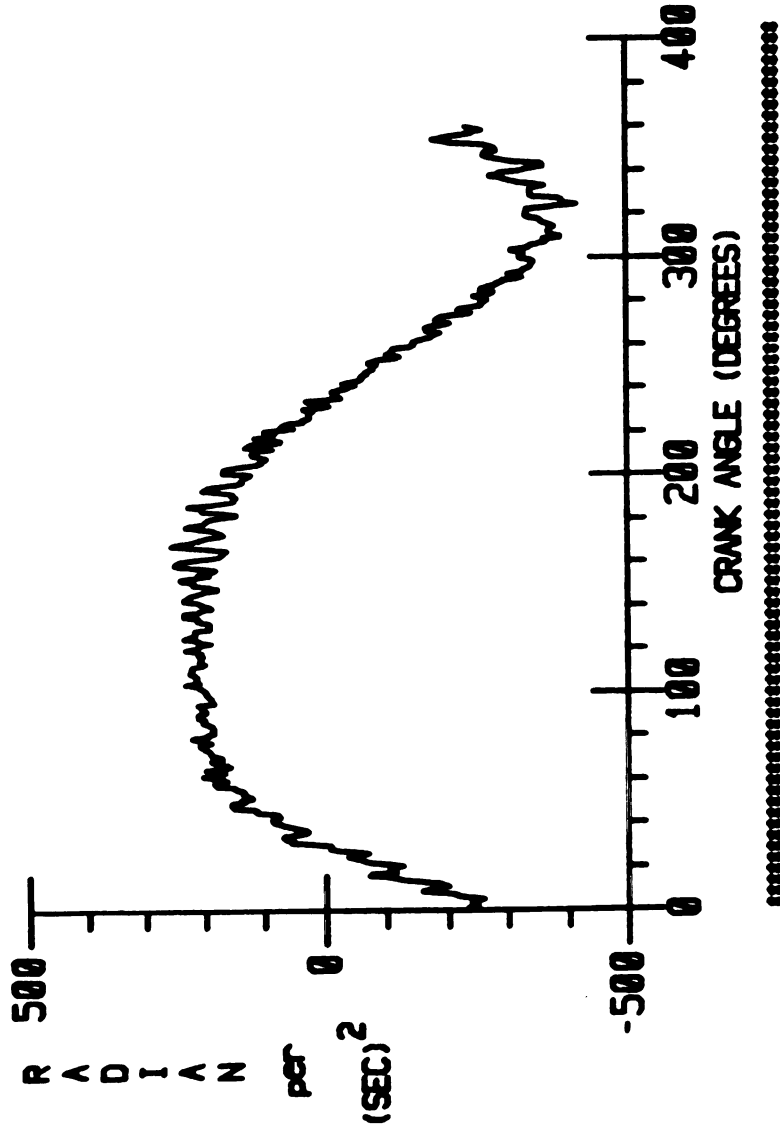
350 RPM. 0.010 in CLR IN C-R JOINT

FIGURE 7.15c. COUPLER ANGULAR ACCELERATION
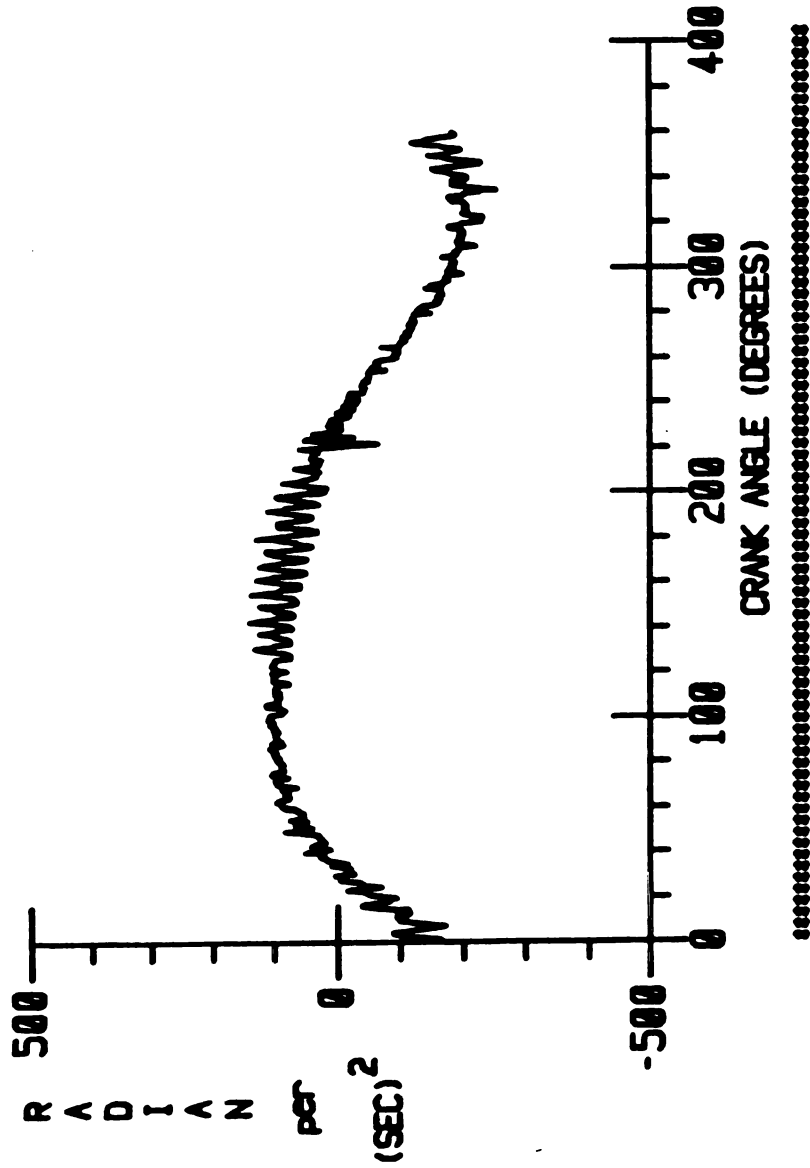
250 RPM. 0.0040 in CLR IN C-R JOINT

FIGURE 7.16a. COUPLER ANGULAR ACCELERATION

178
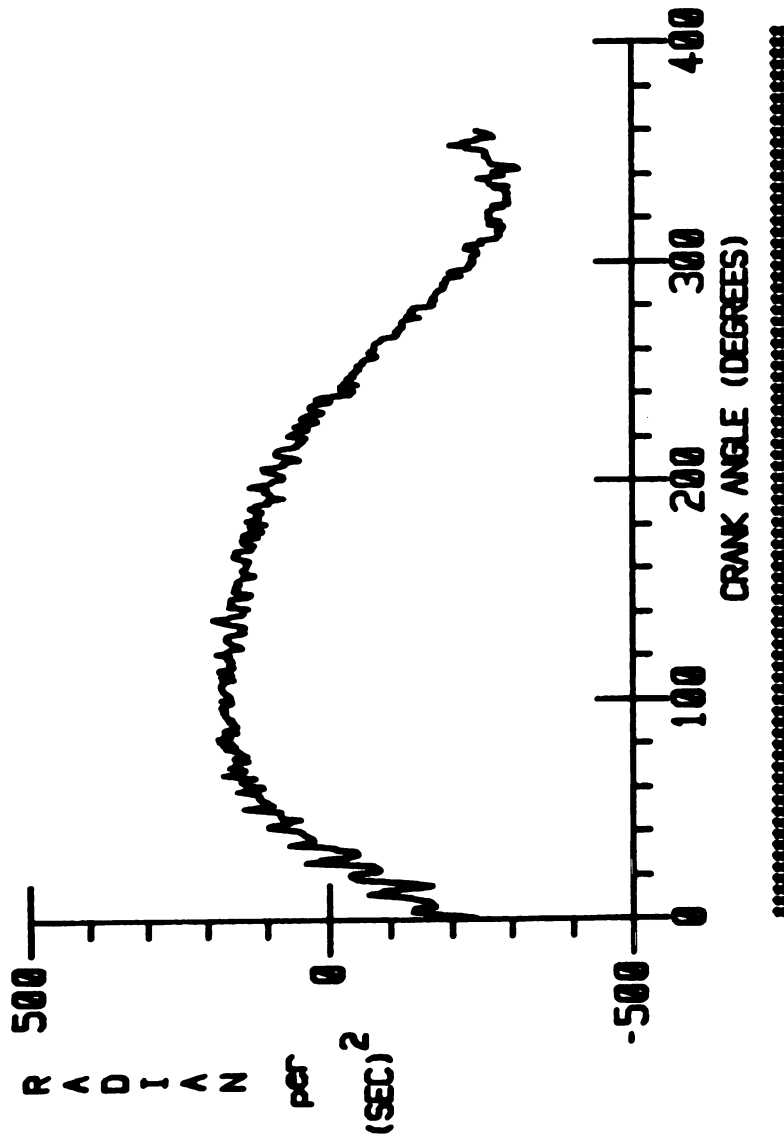
FIGURE 7.16b. COUPLER ANGULAR ACCELERATION
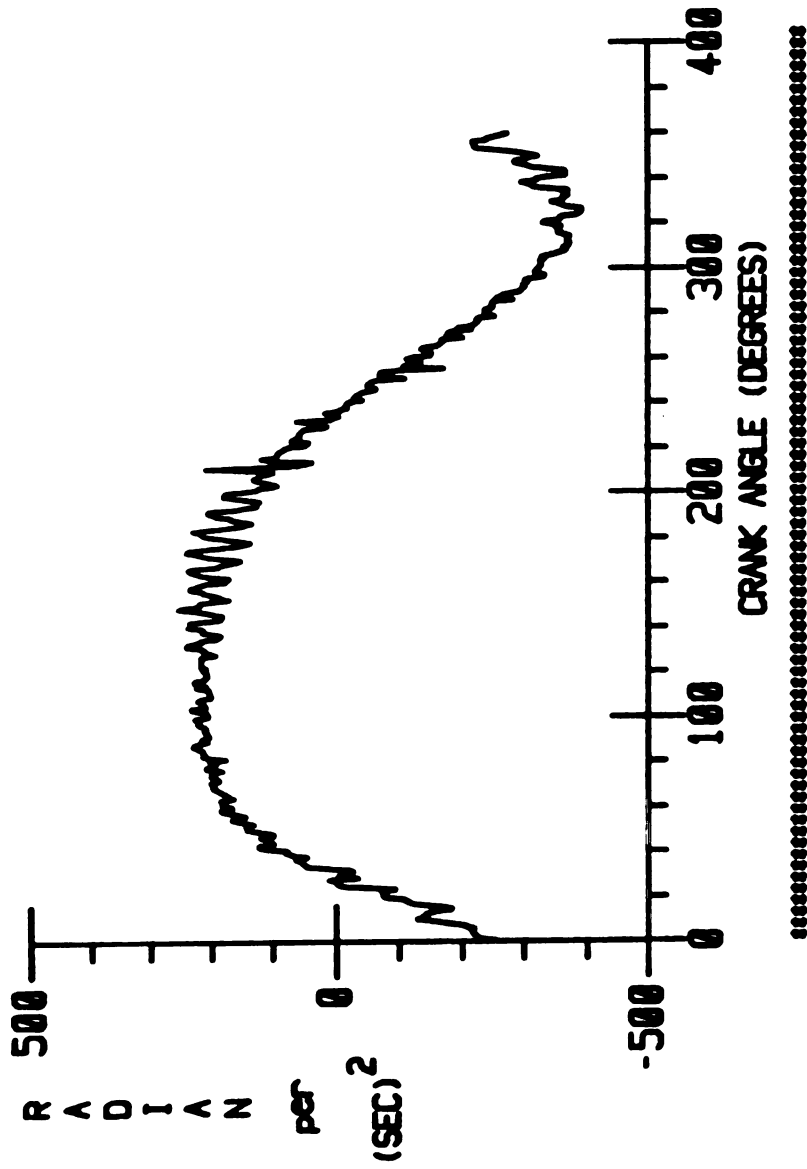
350 RPM, 0.0040 in CLR IN C-R JOINT

FIGURE 7.16c. COUPLER ANGULAR ACCELERATION
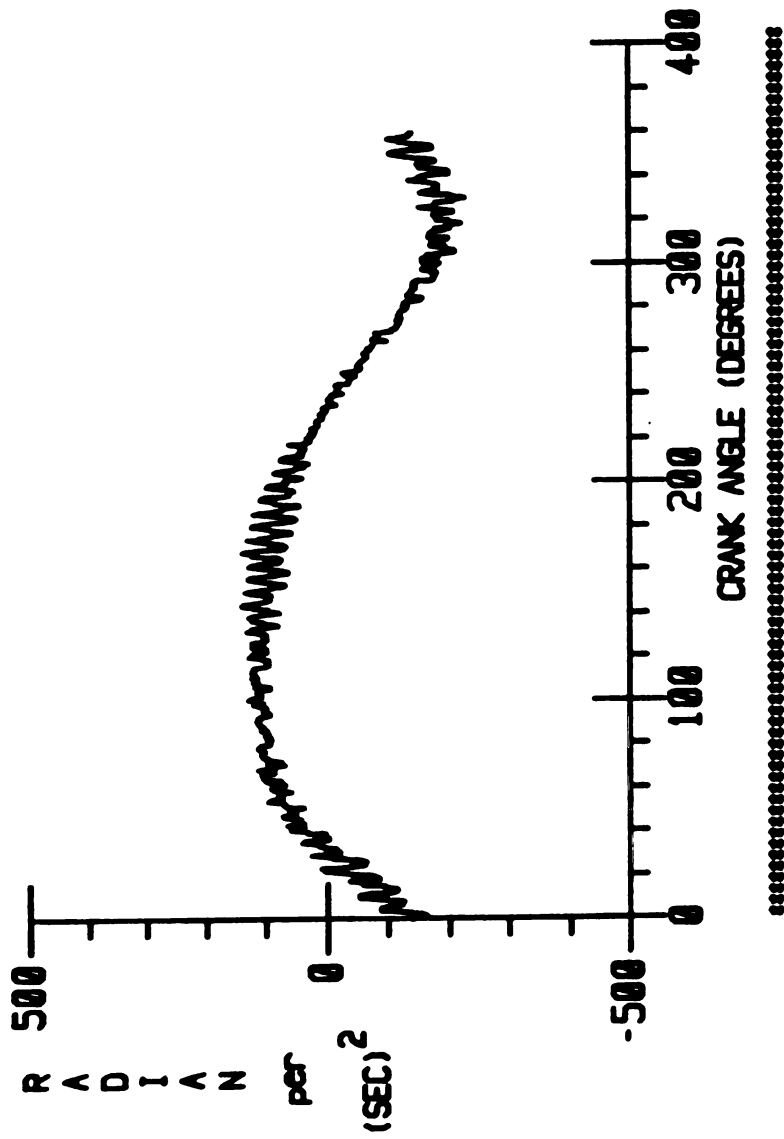
250 RPM. 0.0010 in CLR IN C-R JOINT
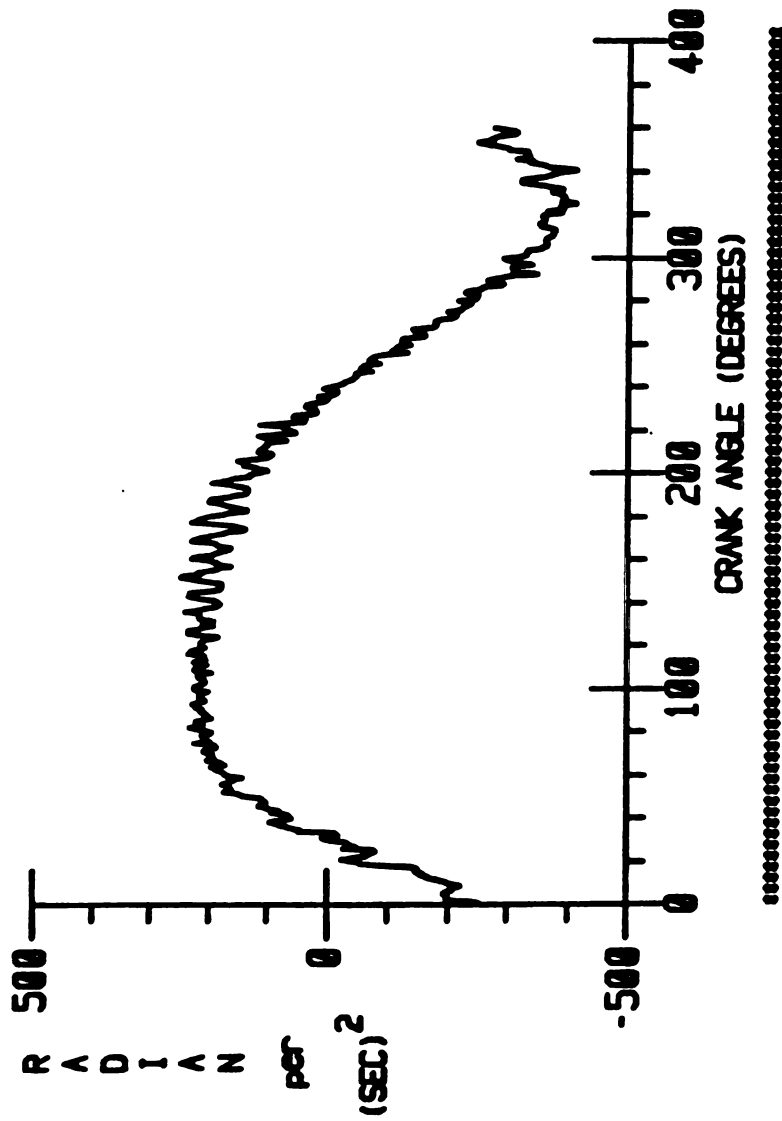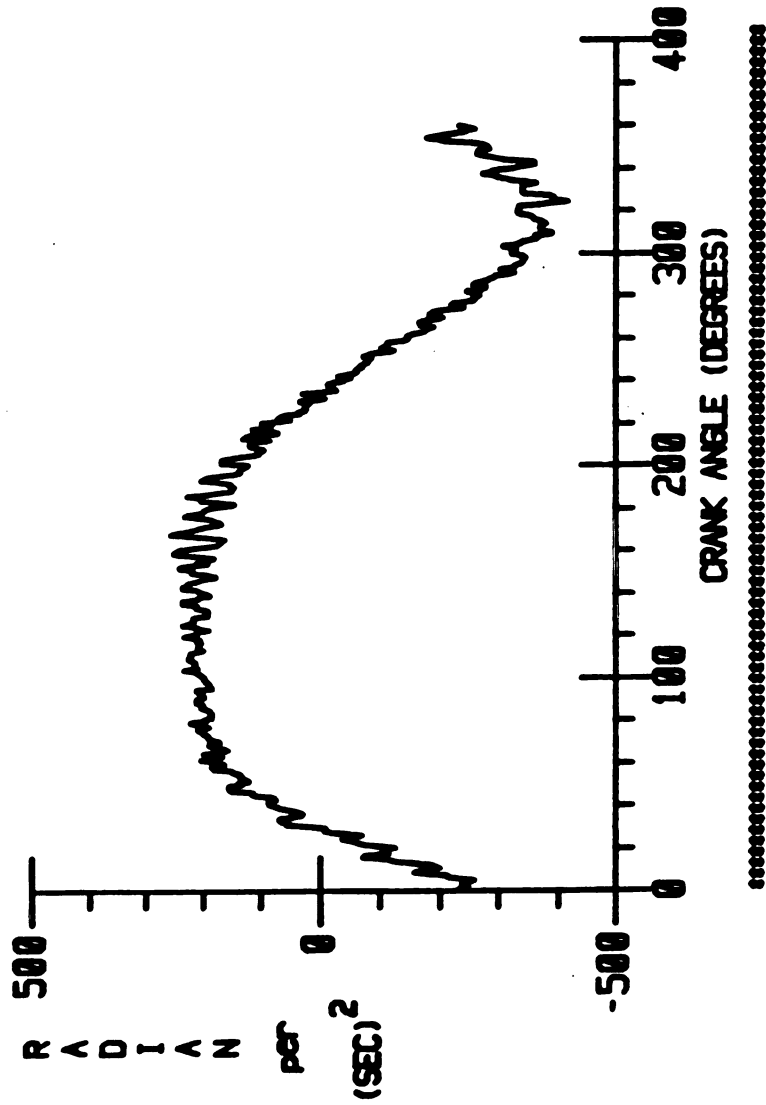
FIGURE 7.17a.   COUPLER ANGULAR ACCELERATION
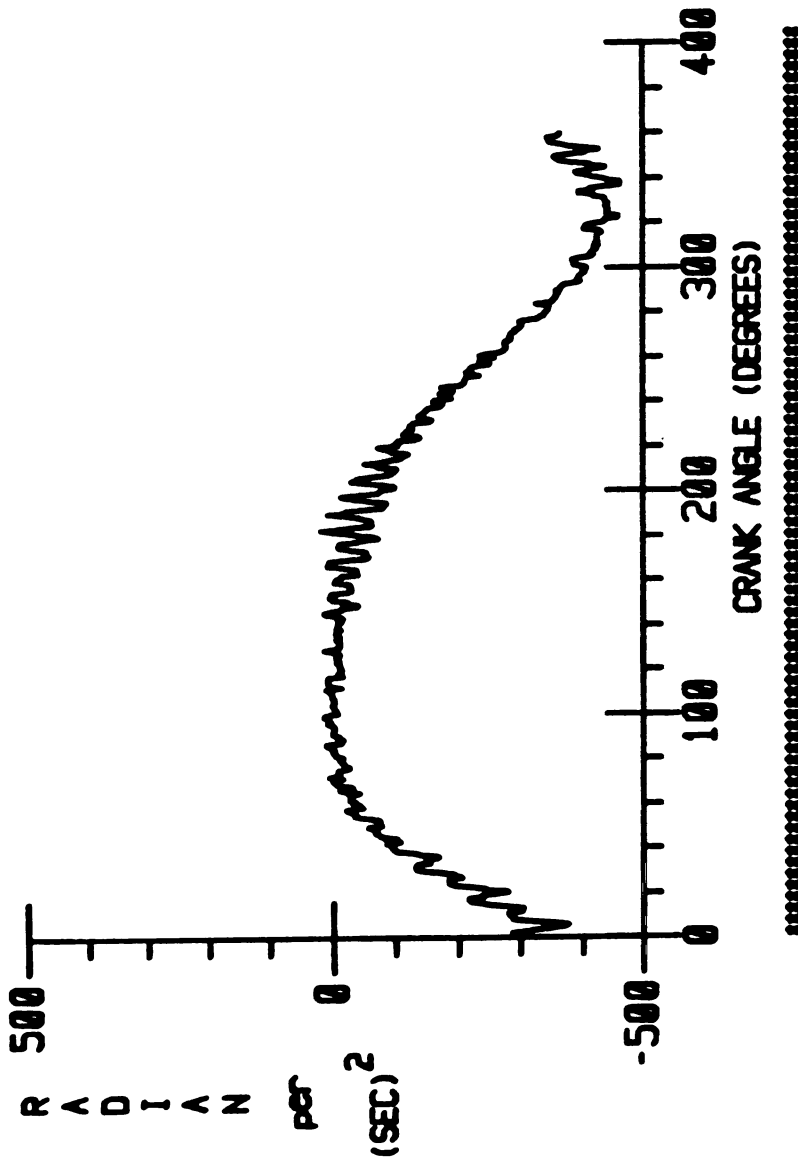
300 RPM, 0.0010 in CLR IN C-R JOINT

FIGURE 7.17b. COUPLER ANGULAR ACCELERATION
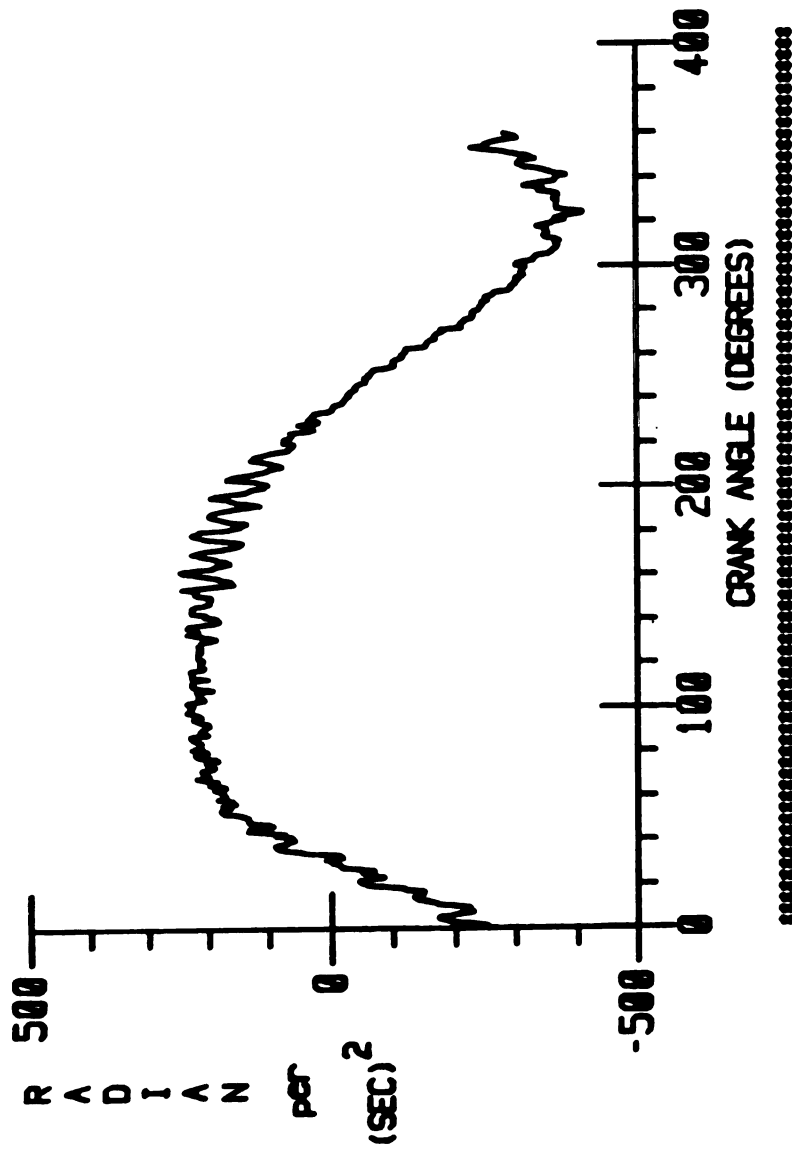
350 RPM, 0.0010 in CLR IN C-R JOINT

FIGURE 7.17c. COUPLER ANGULAR ACCELERATION

The effect of variation of the crank angular velocity can be investigated now. For a clearance size of 0.010 inches, Figures (7.15) illustrate the variation of crank RPM for 250, 300 and, 350 RPM. As the crank angular velocity is increased, the severity of the fluctuations ($\sum F$ or I_n) also increase. However, the number of impacts in one revolution is decreased (Figure 7.11). The same behavior can be observed in Figures (7.16) and (7.17) which correspond to a clearance size of 0.0040 and, 0.0010 inches, respectively.

Based on the experimental results presented in this chapter and, with reference to Figures (7.10) and (7.11), it can be stated that, for practical purposes, one can design a mechanism which is 'tuned' in the sense of having minimal values of $\sum F$ (I_n) (Figure 7.10) with simultaneous minimum number of impacts per revolution.

In the next chapter, attempt has been made to compare and correlate the analytical results obtained by the numerical solution described in the previous chapters with the experimental results presented in this chapter.

CHAPTER EIGHT

COMPARISON OF

ANALYTICAL AND EXPERIMENTAL

RESULTS

In chapter six the complete results of the numerical simulations were studied and, chapter seven dealt with the investigation of the experimental phase of the work. A seperate chapter has been devoted to the comparison and correlation of these two types of results since only the angular velocities and accelerations of the coupler and rocker links can be compared and, the reliability of other parameters obtained by the numerical solution may be deduced from the above. In other words, it is assumed that, any conclusions or remarks drawn from the comparison of, say, angular accelerations of coupler and rocker links will apply to the X- and Y- components of the coupler-rocker bearing reaction, since these parameters are linearly interrelated.

Figures (8.1a) and (8.1b) show the superposition of the numerical and experimental plots of the angular velocities of the coupler and the rocker links, respectively. Note that, unless otherwise specified, in all of the foregoing plots the coefficient of restitution assumed in the numerical simulation is unity. Figures (8.2a) and (8.2b) are analogous to Figures (8.1), but for angular accelerations of the links.

It can be clearly observed that, there is a significant difference between the magnitudes of numerical and experimental results, especially for the angular accelerations (Figures 8.2) in which the numerical results are about 30 times the experimental ones. As previously mentioned, such disagreement in the magnitude and intensity of the experimental and simulation results is primarily due to several reasons such as

1. In the numerical simulation the coefficient of restitution, e, was assumed to be unity. This is hardly the case from practical standpoints. The bushing of the coupler-rocker bearing was made of oil-impregnated brass (chapter seven) which would certainly introduce a finite degree of damping into the system.

By referring to Figure (8.2a) and comparing it to the coupler angular acceleration for e=0.50 (Figure 8.3), it can be observed that, as the coefficient of restitution is reduced the angular acceleration of the coupler becomes less severe and, closer to the experimental results, although it is still about 15 times the experimental results
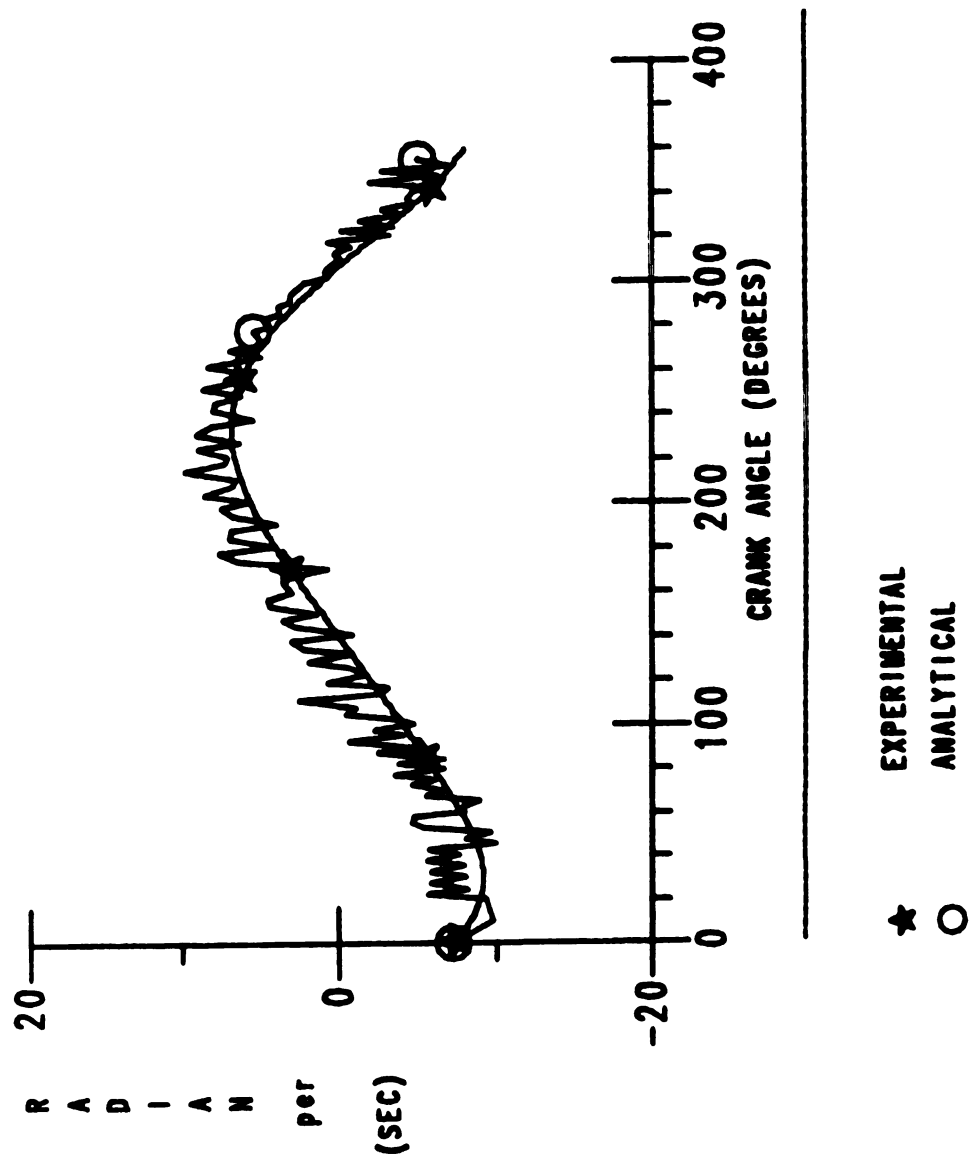
FIGURE 8.1a. COUPLER ANGULAR VELOCITY
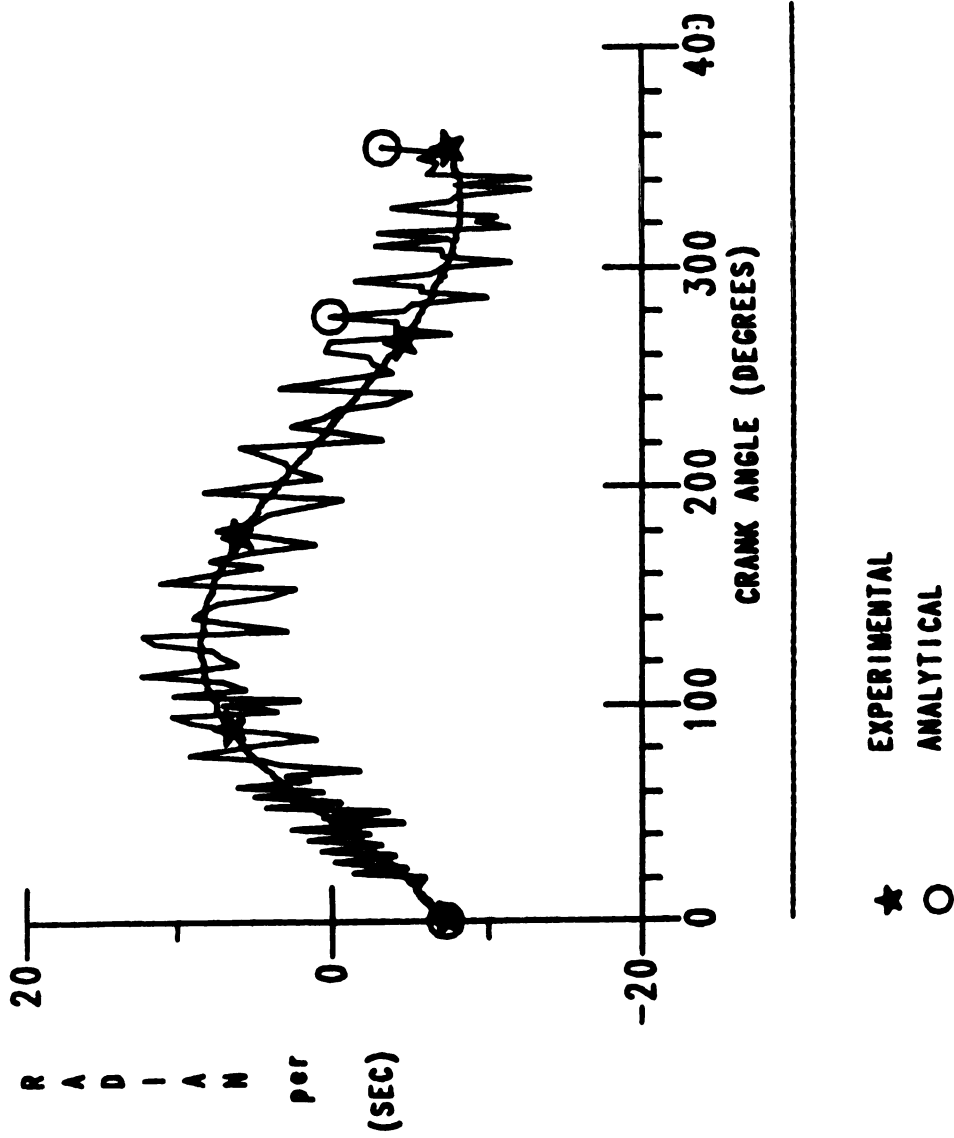
FIGURE 8.1b.   ROCKER ANGULAR VELOCITY

188
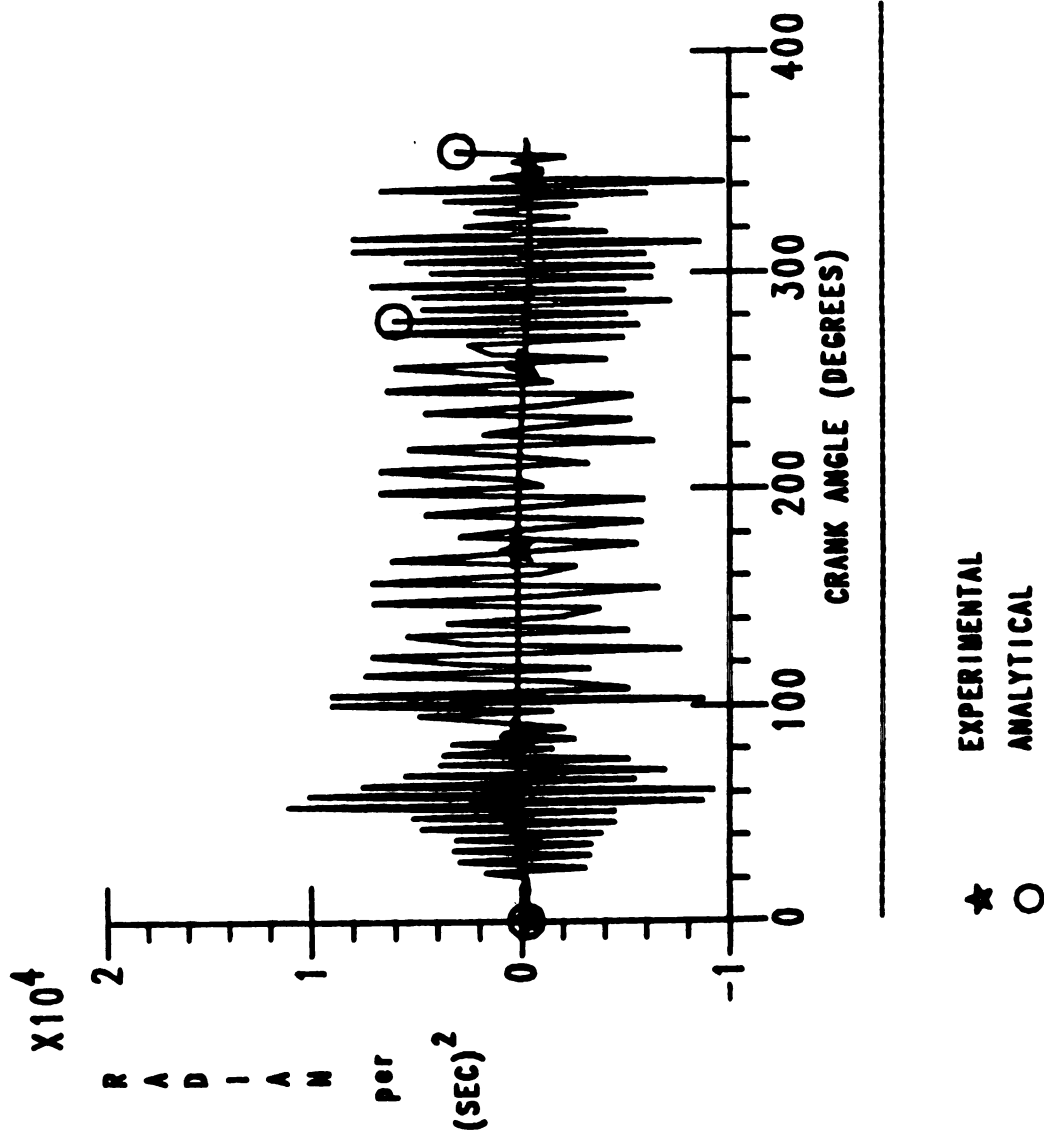
FIGURE 8.2a. COUPLER ANGULAR ACCELERATION

★ EXPERIMENTAL
O ANALYTICAL
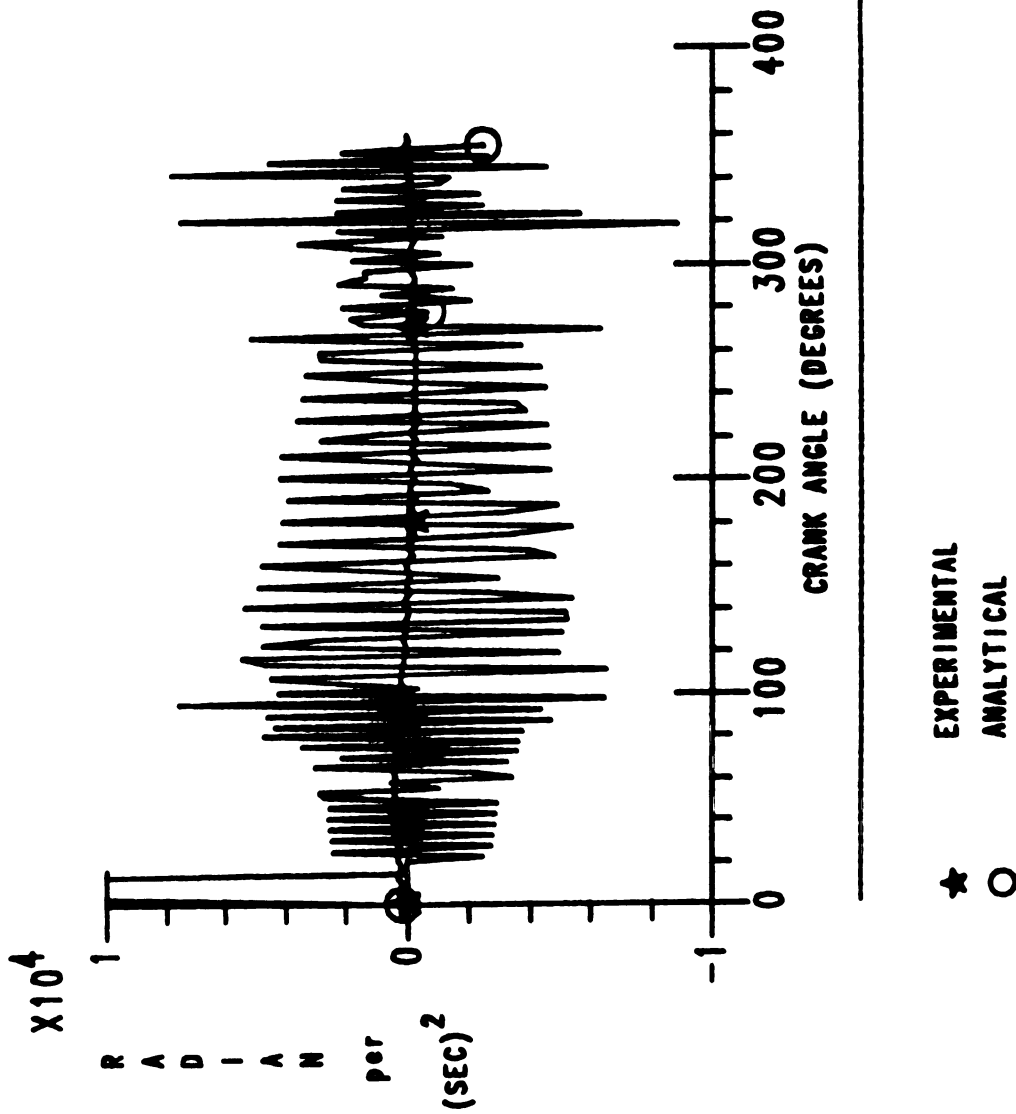
FIGURE 8.2b.   ROCKER ANGULAR ACCELERATION
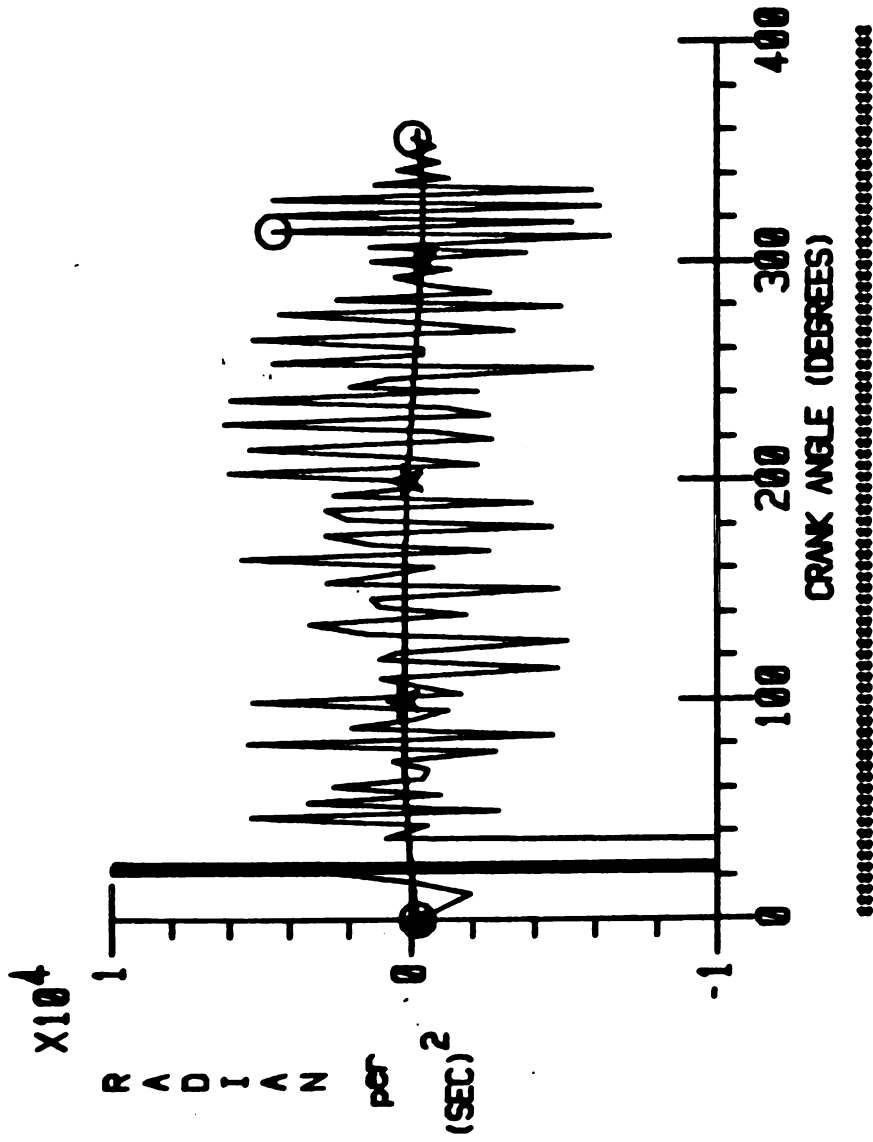
FIGURE 8.3.   COUPLER ANGULAR ACCELERATION (e=0.50)

in scale. Hence, it is conceivable to predict that, as the coefficient of restitution decreases, so does the severity of the analytical results. However, the magnitude of the coefficient of restitution can be reduced down to a realistic value such as 0.10 since e=0.0 implies the sticking of the bearing parts together after impact. Consequently, the value of the parameter e cannot be varied independently without taking other determining factors into consideration such as the Coulomb coefficient of friction.

The above assumption is coupled with the fact that, the Coulomb coefficient of friction in the simulation was assumed to be zero, implying that, the pin can slide against the bushing of the bearing without encountering any resistant frictional forces. This also, is an ideal assumption since in practice there is always some type of frictional force present when two bodies slide against each other. Thus, in real life situation, the combined effect of the coefficient of restitution and, the Coulomb coefficient of friction (or any other type of friction) on the mechanism is to decrease the severity of the motion of the system compared to the simulated results obtained here.

2. The existense of digital/numerical noise in the results of the simulation (chapter six) tends to magnify the aforementioned effects.

Thus, it becomes apparent that, for a realistic simulation of the mechanism investigation, the 'minimal' modifications needed to be performed on the original assumptions outlined in chapter two are as follows

i)- Development of a means of measuring or estimating the true value of the coefficient of restitution.

ii)- Measurement of the Coulomb coefficient of friction in the coupler-rocker bearing by proper means and equipment.

iii)- Simulation of the model on an efficient and fast computing machine with high accuracy.

Up to this point, the primary concern of the discussion on the correlation of the experimental and analytical results was limited to the subject of severity and/or smoothness of each response. It is now appropriate to reflect upon and analyze the reliability of prediction of the points of occurence of such fluctuations, namely, the points of occurence of contact-loss and impact during the interval of motion of the system. The following points are in order

1. When the characteristic parameters in the simulation are as chosen above ($e=1.0$ and $\mu=0.0$), which are almost certainly different from their true values corresponding to the experimental mechanism (say $e=e_1$ and $\mu=\mu_1$), then the contact-loss and subsequent impact points for the latter two systems occur at different instants of time except for a few cases which pertain to the 'geometrical' configuration of the systems. The reason behind this is that, suppose at time $t=t_1$ during the simulation, a point of occurence of contact-loss is detected by the code. Then, after a few time steps in the free-flight mode, the impact mode takes place. Due to the value of e being equal to unity, there is almost always an immediate further contact-loss and, theoret-

ically, it takes infinite time for the system to re-stabilize itself. But, the round up errors tend to increase this so-called stabilization process and decrease the severity of the response after a few time steps. However, in real life situation the coefficient of restitution, e, is less than unity (and more likely to be even less than 0.50) and hence, the rate of dissipation of energy is much faster than in the simulation case.

Another factor is the Coulomb coefficient of friction, μ. For all practical purposes the coefficient μ is always greater than zero, whereas in the simulation the assumption was that $\mu=0.0$. The third factor that dominates the location of the points of occurence of the variations in the plots is the simulated phase of motion of the mechanism. That is, if the simulation corresponds to the transient or the start-up cycles of revolution (which is the case here), then the results will certainly be different than those obtained for higher cycles of revolution or the quasi-steady phase.

The combined effect of the above three simulation characteristics is complex. But, it could be stated that, any disagreement in the values and phases in the simulation with their true states would cause frequent leads and delays in the occurence of the points of contact-loss and impact, with its degree of discrepancy dependent upon how close the assumed cases are to their real ones. Thus, as noted above, the optimum way of improving the results is to use the correct values of the coupler-rocker characteristic parameters (e and μ) with

the simulation performed on a computing machine that would allow the study of the responses in the quasi-steady phase of the motion with optimum accuracy and speed.

Before closing this chapter, a further, simplistic attempt will be made to modify the available simulation results so that they resemble the realistic case as close as possible. The reader should be forewarned that, the following so-called 'modification' of the analytical results simply provides an 'estimation' of the true value of the system parameters and, they are by no means intended to be accurate and exact results. In fact, as will be clear, their accuracy is no greater than the analytical results and, their only advantage is that they are 're-scaled' in such a manner as to be in the range of the experimental results.

8.1- Modification Of The Analytical Results

Ideally, the task of simulating the mechanism under study on a digital computer effectively requires finding the correct values of the coefficient of restitution and the Coulomb coefficient of friction to be used in the numerical simulation of the problem, which in turn is a tedious and time consuming job, provided that the available computing machine is capable of preventing the obstruction of the system response by digital noise which is again a problem by itself. However, an alternate approach can be adapted at this point which, to some extent, 'modifies' the final results of the simulation to compen-

sate for the inaccuracies of the scaling of the numerical results obtained due to the difficulties mentioned above.

Reference is made to Figure (8.2a) which depicts the angular acceleration of the coupler link for the analytical and the experimental cases. Let us express both of these types of results can be expressed in terms of their Fourier expansions. In other words, if the numerical response can be expressed as

$$a_s = \left[B_1 \sin\omega t + B_2 \sin 2\omega t + \ldots + B_m \sin m\omega t \right] +$$
$$\left[A_1 \sin(m+1)\omega t + A_2 \sin(m+2)\omega t + \ldots + A_{n-m} \sin n\omega t \right]$$

$$(8.1.1a)$$

then the experimental results can be stated as

$$a_e = \left[B_1 \sin\omega t + B_2 \sin 2\omega t + \ldots B_m \sin m\omega t \right] +$$
$$\left[C_1 \sin(m+1)\omega t + C_2 \sin(m+2)\omega t + \ldots C_{n-m} \sin n\omega t \right]$$

$$(8.1.1b)$$

Note that, in the above two equations the terms inside the first set of brackets on the right hand side of the equations corresponds to a function defining the 'nominal' response, while the remainder are the superimposed oscillations and fluctuations. Obviously, the nomi-

nal part of these two equations are the same and, the difference occurs in the oscillating parts of the two responses.

In an ideal simulation, both the experimental and analytical results are made up of ideal combinations of sine waves at different frequencies with amplitudes related by a magnification/conversion factor α, i.e.

$$A_1 = \alpha C_1 \quad ; \quad A_2 = \alpha C_2 \quad ; \quad \ldots \quad ; \quad A_{n-m} = \alpha C_{n-m}$$

$$(8.1.2)$$

where, again, for the ideal case, we have

$$\alpha = 1.0$$

Assuming that equations (8.1.1) and (8.1.2) hold for the results shown in Figure (8.2a). The validity of such an assumption will be discussed shortly. But, for present, it is assumed that it holds true. Hence, the only remaining parameter to be determined in equation (8.1.2) is the magnification/conversion factor, α.

Two seperate methods can be adapted to determine the factor α. The first and more accurate method is to obtain the frequency spectrum of the two analytical and experimental results based on the fast fourier transform routine (chapter six) and then, through a simple comparison between the amplitudes of the spectra at a given frequency,

the desired factor a can be determined. Although as mentioned above, this method is preferred to the second one in terms of accuracy, its use has been avoided here due to the extent of noise associated with the rectangular windowing function used in the FFT computer routine.

The second method, which is simpler and less accurate than the first one, deals with the results in their time-domain. In other words, the difference in the magnitudes of the numerical and experimental results at a certain instant of time is compared against each other. After a series of comparisons at several instants of time during the operation of the mechanism, an approximate value for the factor a can be obtained.

From the two methods described above, the latter was used in this work. However, direct comparisons between the experimental and numerical results is not possible in this case. The reason behind this is that, each of the experimental and analytical plots is a collection of several points sampled (or simulated) at different instants of time. This implies that, if there exists a point in the experimental data which has been sampled at time, say $t=t_1$, the corresponding point on the numerical results for $t=t_1$ may not be available and, the next closest point would correspond to a point for $t=t_1\pm\varepsilon$, with ε depending on the integration mesh size (chapter six) on one hand and, the sampling rate of the experimental data (chapter seven) on the other.

Hence, an indirect comparison can be made between the experimen-

tal and the simulation results. This is performed by comparing each of these results to a corresponding 'nominal mechanism' response. The latter is obtained with the aid of the computer routine adapting the nominal mechanism equations described in chapter two. Such a comparison provides enough flexibility that, each of the sets of results can be compared to the nominal response at their specified instants of time. The simplest method of finding the factor a would be to compute the average (or root mean square) of the deviation of each of the plots from the nominal plot. Then, the factor a would equal the (the square root of the) ratio of the two average deviations corresponding to the experimental and nominal mechanisms.

For the responses shown in Figure (8.2a) this factor was found to be in the neighborhood of 30.0 . Thus, in order to construct the 'modified' analytical response, the deviation of the analytical result for each point is divided by this factor and the resulting modified deviation for that point is added algabraically to the 'nominal' response corresponding to the same instant of time. This latter addition yields the final result, called the modified analytical result.

The effect of the utilization of such a conversion/magnification factor on the plots of Figure (8.2a) can be observed in Figure (8.4) which, illustrates the modified analytical coupler angular acceleration superimposed on the experimental response. A note is in order at this point that, the 'disturbance' associated with the original simulated coupler angular acceleration occruing at about zero to 20

degrees of crank angular displacement has been omitted during the pro-
cess of computing the factor a. This step was taken in order to avoid
the offsetting of the value of a due to this localized high-amplitude
disturbance.

As can be seen in Figure (8.4), the simulated response agrees
well with the experimental one. This would be expected, since the
analytical response was in a sense 'forced' to fall within the range
of the experimental response by the use of the factor a. The objec-
tive is now to examine the effect of such a modification on the other
simulated system characteristics with the help of the same
conversion/magnification factor a computed perviously.

Figure (8.5) illustrates the correlation of the experimental and
modified analytical response of the rocker angular acceleration. The
numerical response seems to predict a smoother behavior than the
experimental one. But, there is still a fairly good correlation
between the two curves. Figures (8.6) and (8.7) show the analogous
comparisons for the coupler and, the rocker angular velocities,
respectively. Although in both of the latter figures the modified
analytical results show reasonable correlation to their correponding
experimental responses in terms of smoothness, there exists a small
offsetting of each pair of curves between their end values. This is
primarily attributed to the value of the conversion factor (not to be
mistaken with the factor a) used to convert the experimental results
obtained from the probes in millivolts to meters per second (squared).
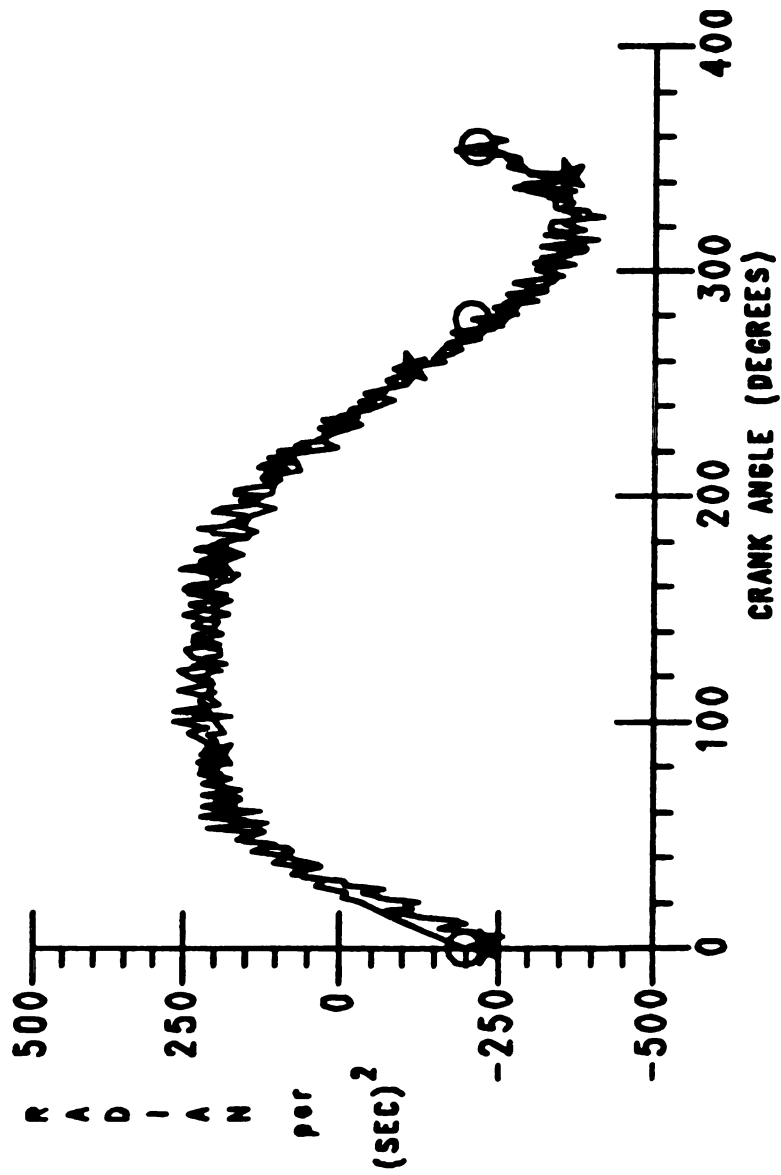
FIGURE 8.4. COUPLER ANGULAR ACCELERATION

★   350 RPM, 0.010" CLEARANCE - EXPERIMENTAL
O   350 RPM, 0.010" CLEARANCE - MODIFIED ANALYTICAL
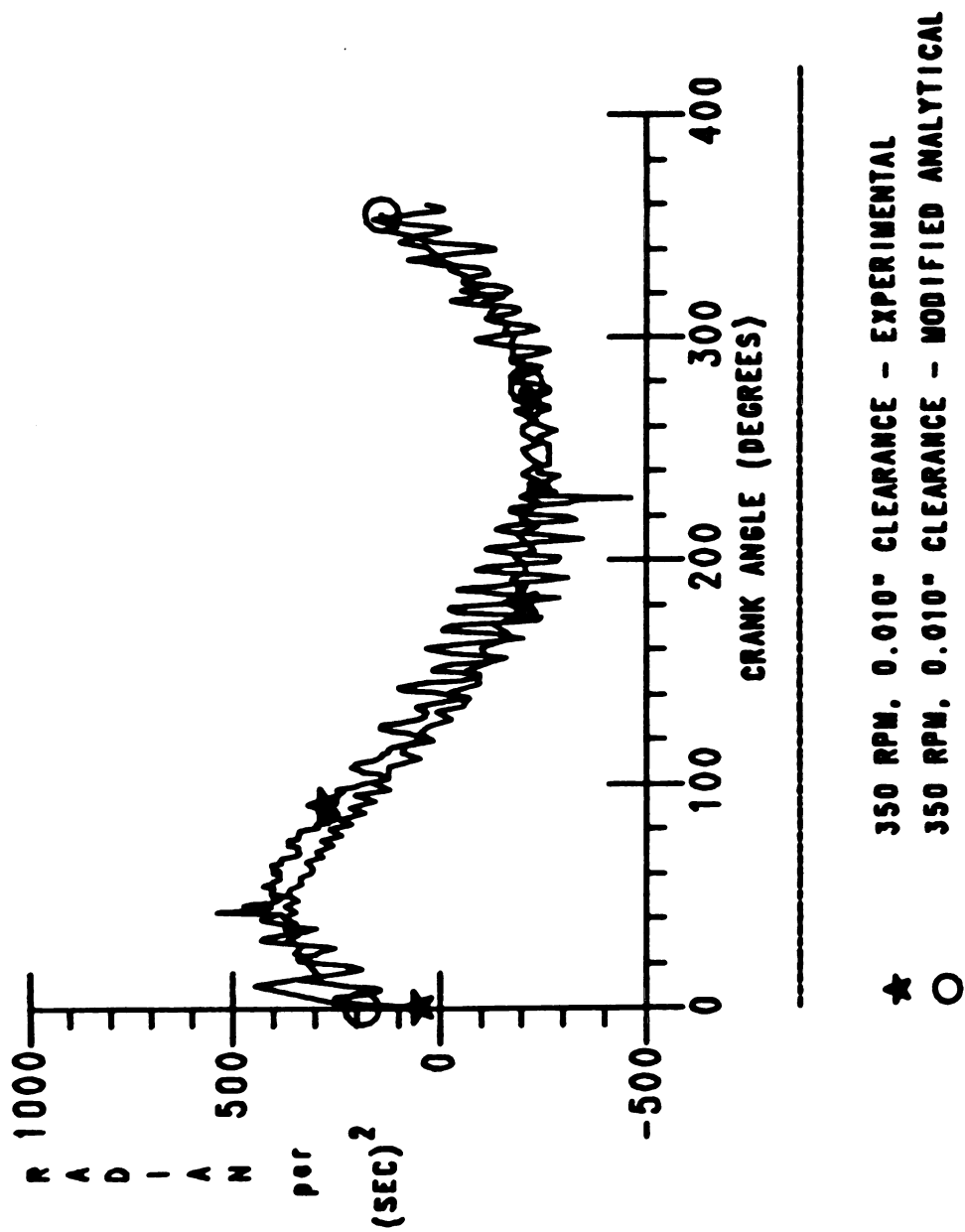
FIGURE 8.5. ROCKER ANGULAR ACCELERATION

★ 350 RPM, 0.010" CLEARANCE - EXPERIMENTAL

O 350 RPM, 0.010" CLEARANCE - MODIFIED ANALYTICAL
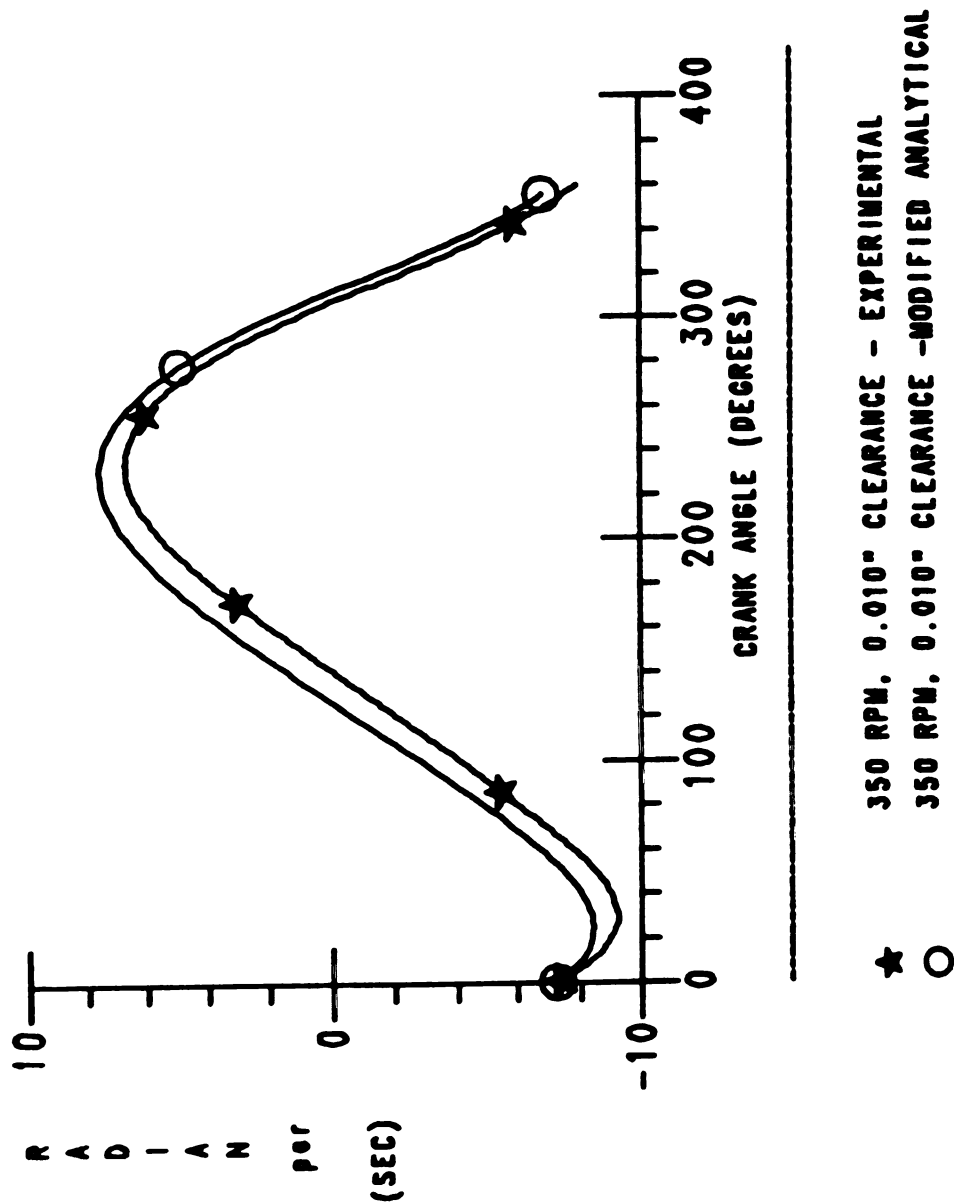
FIGURE 8.6. COUPLER ANGULAR VELOCITY

★ 350 RPM. 0.010" CLEARANCE - EXPERIMENTAL
O 350 RPM. 0.010" CLEARANCE -MODIFIED ANALYTICAL
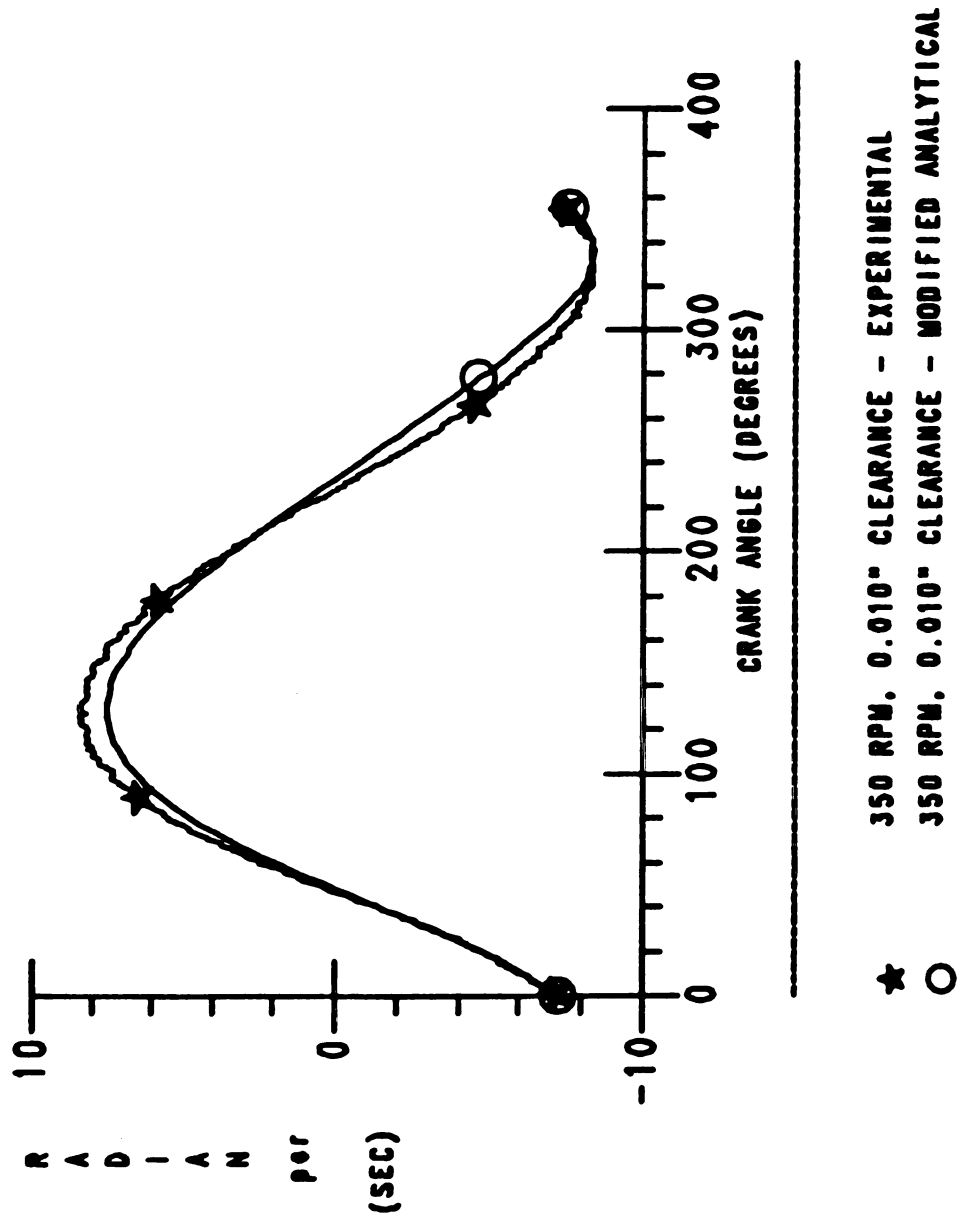
FIGURE 8.7. ROCKER ANGULAR VELOCITY

★ 350 RPM, 0.010" CLEARANCE - EXPERIMENTAL
O 350 RPM, 0.010" CLEARANCE - MODIFIED ANALYTICAL

The above comparisons indicate that, there is a good correlation between the experimental and the modified analytical results in terms of scaling. Hence, the modified analytical response of other system characteristics for which there is no experimental data available, can be studied with caution based on the notions and remarks deduced from the aforementioned correlations. (Figures 8.4 to 8.7). Figures (8.8) and (8.9) show the modified analytical responses of the X- and the Y-components of the coupler-rocker bearing reaction. Also, Figure (8.10) depicts the simulated torque required to drive the crank link at the specified angular velocity.

Obviously, by now the reader has realized that, although based on the preceding discussions the X- and Y- components of the coupler-rocker bearing reaction (Figures 8.8 and 8.9) would predictably correlate reasonably with their experimental counterparts (from scaling point of view), probably the only case of misrepresentation of these two latter plots caused by the use of the factor a occurs for the intervals of time during which the mechanism is in the free-flight mode. In other words, during the free-flight mode, there should be no interaction between the two components of the coupler-rocker bearing, namely, the pin and the bushing. This implies that, for these cases, the bearing reaction components should necessarily reduce to zero. Hence, there should exist some points on the responses shown in Figures (8.7) and (8.8) which indicate such behavior and, as can be seen such points practically do not occur in these plots. This is due to the method by which the conversion factor a has been obtained. That
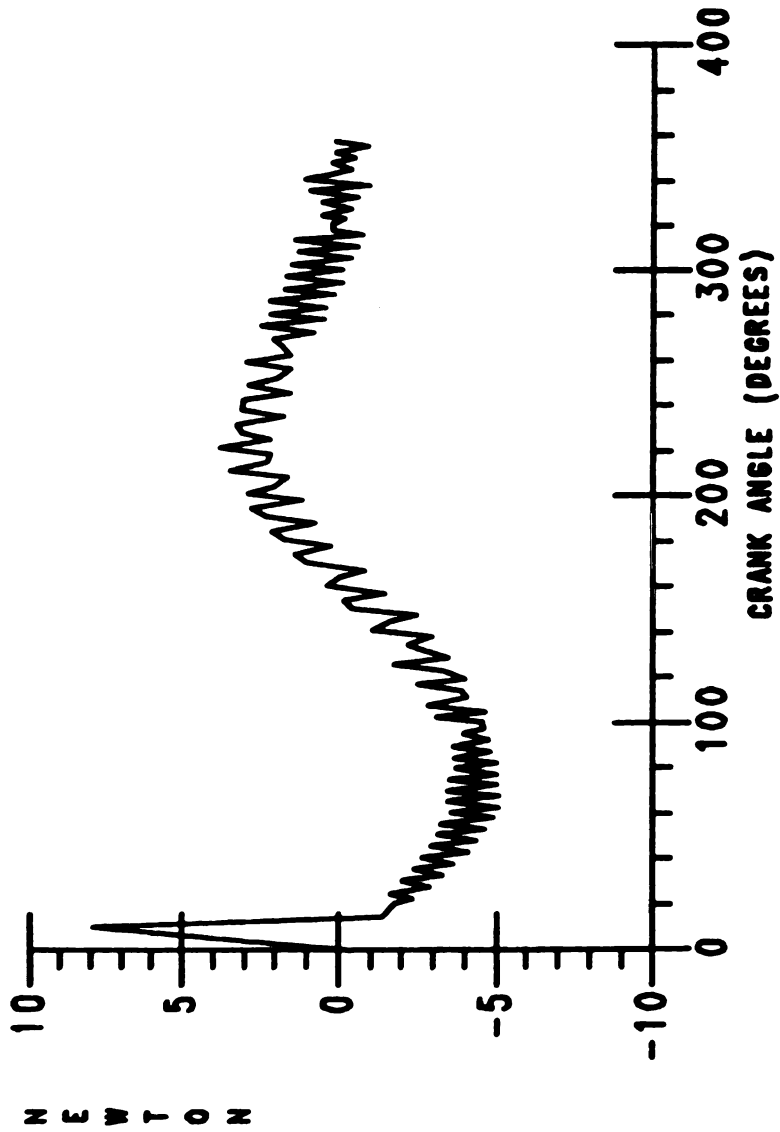
350 RPM, 0.010" CLEARANCE - MODIFIED ANALYTICAL

FIGURE 8.8. C-R BEARING REACTION; X-COMPONENT
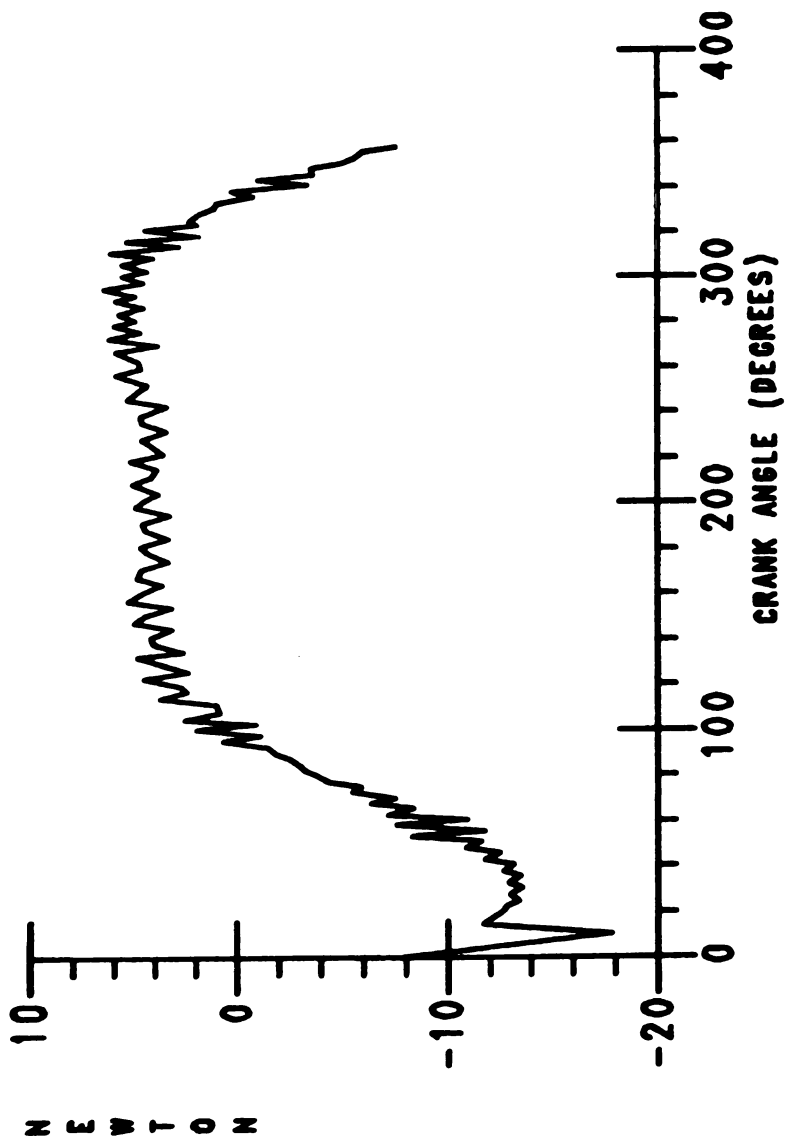
350 RPM, 0.010" CLEARANCE - MODIFIED ANALYTICAL

FIGURE 8.9.   C-R BEARING REACTION: Y-COMPONENT
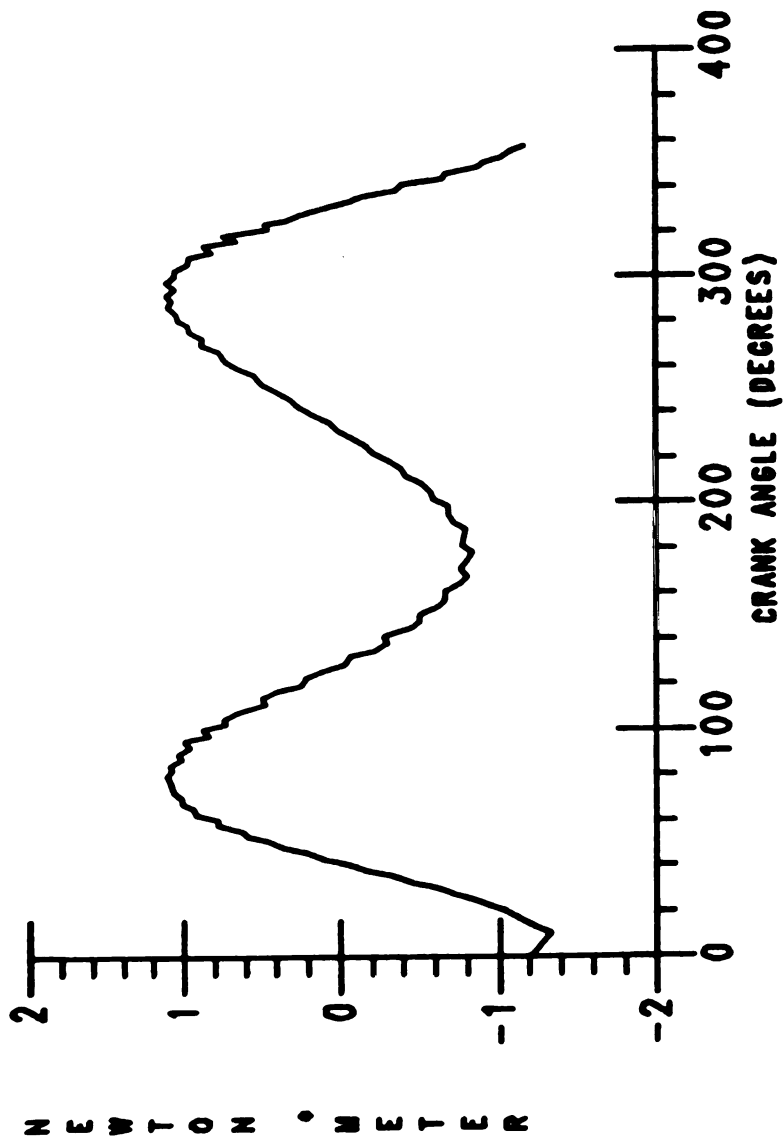
350 RPM, 0.010" CLEARANCE - MODIFIED ANALYTICAL

FIGURE 8.10. CRANK TORQUE

is, once a is used to modify the responses, it does not distinguish between the different modes of motion of the mechanism and, rather it deals with the average of the response throughout the whole period of motion of the system.

However, such a flaw due to the rescaling of the plots is not a serious one since these 'zero's which are not shown on the modified simulated responses do not, in practice, contribute to the severity of the response in terms of questions related to design and, strengths of the mechanism's parts under investigation. Also, as mentioned previously, it is more likely that, the outcome of the modification of the analytical results can be improved greatly if,

1. The conversion/magnification factor, a, is obtained using the fast fourier transform algorithm incorporating an accurate windowing function.

2. Instead of finding the average deviation of the analytical and experimental results from the nominal response which, implicitly assumes a uniform deviation of each response from the nominal one, a more realistic, if not complicated, type of distribution of deviations would be used such as normal distribution and, so forth.

Thus, in practical design applications, once the simulation is carried out using an effective and accurate digital computer, only one variable needs to be measured from the real-life system and, based on the conversion/magnification factor obtained by comparing the sampled

data with its simulation counterpart other system characteristics found by the simulation can be readily modified and studied in terms of their parametric range of values.

Now, for the sake of mentioning a few other points, suppose that the simulation and the experimental results correlate accurately both in scaling and points of variations. Assuming that such a task can be performed easily, other significant plots can be obtained such as the ones presented by Mansour et. al. [7] (although based on two modes of free-flight and impact only) and shown here in Figures (8.11) and (8.12). As can be observed, Figure (8.11) shows the impact spectra for the pin and the bushing of the coupler-rocker bearing. The six largest impacts on these system components are marked as Y_1 to Y_6 in the descending order of their magnitudes, Y_1 being the largest. Note that, these are locally-oriented spectra. That is, for instance, the orientation of the impacts shown for the pin of the bearing are those viewed by an observer moving with the rocker arm. Also, Figure (8.12) shows the largest three impacts acting on the coupler-rocker bearing of the mechanism during its motion. Note that, these figures were obtained from a simulation of the model being in the quasi-steady phase. Thus, based on the above two figures, one can realize the reason behind the out-of-roundness of the bearings that possess a finite clearance.

Assuming that, the capabilities are such that spectra and figures such as the ones in Figures (8.11) and (8.12) can be obtained with

a) IMPULSES ON PIN   b) IMPULSES ON SOCKET
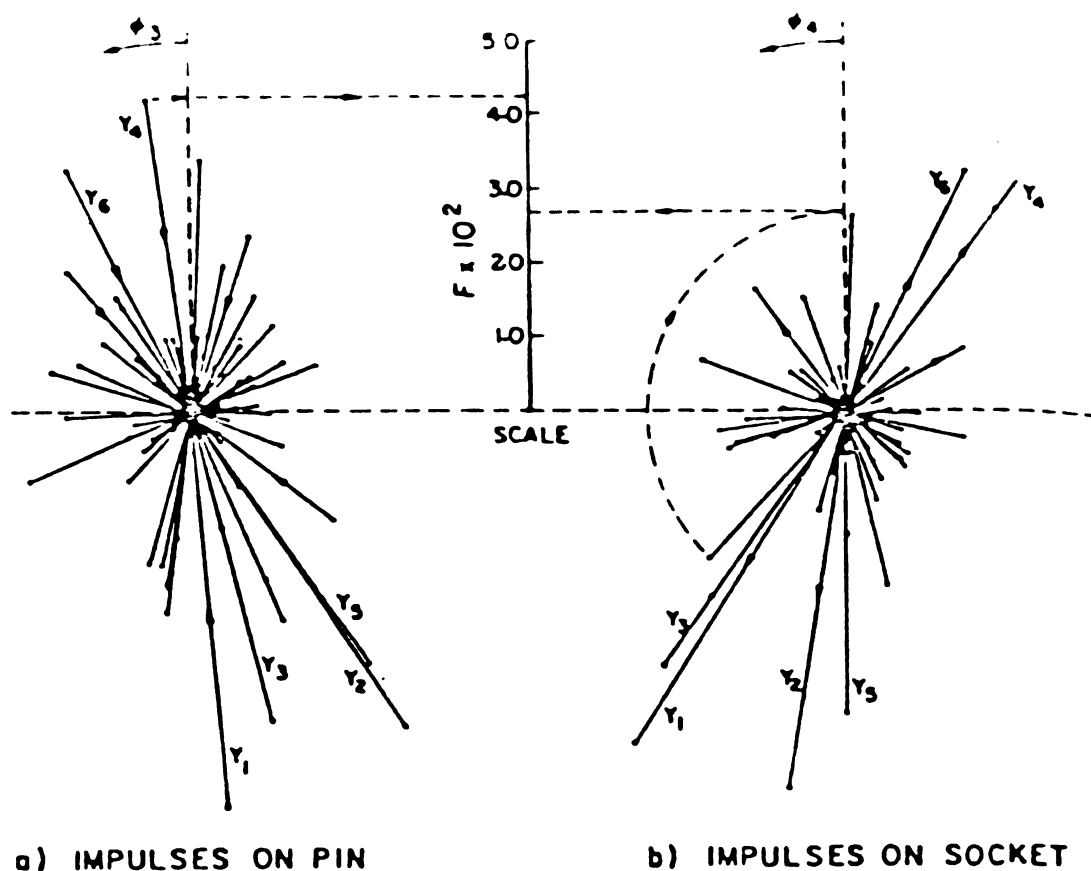
FIGURE 8.11. IMPULSE DIRECTIONS ON THE BEARING COMPONENTS

ARROWS INDICATE IMPULSES
ON SOCKET

(a)   (b)
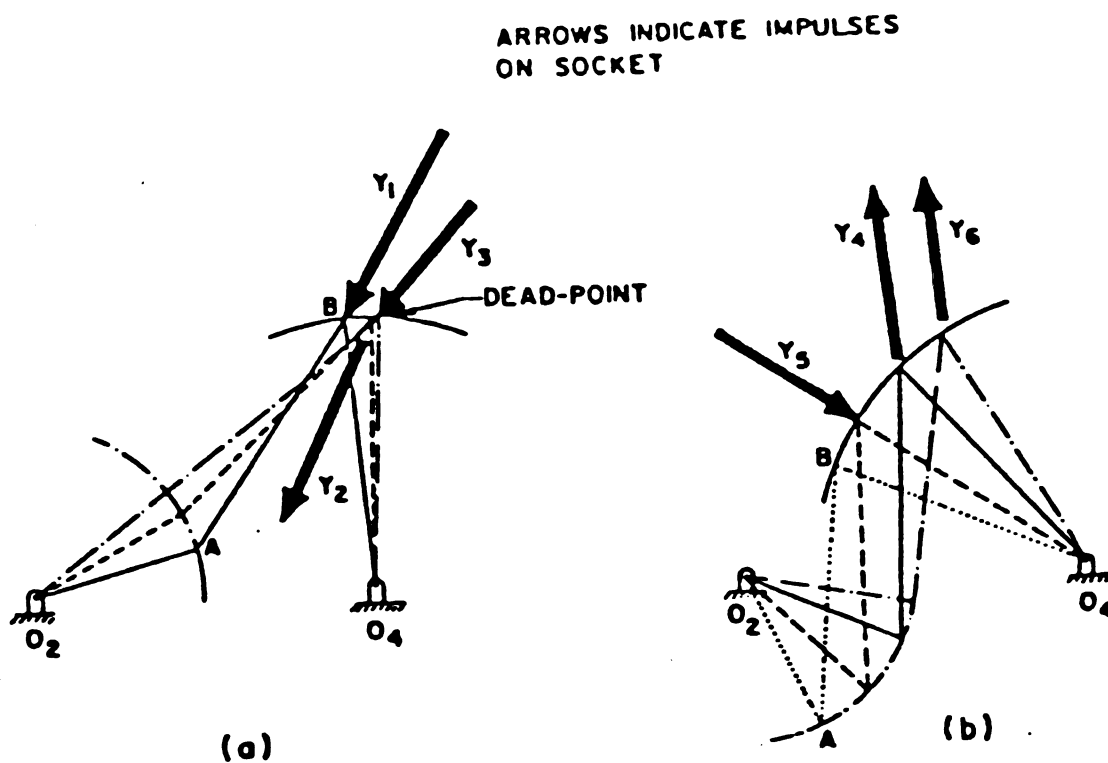
FIGURE 8.12. DIRECTIONS OF THE DOMINANT IMPACTS FOR ONE CYCLE

good reliability, bearings can be tailor-designed to prevent such phenomena. In other words, the bushing of the bearing, for instance, can be made of composite materials with different stiffness and strength regions along its inner surface by locally strengthening the surface of the bushing at regions which are likely to encounter more severe vibro-impact shocks and impulses. This would certainly prolong the working lifespan of the bearing along with a significant reduction of the acoustic noise emitted as a result of these impulses [82].

CHAPTER NINE

CONCLUSIONS

A four bar linkage with rigid links and, with a finite clearance in the coupler-rocker bearing was modelled and simulated. The observed disagreement between the experimental and the analytical results were presumably due to the ideal values assumed for the coefficient of restitution and the Coulomb coefficient of friction, along with the presence of certain level of round up/truncation error, coupled with the existense of manufacturing errors in building the experimental apparatus. Also, the simulation was presented for the start-up or the transient phase of the motion of the mechanism under study, whereas the experimental results corresponded to the quasi-steady phase.

The scaling of the simulation data was modified further using a conversion/magnification factor computed based on the comparison of

the experimental and, the original simulation results. The outcome of such modification suggested reasonable correlation between the analytical and the experimental responses in terms of the parametric scaling of the results. The reliability of those system parameters for which there was only simulation data available, was deduced based on the aforementioned comparison of the experimental data with their simulation counterparts.

Improvements in the simulation results obtained in this work can be achieved by

1. Development of a means of measuring the correct values of the coefficient of restitution and the Coulomb coefficient of friction of the experimental rig under study. The resulting values can be incorporated into the simulation in order to test the threshold of reliability of model assumed in this work and, if possible, enhance the analytical results.

2. Modeling the four bar linkage under study as having elastic links for the coupler and, the rocker links. This, in turn, necessitates the adaption of different approaches to solve and develope the governing equations of motion.

3. Incorporation of the effect of the bearing lubrication and hydrodynamic phenomena occuring within the bearing with finite clearance.

4. Modeling a four bar linkage with simultaneous clearances existing

in more than one bearing of the mechanism.

5. Development of a model to investigate the acoustic radiation due to the existense of clearance in the bearing(s) of the mechanism.

6. Modelling a four bar linkage which encompasses all of the above four cases.

7. Extension of the model to the other types of mechanisms with higher number of links and, more complicated configurations.

8. Construction of a three-dimensional analytical model, which would be able to incorporate the torsional loading on the bearing with clearance due to possible misalignments of the mechanism links.

APPENDIX

APPENDIX

SCHEMATIC FLOWCHART OF THE SIMULATION CODE -SIMUL-

```
                    ┌─────────────┐
                   (    START     )
                    └─────────────┘
                           │
                           ▼
              ┌────────────────────────────┐
              │ Variable type decleration  │
              └────────────────────────────┘
                           │
                           ▼
                  ┌──────────────────┐
                  │  Common blocks   │
                  └──────────────────┘
                           │
                           ▼
              ┌────────────────────────────┐
              │     Primary data input     │
              │  (known system parameters) │
              └────────────────────────────┘
                           │
                           ▼
          ┌──────────────────────────────────┐
          │ Array and vector initialization  │
          └──────────────────────────────────┘
                           │
                           ▼
            ┌──────────────────────────────┐
            │  Set up vector containing the│
            │   values of crank angle at   │
            │      desired intervals       │
            └──────────────────────────────┘
                           │
                           ▼
            ┌──────────────────────────────┐
            │  Compute nominal mechanism   │
            │      system parameters       │
            └──────────────────────────────┘
                           │
                           ▼
          ┌──────────────────────────────────┐
          │ Compute the reaction components  │
          │  of the coupler-rocker bearing   │
          │     of the nominal mechanism     │
          └──────────────────────────────────┘
                           │
                           ▼
                         ( I )
```

```
                                    ( I )
                                      │
                                      ▼
                    ┌─────────────────────────────────┐
                    │   Input the starting value of the │
                    │           crank angle            │
                    └─────────────────────────────────┘
                                      │
                                      ▼
                    ┌─────────────────────────────────┐
                    │  Set up the vector containing the parameter │
                    │   values corresponding to the initial │
                    │     conditions of the simulation  │
                    └─────────────────────────────────┘
                                      │
                                      ▼
                    ┌─────────────────────────────────┐
                    │  Input secondary data. i.e., the integration │
                    │  mesh size, upper bound error size, No. of │
                    │        crank revolutions ...     │
                    └─────────────────────────────────┘
                                      │
                                      ▼
                    ┌─────────────────────────────────┐
                    │  Input the value of the coeficient of │
                    │           restitution            │
                    └─────────────────────────────────┘
                                      │
                                      ▼
                    ┌─────────────────────────────────┐
                    │      Start the simulation        │            ( 5 )
                    └─────────────────────────────────┘
                                      │◄──────────────────────────────┘
                                      ▼
                                    ╱   ╲
                                  ╱       ╲       Y
                                ╱ Contact-loss ╲──────────┐
                                ╲      ?      ╱            │
                                  ╲       ╱                │
                                    ╲   ╱                  │
                                      │ N                  │
                                      ▼                    │
                    ┌─────────────────────────────────┐    │
                    │        Iterate one step          │◄───┘
                    └─────────────────────────────────┘
                                      │
                                      ▼
                                    ╱   ╲
                              Y   ╱       ╲   N
                            ┌───╱   End     ╲───┐
                            │   ╲   time    ╱   │
                            │     ╲   ?   ╱     │
                            │       ╲   ╱       │
                            ▼         ╲╱        ▼
                          ( 4 )              ( II )
```

```
                    ( II )
                      |
                      v
         +--------------------------+
         | Set up new initial conditions |
         +--------------------------+
                      |
          +---------->|
          |           v
          |       /       \
          |      /  Contact \      Y
          |      \    ?     / ------+
          |       \       /         |
          |         | N             |
          |         v               |
          |   +-------------+       |
          +---| Iterate one step |  |
              +-------------+       |
                      |             |
                      |<------------+
                      v
                  /       \
         Y       /  End    \
     +----------/   time    \
     |          \    ?      /
     |           \       /
     v             | N
   ( 4 )           v
         +------------------------------+
         | Compute coupler and rocker angular |
         |     velocities after impact        |
         +------------------------------+
                      |
                      v
         +------------------------------+
         | Set up new initial conditions for |
         |      the following mode           |
         +------------------------------+
                      |
                      v
                    ( 5 )
```

(4)

Write down the result of the
simulation into seperate
output files

STOP

SUBROUTINES AND FUNCTIONS USED

IN CONJUNCTION WITH THE CODE

-STMUL-

ANGLE : Given the two orthogonal sides of a right triangle, computes the corresponding angles in the range of 0 to 2π.

CLANG : Given the X- and Y- components of the coupler-rocker bearing reaction of the nominal mechanism, computes the angular displacement, velocity and, acceleration of the total force at a given time $t=t_1$, where t_1 is the starting time of the integration. Note that, these angular parameters correspond to those of the 'clearance link' at initial conditions.

CRKSET : Given an initial starting crank angle, computes the values of the crank angular displacement at prescribed intervals and, stores them in a pre-initialized vector.

DIFF : Given an array containing one of the system parameters corresponding to equal time intervals, computes the first and second derivatives of the array with respect to time. The differentiation is crried out using difference folmulae (backward, central and, forward).

FCT : Used in conjunction with the numerical integration package

HPCG, computes the values of the unknowns of equation 3.3-7 at each time step. Corresponds to the following mode.

FCT^R : Used in conjunction with HPCG, computes the unknowns of the equations 4.1-20 and 4.2-1 at each time step. Corresponds to the free-flight mode.

FORCE : Given the angular displacements, velocties and, accelerations of the links of the nominal mechanism, computes the values of the ^{T}- and ^{V}- components of the coupler-rocker bearing reaction at each time step. The result is fed into a predesignated vector for1 further manipulations. This subroutine also computes the crank torque at each time step.

HPCG : The numerical integration package. Using subroutines FCT and OUTP (following mode) or FCT^R and OUTPF (free-flight mode), along with the integration mesh size, upper bound of the absolute error of the integration and, other secondary inputs, this package solves the given differential equations numerically.

OUTDAT : Generates seperate output files to store the final results of the simulation obtained from HPCG.

OUTP : Used in conjunction with HPCG. When in the following mode, it examines the contact-loss criteria and, signals the main code for such occurence.

OUTPF : Used in conjunction with HPCG. When in the free-flight mode, it examines whether contact has been reestablished. If so, the main code is signaled accordingly.

OUTPUT : Generates seperate output files to store the system parameters of the nominal mechanism.

RADDEG : Given an angle in radians, this function convert the value to degrees.

SMDR1 : Given the geometric data of the nominal mechanism along with the crank angular velocity, it computes the coupler and rocker angular displacements.

SMDR2 : Given both the input and the output of the subroutine SMDR1, computes the angular velocities of the coupler and the rocker links of the nominal mechanism.

SMDR3 : Given both the input and the output of the subroutine SMDR2, computes the angular accelerations of the coupler and rocker links of the nominal mechanism.

LIST OF REFERENCES

1. R. S. Haines, "A Theory of Contact Loss at Revolute Joints With Clearance," Journal of Mechanical Engineering Science, 1980, Vol. 22 No. 3, pp. 129-136

2. C. L. S. Wu and S. W. E. Earles, "A Determination of Contact-Loss at a Bearing of a Linkage Mechanism,"ASME Journal of Engineering for Industry, 1977, paper No. 76-DET-43, pp. 375-380

3. C. L. S. Wu and S. W. E. Earles, "Motion Analysis of a Rigid-Link Mechanism With Clearance at a Bearing, Using Lagrangian Mechanics and Digital Computation," Institution of Mechanical Engineering Conference, Sept. 1972, Paper No. C86/72, pp. 83-89

4. C. L. S. Wu and S. W. E. Earles, "Predicting The Occurence of Contact-Loss and Impact at a Bearing From a Zero-Clearance Analysis," Institute of Mechanical Engineering Conference, 1975

5. B. Miedema and W. M. Mansour, "Mechanical Joints With Clearance: a Three-Mode Model," ASME Journal of Engineering for Industry, 1976, paper No. 76-DET-52, pp. 1319-1323

6. M. A. Townsend and W. M. Mansour, "A Pendulating Model for Mechanisms With Clearances in the Revolutes," ASME Journal of

Engineering for Industry, 1975, paper No. 74-DET-22, pp.354-358

7. M. A. Townsend and W. M. Mansour, "Impact Spectra and Intensities for High-Speed Mechanisms," ASME Journal of Engineering for Industry, 1975, pp.347-353

8. S. J. Grant and J. N. Fawcett, "Effects of Clearance at the Coupler-Rocker Bearing of a 4-Bar Linkage," Mechanism and Machine Theory, 1979, Vol 14, pp.99-110

9. M. O. M. Osman and B. M. Bahgat and T. S. Sankar, "On the Prediction of Journal-Bearing Seperation in High-Speed Mechanisms with Clearances," American Society of Mechanical Engineering, paper No. 80-WA/DSC-36, 1980, pp.1-7

10. M. O. M. Osman and B. M. Bahgat and T. S. Sankar, "An Approach for Dynamic Analysis of Mechanical Systems with Multiple Clearances Using Lagrangian Mechanics," Journal of Mechanical Engineering Science, 1983, Vol 197C, pp.17-23

11. M. O. M. Osman and B. M. Bahgat and T. S. Sankar, "On the Effect of Bearing Clearances in the Dynamic Analysis of Planar Mechanisms," Journal of Mechanical Engineering Science, 1979, Vol 21, No 6, pp.429-437

12. B. S. Thompson and M. T. Bengisu and D. Zuccaro, "An Experi-

mental Investigation on the Effects of Clearance in Plain Journal Bearings on Bending Strains in Flexible Four-Bar Linkages," American Society of Mechanical Engineers, paper No. 82-DET-16

13. R. D. Mindlin and L. E. Goodman, "Beam Vibrations With Time-Dependent Boundary Conditions," ASME Journal of Applied Mechanics, 1930, pp.377-380

14. A. C. Wang and T. W. Lee, "On the Dynamics of Intermittent-Motion Mechanisms-Part I: Dynamic Model and Response," ASME, paper No. 82-DET-64, 1982

15. A. C. Wang and T. W. Lee, "On the Dynamics of Intermittent-Motion Mechanisms-Part II: Geneva Mechanisms, Ratchets, and Escapements," ASME, paper No. 82-DET-65, 1982

16. S. Dubowsky and T. N. Gardner, "Design and Analysis of Multilink Flexible Mechanisms with Multiple Clearance Connections," ASME Journal of Engineering for Industry, 1976

17. S. Dubowsky and T. N. Gardner, "Dynamic Interactions of Link Elasticity and Clearance Connections in Planar Mechanical Systems," ASME Journal of Engineering for Industry, 1975, pp.652-661

18. M. A. Chace, "Analysis of the Time-Dependence of Multi-Freedom Mechanical Systems in Relative Coordinates," ASME Jour-

nal of Engineering for Industry, 1967, pp.119-125

19. S. C. Chu and K. C. Pan, "Dynamic Response of a High-Speed Slider-Crank Mechanism with an Elastic Connecting Rod," ASME Journal of Engineering for Industry, 1975, pp.542-550

20. A. Shabana and R. A. Wehage, "Variable Degree-of-Freedom Component Mode Analysis of Inertia Variant Flexible Mechanisms," ASME Journal of Mechanical Design, 1982

21. Morita, Furuhashi and Matsuura, "Research on Dynamics of Four-Bar Linkage With Clearances at Turning Pairs- 2nd Report : Analysis of Crank-Lever Mechanism with Clearance at Joint of Crank and Coupler Using Continuous Contact Model," Bulletin of JSME, 1978, Vol 21, No. 158, pp.1284-1291

22. Morita, Furuhashi and Matsuura, "Research on Dynamics of Four-Bar Linkage with Clearance at Turning Pairs- 3rd Report : Analysis of Crank-lever Mechanism with Clearance at Joint of Coupler and Lever Using Continuous Contact Model," Bulletin of JSME, 1978, Vol 21, No. 158, pp.1292-1298

23. Morita, Furuhashi and Matsuura, "Research on Dynamics of Four-Bar Linkage with Clearance at Turning Pairs- 4th Report : Forces Acting at Joints of Crank-Lever Mechanism," Bulletin of JSME, Vol 21, No. 158, pp.1299-1305

24. R. Wilson and J. N. Fawcett, "Dynamics of the Slider-Crank Mechanism with Clearance in the Slider Bearing," Mechanism and Machine Theory, 1972, Vol 9, No. 1-E, pp.61-80

25. Horie and Funabashi and Ogawa and Kobayashi, "A Displacwment Analysis of Plane Multilink Mechanisms with Clearances and Tolerances," Bulletin of JSME, 1980, Vol 23, No. 183, pp.1522-1529

26. M. O. M. Osman and B. M. Bahgat and T. S. Sankar, "On the Dynamic Analysis of Planar Mechanisms with Multiple Clearances," Journal of Mechanical Engineering Science, 1983, Vol 197C, pp.89-95

27. S. A. Kolhatkar and K. S. Yajnik, "The Effects of Play in the Joints of a Function-Generating Mechanism," Journal of Mechanisms, Vol 5, pp.521-532

28. R. E. Garret and A. S. Hall Jr., "Effect of Tolerance and Clearance in Linkage Design," ASME Journal of Engineering for Industry, 1969, pp.198-202

29. M. A. Chace and Y. O. Bayazitoglu, "Development and Application of a Generalized d'Alembert Force for Multifreedom Mechanical Systems," ASME Journal of Engineering for Industry, 1971, pp.317-327

30. Doi and Asano, "A method for Analysis of Elasto-dynamic Con-

tact Problems by Finite Element Method," Bulletin of JSME, 1981, Vol24, No. 189, pp.528-533

31. V. A. Eshwar, "Analysis of Clearance Fit Pin Joints," International Journal of Mechanical Science, 1977, Vol 20, pp.477-484

32. A. Francavilla and O. C. Zienkiewicz, "A Note on Numerical Computation of Elastic Contact Problems," International Journal for Numerical Methods in Engineering, 1975, Vol 9, pp.913-924

33. J. J. Kalker, "A Survey of the Mechanics of Contact Between Solid Bodies," Hauptvortrage, 1977, ZAMM 57, pp. T3-T17

34. K. P. Singh and P. Burton, "Numerical Solution of Non-Hertzian Elastic Contact Problems," ASME Journal of Applied Mechanics, 1974, pp.485-490

35. R. J. Rogers and G. C. Andrews, "Dynamic Simulation of Planar Mechanical Systems with Lubricated Bearing Clearances Using Vector-Network Methods," ASME Journal of Engineering for Industry, 1977, pp.131-137

36. S. W. E. Earles and C. L. S. Wu, "Designing to Minimize Impacts in Bearings," Engineering, 1977, pp.866-867

37. C. Bagci, "Dynamic Motion Analysis of Plane Mechanisms with

Coulomb and Viscous Damping via the Joint Force Analysis," ASME Journal of Engineering for Industry, 1975, pp.551-560

38. R. A. Wehage and E. J. Haug, "Dynamic Analysis of Mechanical Systems with Intermittent Motion," ASME Journal of Mechanical Design, 1981, pp.1-7

39. R. A. Wehage and E. J. Haug and N. C. Barman, "Design Sensitivity Analysis of Planar Mechanism and Machine Dynamics," ASME Journal of Mechanical Design, 1980, pp.1-11

40. O. Perera and W. Seering, "Prevention of Impact in Bearings of Four-Bar Linkages," ASME Journal of Mechanical design, 1982, paper No.82-DET-134

41. R. K. Miller and B. Fatemi, "An Efficient Technique for the Approximate Analysis of Vibro-Impact," ASME Journal of Mechanical Design, 1981, paper No.81-DET-16

42. S. W. E. Earles and O. Kilicay, "Predicting Impact Conditions Due to Bearing Clearances in Linkage Mechanisms," Proceedings of the Fifth World Congress on Theory of Machines and Mechanisms, New Castle upon Tyne, Sept. 1979

43. S. Dubowsky and M. F. Moening, "An Experimental and Analytical Study of Impact Forces in Elstic Mechanical Systems with

Clearances," Mechanism and Machine Theory, 1980, Vol 13, pp.451-465

44. S. Dubovsky, "On Predicting the Dynamic Effects of Clearances in Planar Mechanisms," Mechanisms Conference and International Symposium on Gearing and Transmissions, SanFrancisco, California, October 1972, paper No 72-Mech-91

45. S. Dubovsky and S. C. Young, "An Experimental and Analytical Study of Connection Forces in High-Speed Mechanisms," ASME Journal of Engineering for Industry, 1975, pp.1166-1174

46. G. R. Johnson, "Three-Dimensional Analysis of Sliding Surfaces During High Velocity Impact," ASME Journal of Applied Mechanics, 1977, pp.771-773

47. R. G. Herbert and D. C. McWhannell, "Shape and Frequency Composition of Pulses from an Impact Pair," ASME Journal of Engineering for Industry, 1976, paper No.76-DET-36

48. F. R. E. Crossley and A. Oledzki and W. Szydlowski, "On the Modelling of Impacts of Two Elastic Bodies Having Flat And Cylinderical Surfaces with Application to Cam Mechanisms," Proceedings of the Fifth World Congress on Theory of Machines and Mechanisms, Montreal, Canada, July 1979, pp.1090-1092

49. R. C. Azar and F. R. Crossley, "Digital Simulation of Impact

Phenomenon in Spur Gear Systems," ASME, Journal of Engineering for Industry, 1977, Vol 99B, pp.792-798

50. M. A. Veluswami and F. R. E. Crossley, "Multiple Impacts of a Ball Between Two Plates -Part I : Some Experimental Observations," ASME Journal of Engineering for Industry, 1975, pp.820-827

51. M. A. Veluswami and F. R. E. Crossley and G. Horvay, "Multiple Impacts of a Ball Between Two Plates -Part II : Mathematical Modelling," ASME Journal of Engineering for Industry, 1975, pp.828-835

52. T. P. Goodman, "How to Calculate Dynamic Effects of Backlash," Machine Design, 1963, pp.150-157

53. R. C. Johnson, "Impact Forces in Mechanisms," Machine Design, 1958, pp.138-146

54. R. E. Beckett and K. C. Pan and S. C. Chu, "A Numerical Method for the Dynamic Analysis of Mechanical Systems in Impact," ASME Journal of Engineering for Industry, 1977, pp.665-673

55. D. L. Sikarskie and B. Paul, "Periodic Motions of a Two-Body Subjected to Repetitive Impact," Journal of Engineering for Industry, 1969, pp.931-938

56. Y. Tatara, "Effects of External Force on Contacting Times and Coefficient of Restitution in a Periodic Collision," ASME Journal of Applied Mechanics, 1977, pp.773-774

57. M. A. Townsend and W. M. Mansour, "Approximating the Times Between Closely-Spaced Impacts in Mechanisms with Clearances," Mechanism and Machine Theory, 1976, Vol 11, pp.259-265

58. R. E. Beckett and K. C. Pan and S. C. Chu, "A Numerical Method for the Dynamic Analysis of Mechanical Systems in Impact," Journal of Engineering for Industry, 1977, Vol 99B, pp.665-672

59. S. Dubowsky and M. F. Moening, "An Experimental and Analytical Study of Impact Forces in Elastic Mechanisms with Clearance," Mechanism and Machine Theory, 1978, Vol 13, pp.451-465

60. T. Hayashi and F. R. E. Crossley and D. Larionescu, "Analog Simulation of Repetitive Impacts," Proceedings of the Fourth World Congress on Mechanism and Machine Theory -1975, pp.1073-1077

61. K. H. Hunt and F. R. E. Crossley, "Coefficient of Restitution Interpreted as Damping in Vibro-Impact," ASME Journal of Applied Mechanics, 1975, Vol 42E, pp.440-445

62. N. Maw and J. R. Barber and J. N. Fawcett, "The Oblique Impact of Elastic Spheres," Wear, 1976, Vol 38, pp.101-114

63. B. S. Thompson, "Variational Formulations for the Finite Element Analysis of Noise Radiation from High-Speed Machinery," ASME Journal of Engineering for Industry, 1981, Vol 103/385, pp.385-391

64. A. J. Ruffini, "Bearing Noise -Part II : Analysis of Sliding Bearings," Machine Design, 1963, pp.158-166

65. A. Akay and M. T. Bengisu and M. Latcha, "Transient Acoustic Radiation from Impacted Beam-Like Structures," Journal of Sound and Vibration, 1983, Vol 91, pp.135-145

66. E. J. Richards, "Energy Input, Vibrational Level and Machinery Noise; Some Simple Relationships," ASME, paper No. 81-DET-96, 1982

67. D. A. Turcic and A. Midha, "Modelling of High Speed Elastic Mechanisms for Vibration Response," ASME, Int. Comp. Conf. Exhibit, pp.81-92, 1983

68. Perrera Noel Duke, "Noise Generation in High-Speed Mechanical Systems," Ph.D. Dissertation, 1977

69. N. D. Perrera and S. Dubowsky, "Predicting Acoustical Noise Generation in Complex Mechanical Systems," ASME Journal of Mechanical Design, 1978, paper No. 78-DET-60

70. N. D. Perrera and S. Dubowsky, "Analytical Method to Predict Noise Generation From Vibrating Machine Systems," ASME Journal of Acoustics, 1980, Vol 67, No 2, pp.551-563

71. S. Dubowsky and T. L. Morris, "An Analytical and Experimental Study of the Acoustical Noise Produced by Machine Links," ASME Journal of Vibration, Acoustics, Stress, and Reliability in Design, 1983, Vol 105, pp.393-401

72. M. R. Smith and L. Maunder, "Inertia Forces in a Four Bar Linkage," Journal of Mechanical Engineering Science, 1967, Vol 9, No 3, pp.218-225

73. J. L. Meriam, "Dynamics," New York : John Wiley Sons, 1975

74. A. Frank D'Souza and Vijay K. Garg, "Advanced Dynamics, Modelling and Analysis," New Jersey : Prentice Hall, 1984

75. K. M. Yudin, "On a Problem of the Dynamics of Mechanical Systems with Clearance," Proceedings of the Third World Congress of IFTOMM, Vol A, 1971, pp.197-208

76. S. Dubowsky and F. Freudenstein, "Dynamic Analysis of Mechanical Systems with Clearances, Parts 1 _2 ," ASME Journal of Engineering for Industry, Series B, Vol 93, No. 1, 1971, pp.305-316

77. S. Dubowsky, "On Predicting the Dynamic Effects of Clearances in One-Dimensional Closed Loop Systems," ASME Journal of Engineering for Industry, Series B, Vol 96, No. 1, 1974, pp.317-323

78. M. A. Veluswami and F. R. E. Crossley and G. Horvay, "Some Experiments on the Nature of Repetitive Impacts," ASME Journal of Engineering for Industry, Transactions of the ASME, 1974

79. D. Benson, "Simulating Anelastic mechanisms Using Vector Processors," Computers in Mechanical Engineering, Jan. 1983, pp.59-64

80. L. Meirovitch, "Analytical Methods in Vibrations," London : The Macmillan, 1967

81. Theodore Baumeister (Editor-in-Chief), "Marks Standard Handbook for Engineers," New York : McGraw-Hill, 1978, Eighth Edition

82. M. Sharif-Bakhtiar and B. S. Thompson, "Reducing Acoustical Noise Radiation From High-Speed Mechanisms by Judicious Material Selection : An Experimental Study," ASME Paper No. 84-DET-38

83. R. S. Haines, "Survey: 2-Dimensional Motion and Impact at Revolute Joints," Mechanism and Machine Theory, Vol 15, pp.361-370

84. S. J. Grant and J. N. Fawcett, "Comparison of Relative Motion at Form-Closed and Force-Form-Closed Connections," Proceedings

of the Second World congress on IFToMM, International Symposium of Linkages and Computer Aided Design Methods, Bucharest, Romania, 1977, 1(2), pp.269-280

85. Ralston, Wilf, "Mathematical Methods for Digital Computers," Wiley, New York/London, 1960, pp.95-109

86. Ralston, "Runge-Kutta Methods with Minimum Error Bounds," MTAC, Vol.16, ISS.80, 1962, pp.431-437

87. E. Oran Brigham, "The Fast Fourier Transform," Prentice-Hall, New Jersey, 1974

88. P. A. Stark, "Introduction to Numerical Methods," Macmillan, New York/London, 1970